

TECTONIC EVOLUTION OF A CALEDONIAN-AGED CONTINENTAL
BASEMENT ECLOGITE TERRANE IN LIVERPOOL LAND,
EAST GREENLAND

Except where reference is made to the work of others, the work described in this thesis is my own or was done in collaboration with my advisory committee. This thesis does not include proprietary or classified information.

John Wesley Buchanan II

Certificate of Approval:

Willis E. Hames
Professor
Geology

Mark G. Steltenpohl, Chair
Professor
Geology

Ashraf Uddin
Associate Professor
Geology

Joe F. Pittman
Interim Dean
Graduate School

TECTONIC EVOLUTION OF A CALEDONIAN-AGED CONTINENTAL
BASEMENT ECLOGITE TERRANE IN LIVERPOOL LAND,
EAST GREENLAND

John Wesley Buchanan II

A Thesis

Submitted to

the Graduate Faculty of

Auburn University

in Partial Fulfillment of the

Requirements for the

Degree of

Master of Science

Auburn, Alabama
May 10, 2008

TECTONIC EVOLUTION OF A CALEDONIAN-AGED CONTINENTAL
BASEMENT ECLOGITE TERRANE IN LIVERPOOL LAND,
EAST GREENLAND

John Wesley Buchanan II

Permission is granted to Auburn University to make copies of this thesis at its discretion,
upon request of individuals or institutions and at their expense. The author reserves all
publication rights.

Signature of Author

Date of Graduation

VITA

John Wesley Buchanan II, son of Jerry Wesley and Patricia Ann Buchanan was born on November 29, 1983 in Franklin, Tennessee. During Wesley's middle and high school years, he was involved in the Boy Scouts of America and earned the rank of Eagle Scout. During his scouting years, he hiked in the southern Rocky Mountains, the Appalachians, and the Canadian interior, learning to navigate backcountry lands by map and compass a skill that would later become very valuable. He graduated with honors from Battle Ground Academy in Franklin, Tennessee in 2002. Upon graduation, Wesley enrolled at the University of Kentucky, where by a rather circuitous route found and fell in love with geology. While at the University of Kentucky, Wesley enjoyed geology based field trips in the states of Kentucky, Tennessee, North Carolina, South Carolina, Georgia, Alabama, Mississippi, Louisiana, Missouri, Kansas, Colorado, Utah, Arizona, and New Mexico. After completing almost all of his course work, he entered the graduate program at Auburn University in the fall of 2006. By the wonders of a correspondence course he graduated in August 2007 with a Bachelor of Science in Geology. While attending Auburn University, Wesley performed field work in East Greenland, North Norway, and the Southern Appalachians. In the spring of 2008, Wesley graduated from Auburn University with a Masters of Science in Geology.

THESIS ABSTRACT

TECTONIC EVOLUTION OF A CALEDONIAN-AGED CONTINENTAL
BASEMENT ECLOGITE TERRANE IN LIVERPOOL LAND,
EAST GREENLAND

John Wesley Buchanan II

Master of Science, May 10, 2008
(M.S., Auburn University, 2008)
(B.S., University of Kentucky, 2007)

122 Typed Pages

Directed by Mark G. Steltenpohl

Liverpool Land is located in an interior position within the East Greenland Caledonides. Due to the remoteness of the field locality, very little work has been published on the rocks and structures of Liverpool Land. The main focus of this thesis work, therefore, has been to aid in establishing a metamorphic and deformational framework for rocks in the area. Southern Liverpool Land is divided by the Gubbedalen Shear Zone, a greenschist-facies, ~500 m thick, N-dipping high-strain zone with a polyphase history, including tops-south (contraction) as well as tops-north (extension) displacement (discovered and documented in this study). The hanging wall to the north

is characterized by the Krummedal Sequence, which is intruded by the Caledonian, Silurian Hurry Inlet Granite and Hodal-Storefjord Monzodiorite plutons. The Krummedal Sequence and Monzodiorite unit are intruded by several north-south striking lamprophyre dikes that are herein dated to 262 and 264 Ma by $^{40}\text{Ar}/^{39}\text{Ar}$ methods performed on crystals of phlogopite.

The footwall block of the Gubbedalen Shear Zone is characterized by a migmatitic orthogneiss basement complex, with felsic and mafic phases. Included within the felsic orthogneiss are eclogites, garnet-pyroxenites, amphibolites, and ultramafic bodies. These mafic bodies occur as boudins and pods wrapped by crystal-plastic mylonites that overprint the gneissosity in the country rocks. Peak temperature and pressure conditions of eclogitization are herein constrained by geothermobarometry on minerals forming the eclogite-facies assemblage (i.e., garnet and omphacite), and are $\sim 867^\circ\text{C}$ and a minimum pressure of 18.2 kbars. Cutting across all lithologies in the footwall is a stockwork of granitic veins and dikes.

Similarities between the orthogneiss complex of the footwall block and parts of the Western Gneiss Region in Norway imply that the footwall block may in fact be an orphaned crustal slice from the Baltic craton. This interpretation explains how the eclogites of southern Liverpool Land occur within the supposed upper plate of the Caledonian collisional event.

ACKNOWLEDGEMENTS

The author thanks the Geological Society of America for the financial support of this work. Many thanks are also extended to Dr. Muriel Erambert, University of Oslo, for her knowledge and guidance while performing microprobe analysis; Dr. David Moecher, University of Kentucky, for his knowledge of high pressure rocks and microprobe analysis and for conducting detailed mineral element mapping; Dr. Willis Hames, Auburn University, for use of his lab, ANIMAL, and for many discussions on mineral chemistry; Lars Eivind Augland and Dannena Bowman, for helping to unravel the complicated history of Liverpool Land; Per Inge Myhre, for helping us set up and run base camp in East Greenland; and Dr. Arild Andresen, University of Oslo, for being himself and everything that entails.

Style manual used: United States Geological Survey Suggestions to Authors – 6th Edition

Computer software used: Microsoft Word 2003, Microsoft Excel 2003, Microsoft Powerpoint 2003, Adobe Photoshop, Isoplot, Corel Designer 12

TABLE OF CONTENTS

LIST OF FIGURES	xi
LIST OF TABLES	xvi
I. INTRODUCTION	1
General Geology of East Greenland	1
Introduction to the Problem	4
Thesis Objectives and Methods of Investigation	7
II. GEOLOGY OF SOUTHERN LIVERPOOL LAND	9
General Statement	9
Northern Hanging Wall Block	11
Southern Footwall Block	13
Gubbedalen Shear Zone	25
III. PETROLOGY AND PETROGRAPHY OF ECLOGITES	34
Petrography	34
Mineral Chemistry	37
Geothermobarometry	40
Thermometry Calculations	40
Barometry Calculations	43
Results	44
IV. $^{40}\text{Ar}/^{39}\text{Ar}$ GEOCHRONOLOGY OF LAMPROPHYRE DIKES	46
Petrography	46
$^{40}\text{Ar}/^{39}\text{Ar}$ Methods	48
$^{40}\text{Ar}/^{39}\text{Ar}$ Results	48
V. DISCUSSION	52
Alternate Explanation of Liverpool Land Eclogites	58
VI. CONCLUSIONS	62
REFERENCES CITED	65
APPENDIX A	70

APPENDIX B	80
APPENDIX C	98

LIST OF FIGURES

- Figure 1. Map showing the extent of the Caledonian-Appalachian mountain belt (blue areas). The yellow-orange areas represent basement shield rocks (Stampfli, 2004) 2
- Figure 2. Cartoon representing the subduction of Baltica beneath the Laurentian margin (modified from H. Fossen, personal communication to Steltenpohl, 2005) 2
- Figure 3. Geologic map of the East Greenland Caledonides, showing the major rock units and fault structure (Modified after Mandler and Jokat, 1998). Black rectangle outlines the area of the Liverpool Land geologic map shown in Figure 4. Cross section along red line is illustrated in color beneath the geologic map (Henricksen et al., 2000) 3
- Figure 4. Geologic map of the central portion of Liverpool Land East Greenland with northern and southern field areas outlined with black boxes (Modified from Friderichsen and Surlyk, 1976) 5
- Figure 5. Images of rocks from the hanging wall of the Gubbedalen Shear Zone. A. Krummedal Sequence showing weak gneissic foliation with a metasedimentary biotite schist inclusion. B. Boulder of Hurry Inlet Granite showing lighter felsic injections into a mafic-rich phase with inclusion of coarse grained granite in the top of boulder. C. Photomicrograph in cross polars of Hodal-Storefjord Monzodiorite showing little internal deformation. D. Lamprophyre dike located within the northern field area. Notice the inclusions of country wall rock within the dike. E. Phlogopite and plagioclase phenocrysts contained within the lamprophyre dike. F. Dolerite dike intruding the Hodal-Storefjord Monzodiorite with contact metamorphic areoles. Notice fining (darkening) of igneous fabric in the dolerite as the contact (in red) is approached 12
- Figure 6. General geologic map of the southern field area depicting the location of the Gubbedalen Shear Zone. Refer to Figure 4 for location of the field area within Liverpool Land. Contour lines are represented as dashed lines (contour interval = 100 meters). Blue lines represent rivers and streams. Blue closed polygons represent lakes. A to A' indicates the location of the cross section produced in Figure 16B 14
- Figure 7. Rocks within the footwall of the Gubbedalen Shear Zone. A. Mafic orthogneiss near the bottom of the shear zone. Note the sheared felsic stringers of

quartz and feldspar, sigma clasts indicating tops right in the photo, S_2 mylonitic foliation parallels pencil. B. Photomicrograph in plane light of mafic orthogneiss showing S_0 gneissic foliation composed of alternating biotite layers with quartz-feldspar layers. C. Felsic orthogneiss preserving S_0 gneissic foliation (looking perpendicular to foliation). D. Photomicrograph in plane light of felsic orthogneiss showing S_0 gneissic foliation composed of less mafic alternating biotite and hornblende layers with quartz-feldspar layers. E. Highly folded and sheared felsic migmatite. F. Blebby migmatite gneiss with stretched cigar shaped neosomes (looking to the north, parallel to lineation). Note the migmatite foliation S_1 sheared into a tops-left mylonitic shear zone in the top of the image. 15

Figure 8. Geologic map illustrating S_0/S_1 foliation planes measured in the southern field area. Inset is a lower hemisphere stereographic projection of poles to S_0/S_1 ; $n = 22$ 17

Figure 9. Geologic map illustrating L_0/L_1 lineations measured in the southern field area. Inset is a lower hemisphere stereographic projection of L_0/L_1 lineations; $n = 11$ 19

Figure 10. Field images of eclogites and related mylonites within the footwall of the Gubbedalen Shear Zone. A. Boudinaged eclogite pod within the felsic orthogneiss. Note the mylonitization (S_2) of the migmatite around the boudin and the presence of felsic veins interpreted to be decompressional melts. B. Eclogite CP-52A with garnet-rich layers (S_2 , eclogite-facies compositional layering) and felsic decompressional melt veins with large amphibole crystals 20

Figure 11. A. View of a sigmoidal shaped crystal-plastic mylonite wrapping over the top of a small mafic boudin (backpack for scale). B. Line drawing of a mylonite sheathed boudin in A. Solid lines represent mineral elongation lineation and dashed lines represent the vertical joint faces. C. Mylonite (looking perpendicular to foliation and parallel to lineation) from vertical face of a boudin sheathing a mafic lens with large (2.5 cm) potassium feldspar sigma clasts entrained and rotated with tops-right movement. D. Stereogram of data for outcrop shown in A, B, and C, with S_2 mylonitic foliation in blue and L_2 mineral elongation lineation in black. E. Photomicrograph in cross polarized light of a mylonite wrapping an eclogite boudin. S-C fabric is preserved indicating dextral movement. The shear fabric has been mostly recrystallized and annealed. F. Photomicrograph of myrmekite grains found throughout the boudin wrapping mylonites 22

Figure 12. Geologic map illustrating S_2 and S_3/S_4 foliation planes measured in the southern field area. Inset is a lower hemisphere stereographic projection of poles to foliation planes. A. S_3/S_4 foliations within the Gubbedalen Shear Zone; $n = 24$. Dashed red line is an average S_0/S_1 foliation plane. Small circle fit through data

(red partial circle) indicates a cone axis at N32°W, 25°W. B. S₂ foliations of mylonite shear zones associated with eclogite boudins and “rogue” shears; n = 14. 23

Figure 13. Geologic map illustrating L₂ and L₃/L₄ lineations. Inset is a lower hemisphere stereographic projection of elongation lineations. A. L₃/L₄ lineations within the Gubbedalen Shear Zone; n = 34. Dashed red line is an average S₀/S₁ foliation plane. B. L₂ lineations of shear zones associated with eclogite boudins and “rogue” shears; n = 25. Small circle fit through data (red circle) indicates a cone axis at N27°W, 19°NW 24

Figure 14. Images and photomicrographs of the contractional lower part of the Gubbedalen Shear Zone. All photos perpendicular to foliation and parallel to lineation. A. Mylonitized migmatitic gneiss and syntectonic granite found within the lower part of the shear zone . B. Mafic-rich ultramylonites with feldspar sigma clasts indicating tops-right (south) thrust movement. C. Ultramylonite (S₃) cutting across a mylonitized migmatite (S₂), documenting tops-right (south) thrust movement. D. Photomicrograph in cross polarized light from granitic mylonite in image A. Micafish and sigma clasts indicate dextral (tops-up and south) reverse slip movement. Note quartz has subgrains and the shear fabric is dynamically recrystallized. E. Photomicrograph in cross polars from same thin section as D showing a dextral quartz and feldspar aggregate sigma clast 27

Figure 15. Studies from the extensional overprint in the upper parts of the Gubbedalen Shear Zone. A. Ultramylonitic extensional shear zone (S₄) cutting across and retrograding the prior contractional mylonitic fabric (S₃). B. S₄ extensional shear zone cutting a granitic injection. C. Reverse-slip crenulations documenting tops-down-to-the left (north) extension. D. Carbonate breccia zone at the northern margin of the shear zone in contact with the Hurry Inlet Granite. E. Photomicrograph in plane light of extensional overprint upon the S₃ mylonitic fabric. Note the microfolds within the quartz ribbons, and C’ shear bands. F. Photomicrograph in cross polarized light of dextral mica fish. Polycrystalline quartz ribbons contain sugbrains and recrystallized grain shape preferred orientation documenting sinistral extensional shear 29

Figure 16. A. Photo mosaic of the Gubbedalen Shear Zone (outlined in red) looking to the east along a valley wall. Extensional and contractional zones are separated by the blue line. B. Schematic cross section from A to A’ of the Gubbedalen Shear Zone and surrounding terranes (location of cross section marked in Figure 6). Shear couples within the shear zone represent the direction of shear. Straight lines represent the mylonitic foliation and wavy lines represent the migmatitic foliation. C. Felsic dikes within the bottom of the shear zone (looking north) pulled into parallelism with the shear zone’s foliation. D. Unaffected felsic dikes from a canyon wall (looking east) well south of the shear zone 31

Figure 17. A. Stereographic projection of poles to planes from all foliation data (S_0 , S_1 , S_2 , S_3 , and S_4) collected in the southern field area. B. Stereographic projection of all lineations (L_0 , L_1 , L_2 , L_3 , and L_4) collected in the southern field area (n equals the number of measurements) 33

Figure 18. Simplified geologic map showing the location of eclogite samples that were petrographically and chemically analyzed (CP-47: 70° 34.937'N, 22° 13.770'W; CP-52A: 70° 34.633'N, 22° 15.220'W; and CP-92: 70° 35.362'N, 22° 12.106'W) 35

Figure 19. A. Eclogite CP-52A in plane light, notice the thin rim of retrograde hornblende growing on the omphacite grain. B. Eclogite CP-92 in plane light with fine-grained lamellar plagioclase-clinopyroxene-hornblende symplectites. C. Zoomed in Back Scatter Electron image of the area depicted in B. D. Eclogite CP-47 in plane light showing coarse grained wormy plagioclase-clinopyroxene-hornblende symplectites. E. Back Scatter Electron image of sample CP-47 (field of view is ~1 cm). F. Quartz exsolution rods within remnant omphacite grain and small low-sodium clinopyroxene nucleating in plagioclase within sample CP-47 in plane light. Abbreviations used in figure. Grt = Garnet, Cpx = low-Na clinopyroxene, Qtz = quartz, Plag = Plagioclase, Zr = Zircon, Omp = Omphacite, Hbl = Hornblende 36

Figure 20. End member compositions of analyzed garnet grains from eclogite samples displayed on a ternary diagram (after Coleman et al., 1965) 39

Figure 21. End member compositions of analyzed clinopyroxene grains from eclogite samples displayed on a ternary diagram (after Morimoto et al., 1988) 41

Figure 22. Element maps of calcium (left) and sodium (right) of eclogite CP-52A, with lighter colors being more enriched in the element. The central grain is an omphacite with a garnet grain to the top left of each image. Notice the fine grained symplectite that is forming along some fractures within the omphacite. Image is approximately 1 cm 42

Figure 23. End member compositions of analyzed amphibole grains from eclogite samples on a Silicon versus Na+K diagram (after Deer et al., 1992) 42

Figure 24. A. Photomicrograph in plane light from sample M-14C of euhedral phlogopite and plagioclase phenocrysts within a matrix of phlogopite, plagioclase, and opaques (in images Phl = phlogopite and Plag = plagioclase). B. Optically zoned plagioclase phenocryst within M-14C (cross-polarized light). Steel blue birefringence of the plagioclase is believed to be a result of the thin section being slightly too thick. C. Phlogopite and plagioclase phenocrysts within M-21 (plane light). Note the radiogenic halo within the tan-brown phlogopite grain in contact with matrix feldspar (lower right) 47

Figure 25. Plateau diagram produced from the incremental heating data collected from sample M-14C. Inset. Probability density diagram created from the SCTF data from sample M-14C. Individual crystal data represented as points with error bars (error bars are 1σ). Prob. = the probability that the SCTF data could be part of a normal distribution	49
Figure 26. Plateau diagram produced from the incremental heating data collected from sample M-21. Inset. Probability density diagram created from the SCTF data from sample M-21. Individual crystal data represented as points with error bars (error bars are 1σ). Prob. = the probability that the SCTF data could be part of a normal distribution	50
Figure 27. A. Subduction of the Baltic lithospheric slab underneath Laurentia during continental subduction. B. Failure of the crust after reaching eclogite-facies conditions, resulting in the uplift of a crustal slice (orthogneiss footwall terrane), creating a sense of normal movement along the contact with the overriding plate. X's represent brittle faulting occurring in the overriding Laurentian crust. C. Continued uplift of the crustal slice to shallow crustal levels (modified from Chemenda et al., 1995)	54
Figure 28. Devonian detachment faults within the East Greenland and Scandinavian Caledonides (Ebbing et al., 2006)	57
Figure 29. Paleogeographic plate reconstruction during the Permian (~260 Ma) showing the Liverpool Land region (red star) against Lofoten, Norway (blue star) (Blakey, 2007)	59
Figure 30. A and B. Location of the Lofoten Islands of northern Norway (Steltenpohl et al., 2004). C. Probability density diagram with hydrothermal muscovite age from Lofoten fault zone in black (data from Steltenpohl et al., 2004) and phlogopite crystallization age from Liverpool Land lamprophyres in blue and red. D. Diagram depicting the Permian metamorphic core complex of Lofoten (Steltenpohl et al., 2004)	60

LIST OF TABLES

Table 1. Metamorphic and structural history of Liverpool Land comparing hanging wall and footwall blocks to the Gubbedalen Shear Zone (¹ This study; ² Bowman, 2008; ³ Augland, 2007; ⁴ personal communication to Augland, 2008; ⁵ Strachan et al., 1995; ⁶ Kalsbeek et al., 1998)	10
Table 2. Table contains averaged weight percent oxides from multiple (n = number) microprobe analyses of garnet, pyroxene, plagioclase, and amphibole	38
Table 3. Summary table of geothermobarometric calculations.	45

I. INTRODUCTION

General Geology of East Greenland

The Caledonian mountain belt is the northern most continuation of the Appalachian mountain belt that stretches over 10,000 kilometers and represents the suturing together of the Pangaeon supercontinent (Figure 1). This study focuses on East Greenland, which comprises the western side of the Caledonian collisional mountain belt; the eastern side of the mountain belt lies in Norway, Sweden, and the United Kingdom. The East Greenland Caledonides are dominated by Precambrian and Paleozoic metamorphic rocks that average ~300 kilometers wide and extend for 1,400 kilometers between 70° - 82° N and 20° - 30° W, roughly parallel to the coast (Haller, 1971).

The classic model for the formation of the Caledonian orogen evokes the Silurian collision and partial subduction of the Baltic craton beneath the Laurentian craton (Figure 2). The polarity of the collisional zone is documented by a Caledonian-aged calc-alkaline plutonic arc in East Greenland and high pressure and ultra-high pressure eclogites exposed in the Western Gneiss Region of coastal Norway (Hodges et al., 1982). The collision emplaced a westward-verging thrust complex upon the ancient Laurentian margin (Figures 2 and 3). “Thick-skinned” west-directed thrusting in coastal areas of East Greenland grade into multiple “thin-skinned” fold and thrust belts farther west into the foreland (Higgins and Leslie, 2000). A mirror image east-verging fold and thrust belt is seen in the Scandinavian Caledonides (Figure 2; Roberts and Gee, 1985).

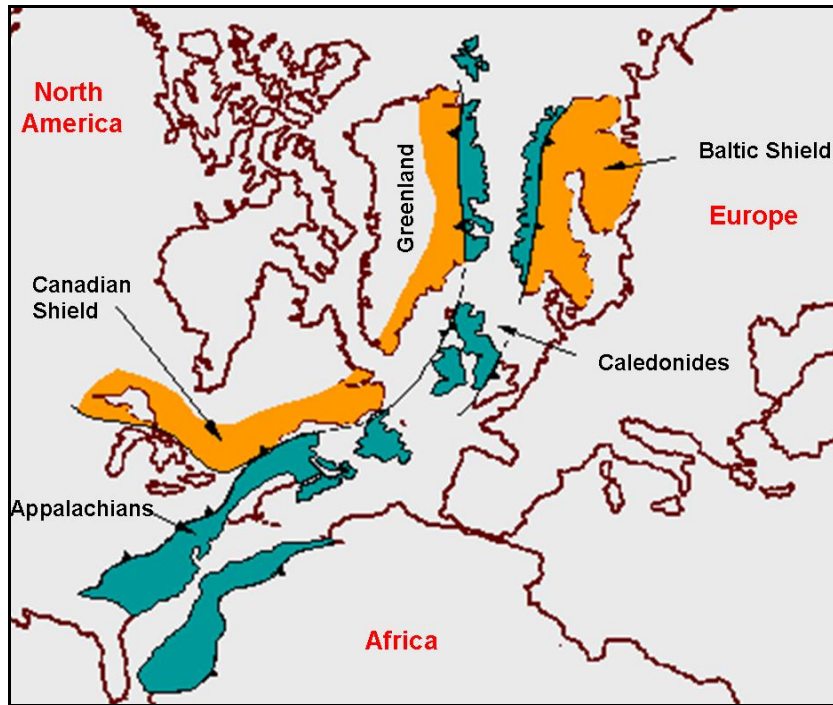


Figure 1. Map showing the extent of the Caledonian-Appalachian mountain belt (blue areas). The yellow-orange areas represent basement shield rocks (Stampfli, 2004).

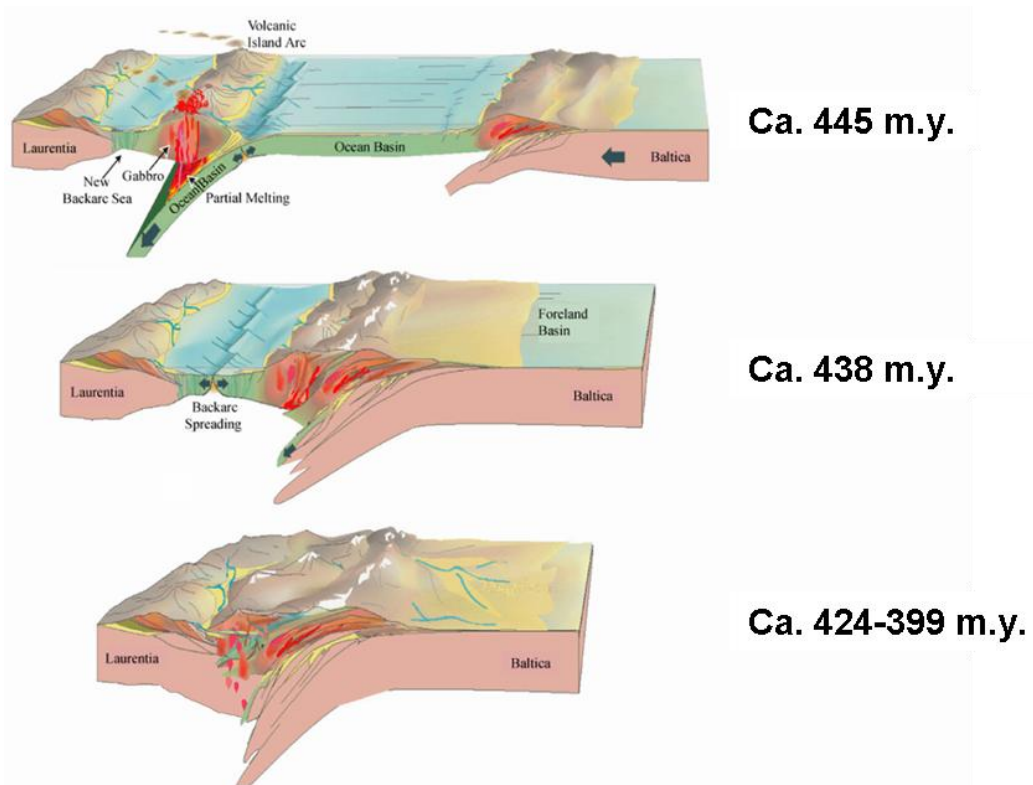


Figure 2. Cartoon representing the subduction of Baltica beneath the Laurentian margin (modified from H. Fossen, personal communication to Steltenpohl, 2005).

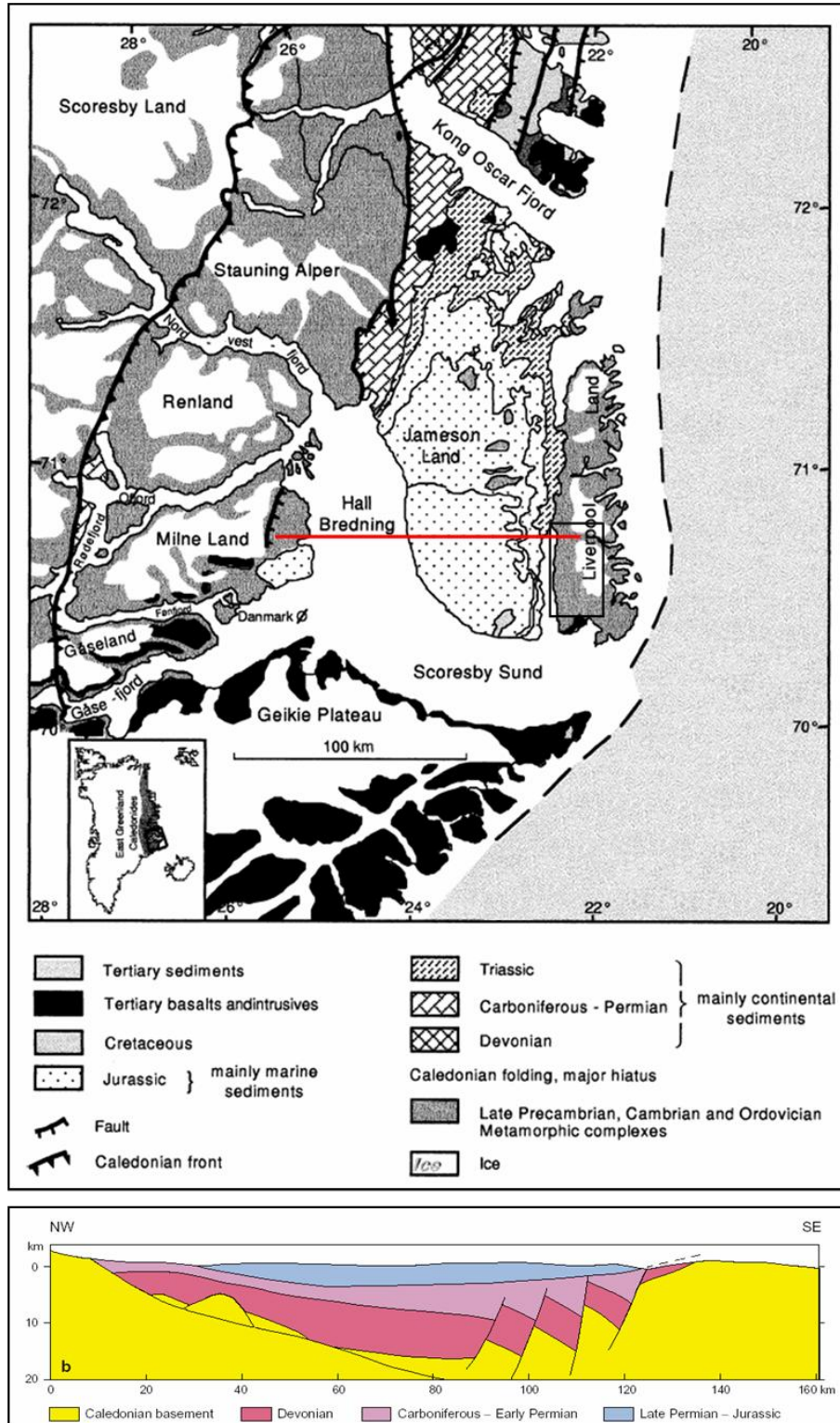


Figure 3. Geologic map of the East Greenland Caledonides, showing the major rock units and fault structures (modified from Mandler and Jokat, 1998). Black rectangle outlines the area of the Liverpool Land geologic map shown in Figure 4. Cross section along red line is illustrated in color beneath the geologic map (Henricksen et al., 2000).

Introduction to the Problem

Liverpool Land is a horst-block (Figure 3) of Archean-Caledonian crystalline basement that is intruded by Caledonian plutons (Figure 4). Eclogites have been known to exist within the crystalline basement of Liverpool Land since the 1930's (Kranck, 1935; Sahlstein, 1935). Eclogites are high temperature and (ultra-) high pressure metamorphic rocks formed under extreme crustal conditions, and are vital indicators of plate tectonic processes. Classically, eclogite formation is predicted to occur within the subducting crustal slab. Contrary to this prediction however, Liverpool Land eclogites occur within the supposed upper plate (Laurentian) of the collisional zone, posing a problem to the model of wholesale asymmetric subduction of Baltica beneath Laurentia.

The Liverpool Land eclogites were recently "rediscovered" using more modern analytical techniques, but all that is published is an abstract by Hartz et al. (2005). Hartz et al. (2005) report a ~395 Ma date on zircons from a Liverpool Land eclogite, using U-Pb TIMS analysis. Likewise, Hartz et al. (2005) report that these eclogites were formed under ultra-high pressure (~850°C and >25kbars). The presence of Caledonian (~395 Ma) eclogites poses another geologic problem in that an adjacent Caledonian granitic pluton imprecisely dated to ~435 Ma (Hansen and Steiger, 1971; Coe and Cheney, 1972; Coe, 1975) completely escaped the eclogite-facies metamorphism. The goal of present thesis research is to unravel the tectonic evolution of southern Liverpool Land in an attempt to explain the presence of Caledonian eclogites, possibly ultra-high pressure ones, within the supposed upper plate of the collisional orogen, and to reconcile the boundary between the eclogite-bearing basement terrane and its adjacent terrane containing earlier intruded and unmetamorphosed Caledonian plutons.

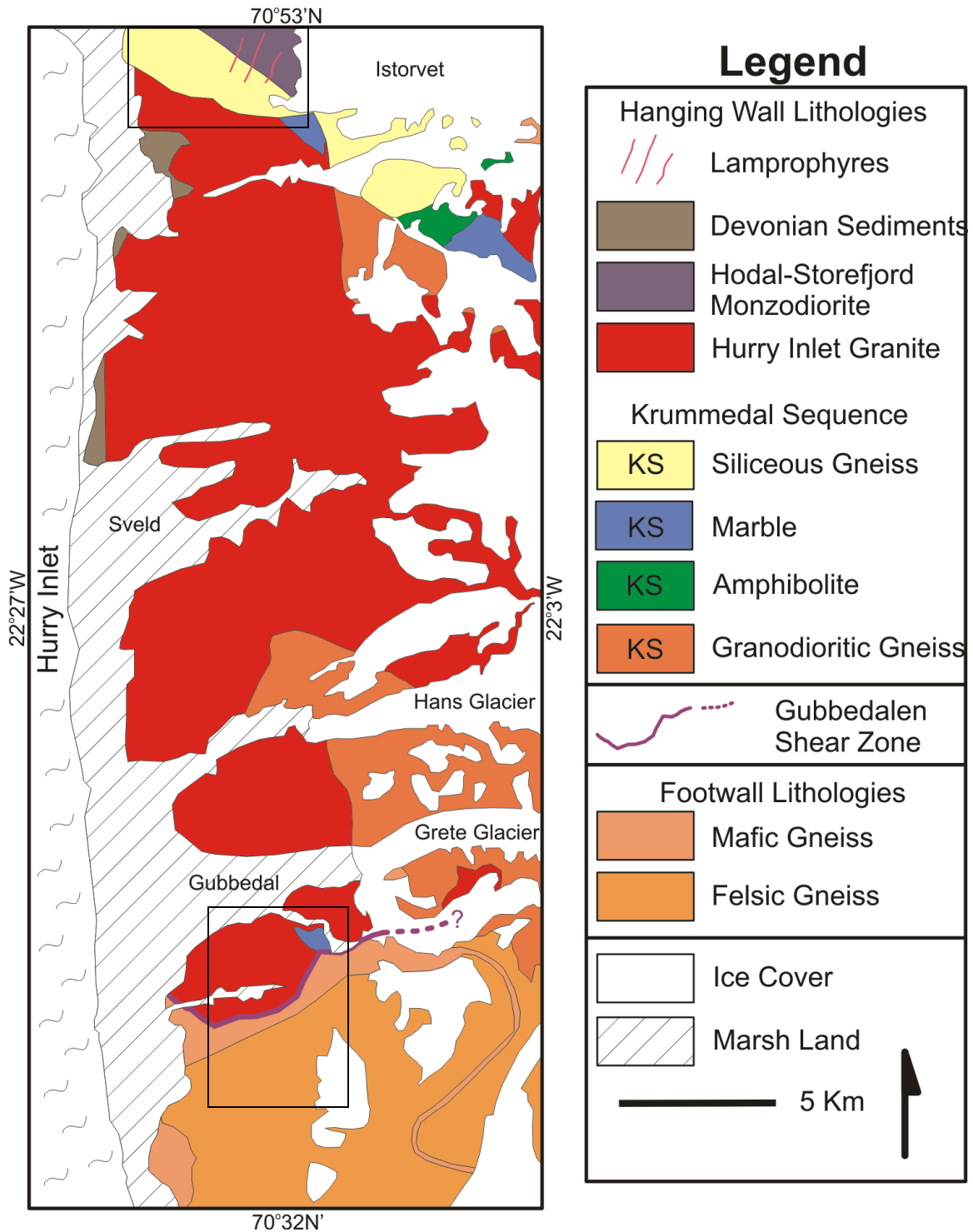


Figure 4. Geologic map of the central portion of Liverpool Land East Greenland with northern and southern field areas outlined with black boxes (modified from Friderichsen and Surlyk, 1976).

In the summer of 2006, field work was focused on two areas within Liverpool Land (Figure 4). The individual objectives for the two field areas varied and more field time was allotted to the southern one. The southern field area, containing the Gubbedalen Shear Zone, was the center of attention for my thesis study and geologic mapping and structural analysis was focused there. The goals for field work in the northern area were to understand the intrusive relationships and to characterize the lamprophyre dikes present in that area.

Field investigations in Liverpool Land were performed in conjunction with a research expedition from the University of Oslo, Norway. The research team consisted of three Auburn University participants, Wesley Buchanan, Dannena Bowman, and Dr. Mark Steltenpohl, and three University of Oslo workers, Lars Eivind Augland, Per Inge Myhre, and Dr. Arild Andresen. Field and laboratory studies were divided among the three Master's candidates, in an effort to piece together the tectonic evolution of the area. As part of the expedition, I was charged to characterize the structural and kinematic relationships of the different lithologic units and combine these observations with previous work to define the deformation sequence for southern Liverpool Land. I was also charged with the petrology and petrography of the eclogites and lamprophyre dikes. Dannena Bowman was responsible for petrographically describing the country rocks of the terrane and performing $^{40}\text{Ar}/^{39}\text{Ar}$ thermochronology to constrain their cooling history (Bowman, 2008). Lars Eivind Augland was charged with conducting U-Pb isotopic studies to determine the absolute ages of igneous crystallization and eclogitization (Augland, 2007).

Thesis Objectives and Methods of Investigation

Five objectives of the present investigation needed to resolve the tectonic evolution of Liverpool Land are as follows: (1) to map and describe the lithologies and structures within the region; (2) to characterize the structural framework of the eclogites; (3) to estimate the pressure and temperature of eclogitization; (4) to constrain the timing of the lamprophyre dikes; and (5) to synthesize the results and incorporate them with those of the 2006 expedition colleagues to develop a tectonic model for the region.

Standard structural mapping techniques were used in the field to characterize the kinematic and geometric relationships of lithologic units. A Brunton compass was used to obtain attitudes of pertinent rock features (i.e., foliation planes and lineations). The structural data was analyzed using lower-hemisphere stereographic projection software to characterize meso- and macroscopic relationships.

Rock samples were collected from eclogites, lamprophyres, and mylonites for laboratory analysis. Sample locations were recorded with a handheld GPS unit. Polished thin sections of eclogite samples and standard thin sections of lamprophyre samples were commercially made. Oriented samples of mylonites were collected and thin sections commercially made in order to determine the kinematics of the samples. Using petrographic microscopes at Auburn University, mineralogical, textural, kinematic, and microstructural analyses were performed to characterize the metamorphic and structural framework of the field area.

Microprobe analysis was performed on eclogite samples using the facilities at the University of Oslo under the direct supervision of Dr. Muriel Erambert, an expert on Caledonian eclogites. Further microprobe analysis was performed using the facilities at

the University of Kentucky, with the guidance of Dr. David Moecher. The chemical compositions of garnet, pyroxene, plagioclase, and amphibole were determined using Wavelength-Dispersive System (WDS) analysis. Other previously unknown minerals were identified using Energy-Dispersive System (EDS) analysis. The wavelength-dispersive system analyses were used to quantify the temperature and pressure of eclogite formation, using elemental partitioning geothermobarometry and Excel® worksheets developed by the author. Phlogopite grains were separated from lamprophyre dikes and dated using $^{40}\text{Ar}/^{39}\text{Ar}$ techniques in the Auburn Noble Isotope Mass Analysis Laboratory (ANIMAL), under the supervision of Dr. Willis Hames.

II. GEOLOGY OF SOUTHERN LIVERPOOL LAND

General Statement

Field investigations conducted in 2006, revealed the presence of a major east-west trending, north-dipping ductile shear zone bisecting southern Liverpool Land, hereafter named the Gubbedalen Shear Zone (Figure 4; Buchanan et al., 2007). This shear zone juxtaposes two vastly distinct terranes both in terms of lithology and their structural and metamorphic development. The hanging wall (Figure 4) is characterized by a partially migmatized metasedimentary package (i.e., Krummedal Sequence) and several Caledonian plutons (i.e., Hurry Inlet Granite and Hodal-Storefjord Monzodiorite). The Caledonian plutons are in contact with the shear zone and are mostly undeformed except where the margin of the shear zone is approached.

The footwall block (Figure 4) to the south is a highly deformed basement orthogneiss complex that contains the eclogites reported by Hartz et al. (2005). Rocks contained within the footwall block record peak and retrograde metamorphic events. An eclogite and granulite-facies event is recorded within the rarely preserved boudinaged eclogites. Amphibolite-facies metamorphic minerals and textures are clearly retrograde within the eclogites, and although it is less obvious in their encapsulating orthogneisses, the latter must have followed the same metamorphic path. Table 1 contains an outline of the structural and metamorphic history of Liverpool Land developed from the results of the 2006 expedition and provides the context of the structural nomenclature used.

Hanging Wall Block	Age	Footwall Block
Dolerite dikes and flood basalts	65 Ma	Dolerite dikes and flood basalts
Sedimentation in Jameson Land	Jurassic and Triassic	Sedimentation in Jameson Land
Intrusion of lamprophyre dikes	262, 264 Ma ¹	
Devonian sediments deposited on top of the Hurry Inlet Granite	380-350 Ma	
D ₄ – Extensional Gubbedalen Shear Zone dated by ⁴⁰ Ar/ ³⁹ Ar – S ₄ mylonites extend and cut S ₃ – Formation of L ₄ mineral elongation lineation	380 Ma ²	D ₄ – Extensional Gubbedalen Shear Zone dated by ⁴⁰ Ar/ ³⁹ Ar – S ₄ mylonites extend and cut S ₃ – Formation of L ₄ mineral elongation lineation
D ₃ – Contractional Gubbedalen Shear Zone dated by syntectonic granitic dikes – S ₃ mylonitic foliation cuts S ₁ and S ₂ – Formation of L ₃ mineral stretching lineation	386 Ma ³	D ₃ – Contractional Gubbedalen Shear Zone dated by syntectonic granitic dikes – S ₃ mylonitic foliation cuts S ₁ and S ₂ – Formation of L ₃ mineral stretching lineation
Joining of the hanging wall and footwall blocks along the Gubbedalen Shear Zone		
	388 Ma ³	Late D ₂ – Amphibolite-facies retrogression - Formation of S ₂ shear zones around boudins, rogue shears, and L ₂ mineral stretching lineations
	399-388 Ma	Middle D ₂ – Granulite-facies retrogression preserved in eclogites
	399 Ma ³	Early D ₂ – Eclogite-facies metamorphism
	400-410 Ma (Caledonian) ⁴	D ₁ – Formation of S ₁ migmatitic foliation and L ₁ constrictional neosome fold axes
Intrusion of Hodal-Storefjord Monzodiorite	424 Ma ³	
Hurry Inlet Granite magma pulses	445, 438 Ma ³	
Amphibolite-facies metamorphism of Krummedal Sequence – formation of weak gneissic foliation	950 Ma ⁵	
	1660-410 Ma (Relative)	D ₀ – Formation of S ₀ gneissic foliation and L ₀ mineral aligning lineations within the orthogneiss – Must postdate protolith emplacement and predate D ₁
Maximum age for the deposition of the Krummedal Sequence	1100 Ma ⁶	
	1660 Ma ³	Protolith age for eclogites

Table 1. Metamorphic and structural history of Liverpool Land comparing hanging wall and footwall blocks to the Gubbedalen Shear Zone (¹This study; ²Bowman, 2008; ³Augland, 2007; ⁴personal communication to Lars E. Augland, 2008; ⁵Strachan et al., 1995; ⁶Kalsbeek et al., 1998).

Northern Hanging Wall Block

The northern hanging wall block to the Gubbedalen Shear Zone is characterized by the Krummedal Sequence, a supracrustal sequence containing Grenvillian and Caledonian rocks and structures. Detrital zircon dates indicate a maximum age of deposition of 1100 Ma, with a major amphibolite-facies metamorphic event at 950 Ma (Strachan et al., 1995; Kalsbeek et al. 1998). Multiple phases of deformation and metamorphism have completely erased pre-existing sedimentary structures. The sequence is known to be roughly 5 to 10 km thick (Higgins, 1988). Compositionally the Krummedal Sequence in the northern study area is mostly a hornblende-biotite-garnet paragneiss folded together with layers of marbles, meta-psammitic rocks (Figure 5A), calc-silicates, and mafic gneisses. The Krummedal Sequence is vertically and laterally a highly variable sequence and correlation between local successions is not possible (Henriksen et al., 2000). Weak gneissic foliation planes measured within the paragneiss record a roughly northwest strike and a moderate northeast dip, and are interpreted to be of Grenvillian origin.

In the study area, the Krummedal Sequence has been intruded by two different Caledonian plutons. The Hurry Inlet Granite (Figures 4 and 5B) is a batholith sized non-deformed pluton with two magma pulses occurring at 445 Ma and 438 Ma (Augland, 2007). Sediments of Devonian age are in unconformable contact with the Hurry Inlet Granite (Figure 4). The fairly homogeneous Hodal-Storefjord Monzodiorite (Figures 4 and 5C) has been dated to 424 Ma (Augland, 2007).

Cutting across both the Krummedal Sequence and the Hodal-Storefjord Monzodiorite in the northern study area are several NNE-SSW trending, vertical

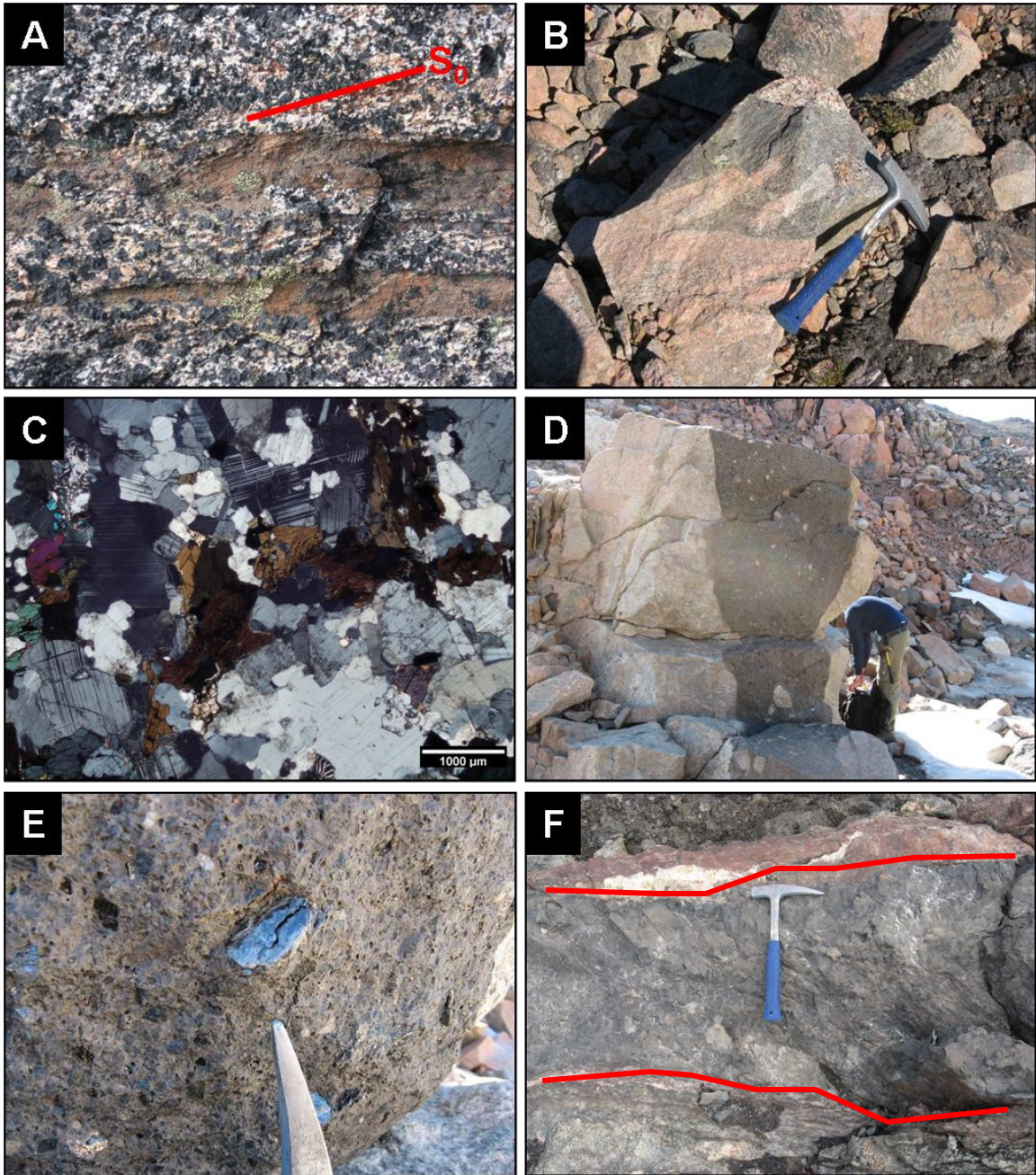


Figure 5. Images of rocks from the hanging wall of the Gubbedalen Shear Zone. **A.** Krummedal Sequence showing weak gneissic foliation with a metasedimentary biotite schist inclusion. **B.** Boulder of Hurry Inlet Granite showing lighter felsic injections into a mafic-rich phase with inclusion of coarse-grained granite in the top of boulder. **C.** Photomicrograph in cross polars of Hodal-Storefjord Monzodiorite showing little internal deformation. **D.** Lamprophyre dike located within the northern field area. Notice the inclusions of country wall rock within the dike. **E.** Phlogopite and plagioclase phenocrysts contained within the lamprophyre dike. **F.** Dolerite dike intruding the Hodal-Storefjord Monzodiorite with contact metamorphic areoles. Notice fining (darkening) of igneous fabric in the dolerite as the contact (in red) is approached.

lamprophyre dikes (Figure 4) ranging between 1 and 2 meters wide with prevalent inclusions of host wall rock (Figure 5D). The lamprophyre dikes contain phenocrysts of large (up to 3 cm across) phlogopite grains (Figure 5E). Mantle xenoliths were not observed within the dikes. Cutting the same units as the lamprophyre dikes are 1-2 meter wide dolerite dikes (Figure 5F). The dolerite dikes have contact metamorphic areoles that are 10-20 centimeters thick. These dikes are presumed to be related to Tertiary basalts and can be seen across Hurry Inlet concordantly and discordantly intruding the Jurassic sedimentary rocks of Jameson Land. Eocene flood basalts are the dominant rock unit exposed south of Liverpool Land, across Scoresby Sund (Figure 3) and are known to be related to the opening of the modern Atlantic Ocean.

Southern Footwall Block

Figure 6 is a lithologic map of the southern field area illustrating rock units of the southern footwall block to the Gubbedalen Shear Zone. A mafic gneiss unit (Figures 4, 6, 7A, and 7B) is structurally the uppermost part of the orthogneiss complex and makes up the lower region of the Gubbedalen Shear Zone. This mafic orthogneiss has a strong gneissic compositional layering (S_0) and a lineation (L_0) created by the alignment of amphibole and biotite grains (Figure 7B). A felsic orthogneiss unit (Figures 4, 6, 7C, and 7D) lies structurally below the mafic orthogneiss and is the main lithology of the gneissic complex within the southern field area.

The felsic unit has the same gneissic banding and mineral aligning lineation of the mafic unit and it carries identical fabrics and structures, indicating synchronous formation. The felsic unit's gneissosity is composed of alternating layers of quartz and

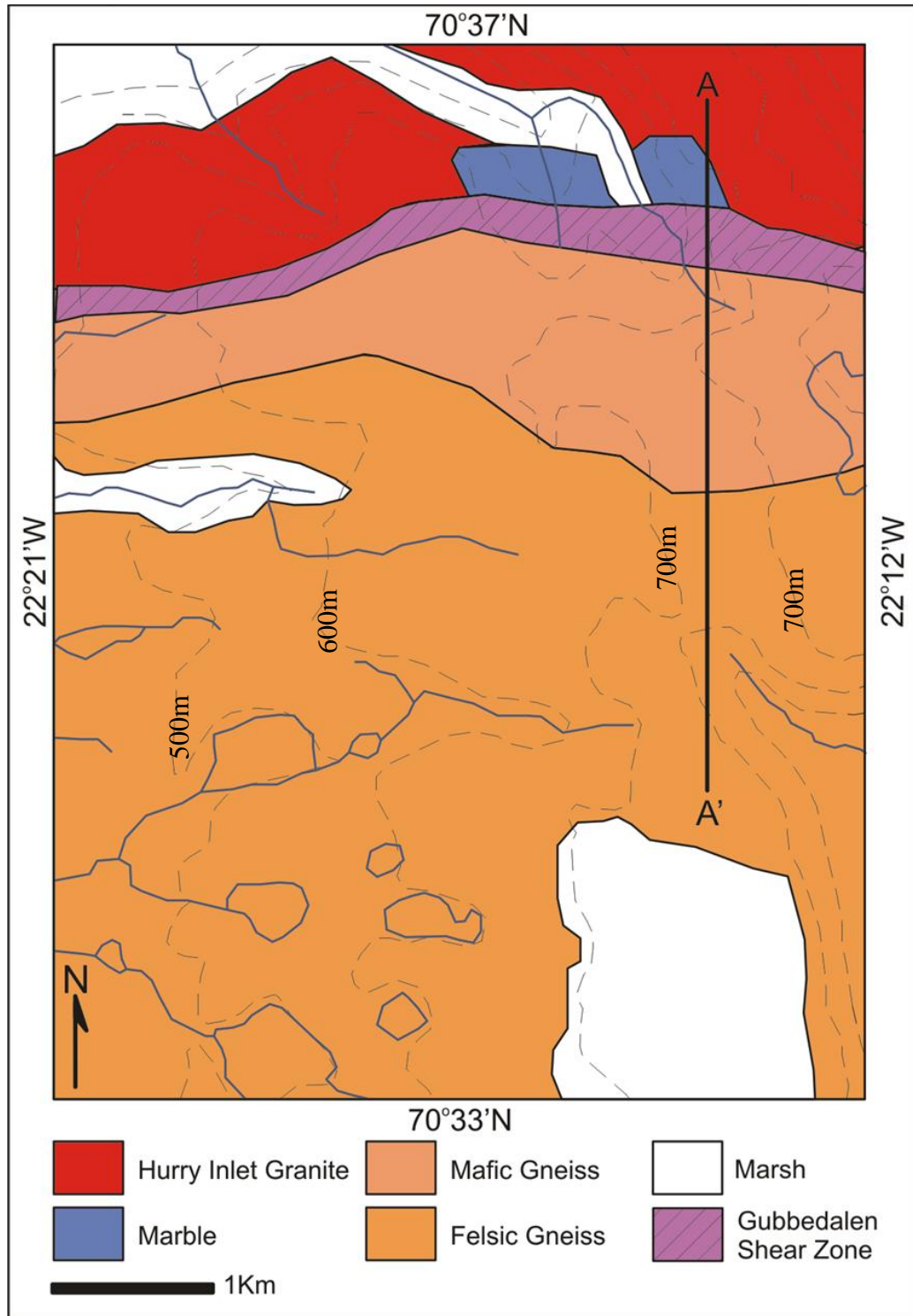


Figure 6. General geologic map of the southern field area depicting the location of the Gubbedalen Shear Zone. Refer to Figure 4 for location of the field area within Liverpool Land. Contour lines are represented as dashed lines (contour interval = 100 meters). Blue lines represent rivers and streams. Blue closed polygons represent lakes. A to A' indicates the location of the cross section produced in Figure 16B.

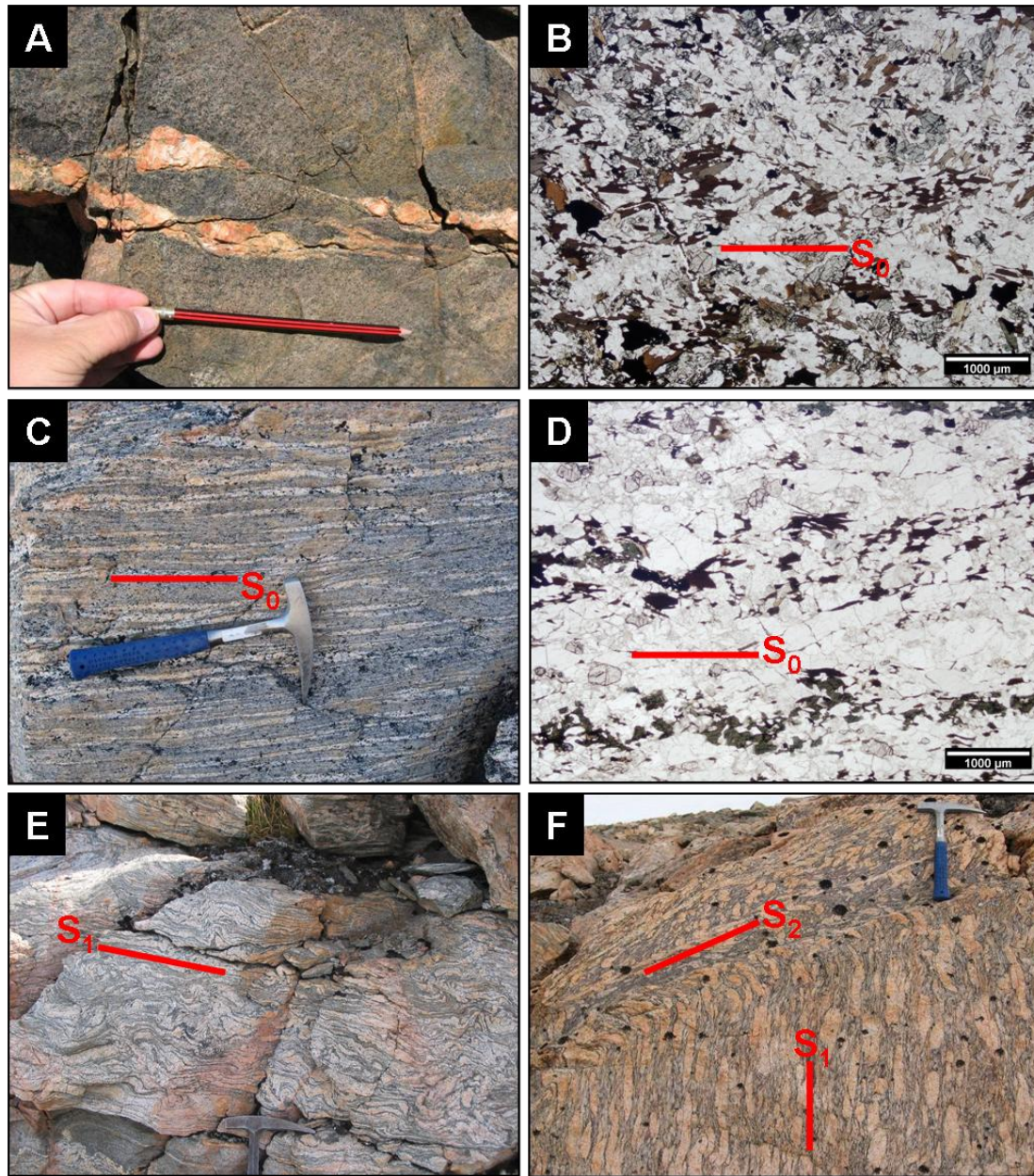


Figure 7. Rocks within the footwall of the Gubbedalen Shear Zone. **A.** Mafic orthogneiss near the bottom of the shear zone. Note the sheared felsic stringers of quartz and feldspar, sigma clasts indicating tops right in the photo, S_2 mylonitic foliation parallels pencil. **B.** Photomicrograph in plane light of mafic orthogneiss showing S_0 gneissic foliation composed of alternating biotite layers with quartz-feldspar layers. **C.** Felsic orthogneiss preserving S_0 gneissic foliation (looking perpendicular to foliation). **D.** Photomicrograph in plane light of felsic orthogneiss showing S_0 gneissic foliation composed of less mafic alternating biotite and hornblende layers with quartz-feldspar layers. **E.** Highly folded and sheared felsic migmatite. **F.** Blebby migmatite gneiss with stretched cigar shaped neosomes (looking to the north, parallel to lineation). Note the migmatite foliation S_1 sheared into a tops-left mylonitic shear zone in the top of the image.

feldspar with biotite and amphibole. Garnet is present within both light and dark layers of the felsic orthogneiss (Figure 7D). The garnet + quartz + feldspar + biotite ± amphibole mineral assemblage of the felsic orthogneiss is indicative of widespread amphibolite-facies retrograde metamorphism within rocks of the footwall to the Gubbedalen Shear Zone. Augland (2007) reports U-Pb zircon data from pegmatites, which based on field relations, he interprets to constrain the age of the amphibolite-facies retrogression to 388 Ma.

Evidence of migmatization is widespread within the felsic orthogneiss complex, although none were observed within the mafic orthogneiss (Figures 7E and 7F). Ongoing work by L. Augland (personal communication, 2008) indicates that migmatization was related to the Caledonian event as well. In some migmatites, constrictional strain has elongated the felsic neosomes into cigar-shaped ellipsoids, which are most prominently developed in areas associated with early fold axes (Figure 7F). It was not possible to confidently separate Caledonian metamorphic folia (i.e., gneissosity and schistosity), S_1 , from Precambrian folia, S_0 , and thus the author has combined them in S_0/S_1 ; likewise, mineral lineations within the orthogneiss and migmatites are combined into L_0/L_1 .

Both the mafic and felsic phases of the orthogneiss complex have been cross cut by several generations of granitic veins and dikes. These fine to coarse-grained granitic units have variable orientations and exhibit a stockwork intrusive pattern. These veins and dikes are not observed within the hanging wall block of the Gubbedalen Shear Zone.

S_0/S_1 foliations measured within rocks of the southern field area are plotted on Figure 8. The S_0/S_1 gneissic foliations are variably striking and have shallow to moderate dips. L_0/L_1 lineations have mostly north-south orientations and mostly shallow to

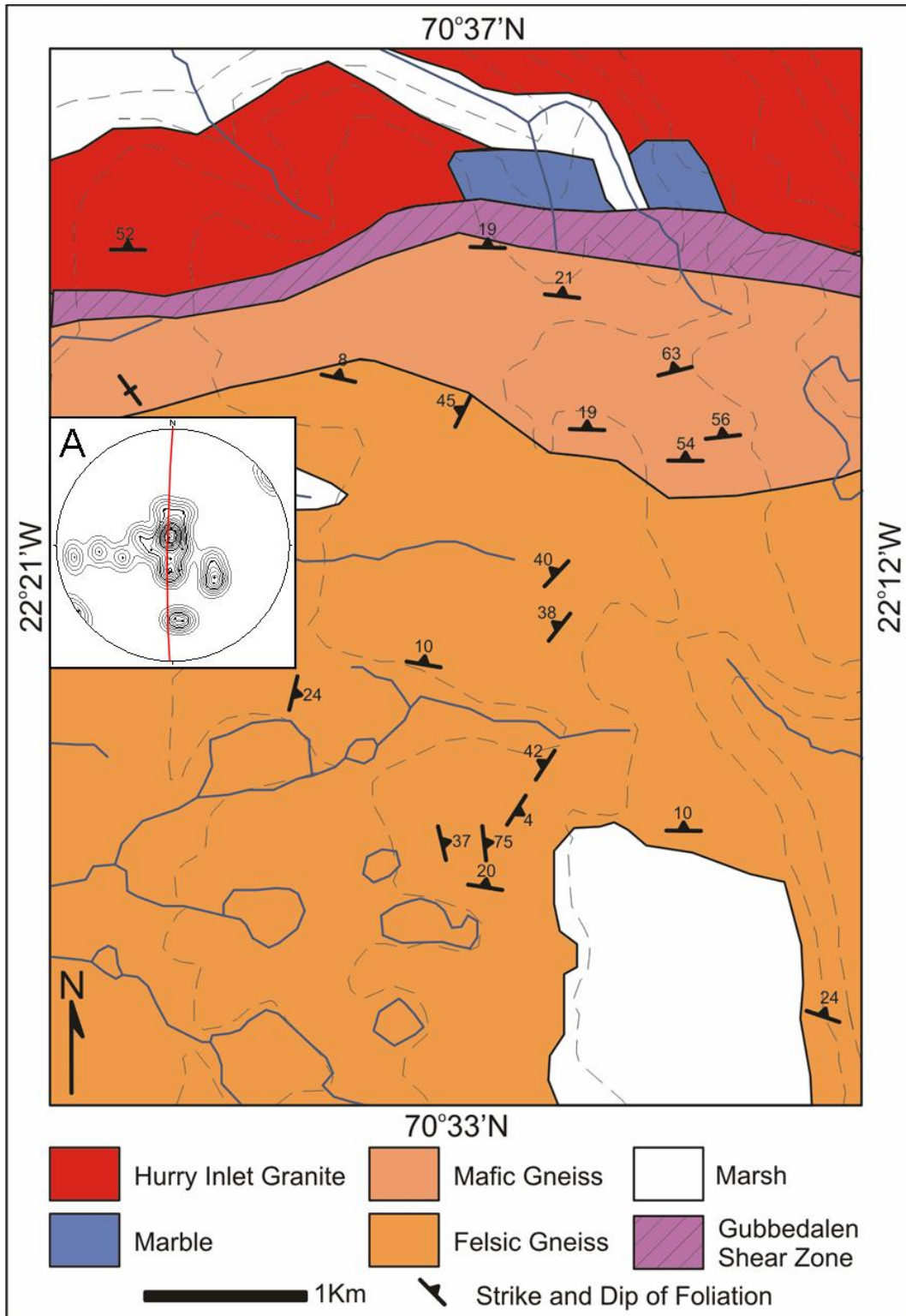


Figure 8. Geologic map illustrating S_0/S_1 foliation planes measured in the southern field area. Inset is a lower hemisphere stereographic projection of poles to S_0/S_1 ; $n = 22$.

moderate plunges (Figure 9) with a visually estimated point concentration trending due north and plunging 9°. Stereographic projections document a general domal, to weak north-south trending partial girdle pattern (Figure 8, inset) that defines a fold (β -) axis at N88°E, 5°NE; L_0/L_1 lineations lie loosely within this great circle. From the foliation and lineation maps and the stereograms, the influence of the Gubbedalen Shear Zone can be seen as all linear and planar fabrics in country rock units in the footwall block are dragged into parallelism with increasing proximity to the shear zone.

Although rare mafic and ultramafic bodies exist within the felsic gneiss complex, the main objective of the present study was to clarify the relationship between the country rock hosts and the eclogites (Figures 10A and 10B). Many small (1-5 meter) bodies of pristine and variably retrograded eclogites were observed. The eclogite pods are interpreted to have originated as mafic injections or enclaves that were incorporated into the orthogneiss complex before eclogite-facies metamorphism. The eclogite pods have been internally deformed in a brittle manner, as evidenced by fractures occurring within them (Figure 10A). Felsic melts with large (3 cm) euhedral amphibole crystals are observed filling these fracture openings, and are interpreted to be decompressional melts developed during the exhumation of the eclogites (Figures 10A and 10B).

Mylonitic shears (S_2) outside of the Gubbedalen Shear Zone and within the orthogneiss footwall block fall into two categories. The first type occur along the margins of boudinaged mafic pods whereas the second type, herein referred to as “rogue” shears, are not associated with mafic lenses at all but occur randomly throughout the footwall block. These “rogue” shears are more tabular, subhorizontal mylonitic bodies that are documented to cut S_0/S_1 foliations within both the mafic (Figure 7A) and felsic

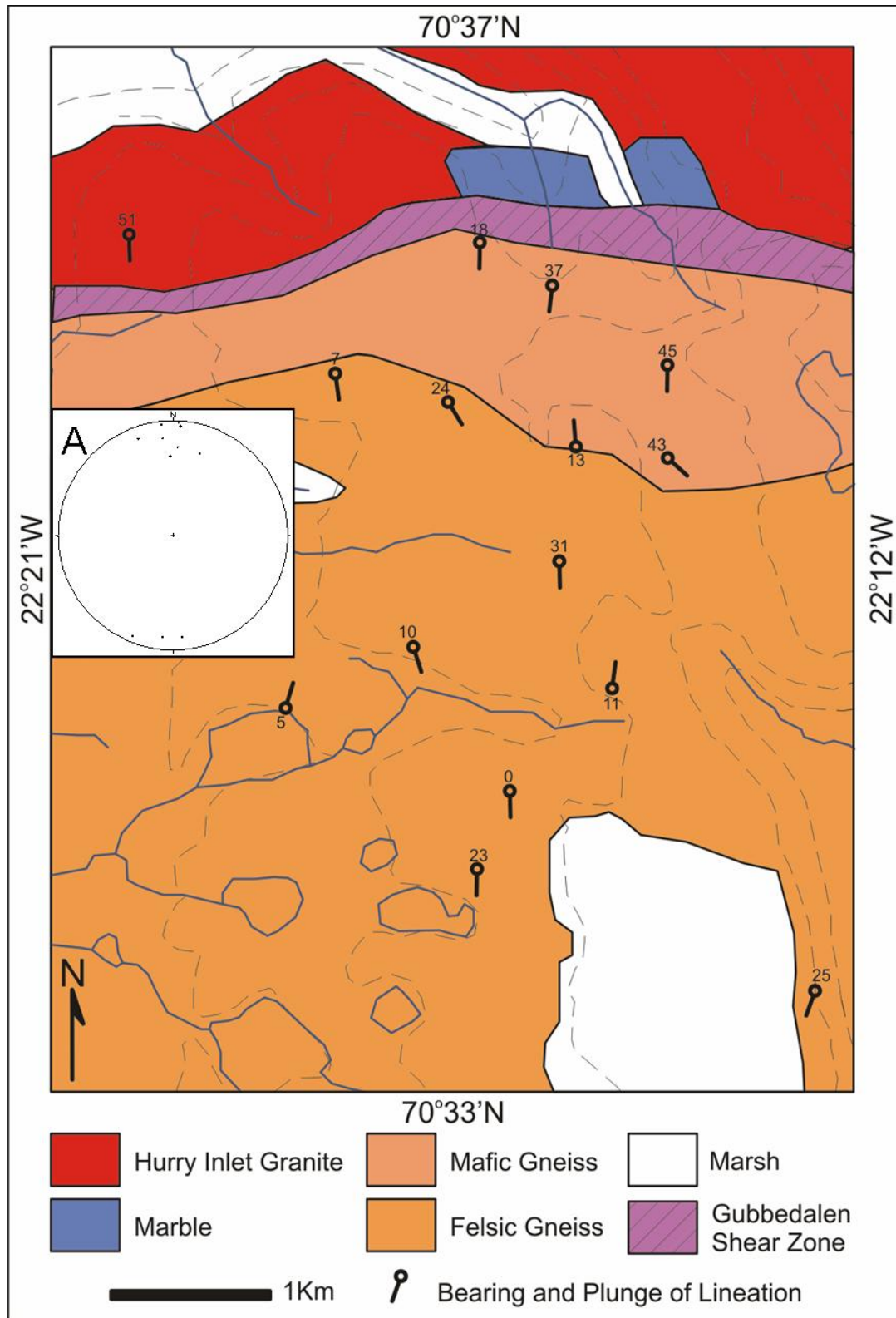


Figure 9. Geologic map illustrating L_0/L_1 lineations measured in the southern field area. Inset is a lower hemisphere stereographic projection of L_0/L_1 lineations; $n = 11$.

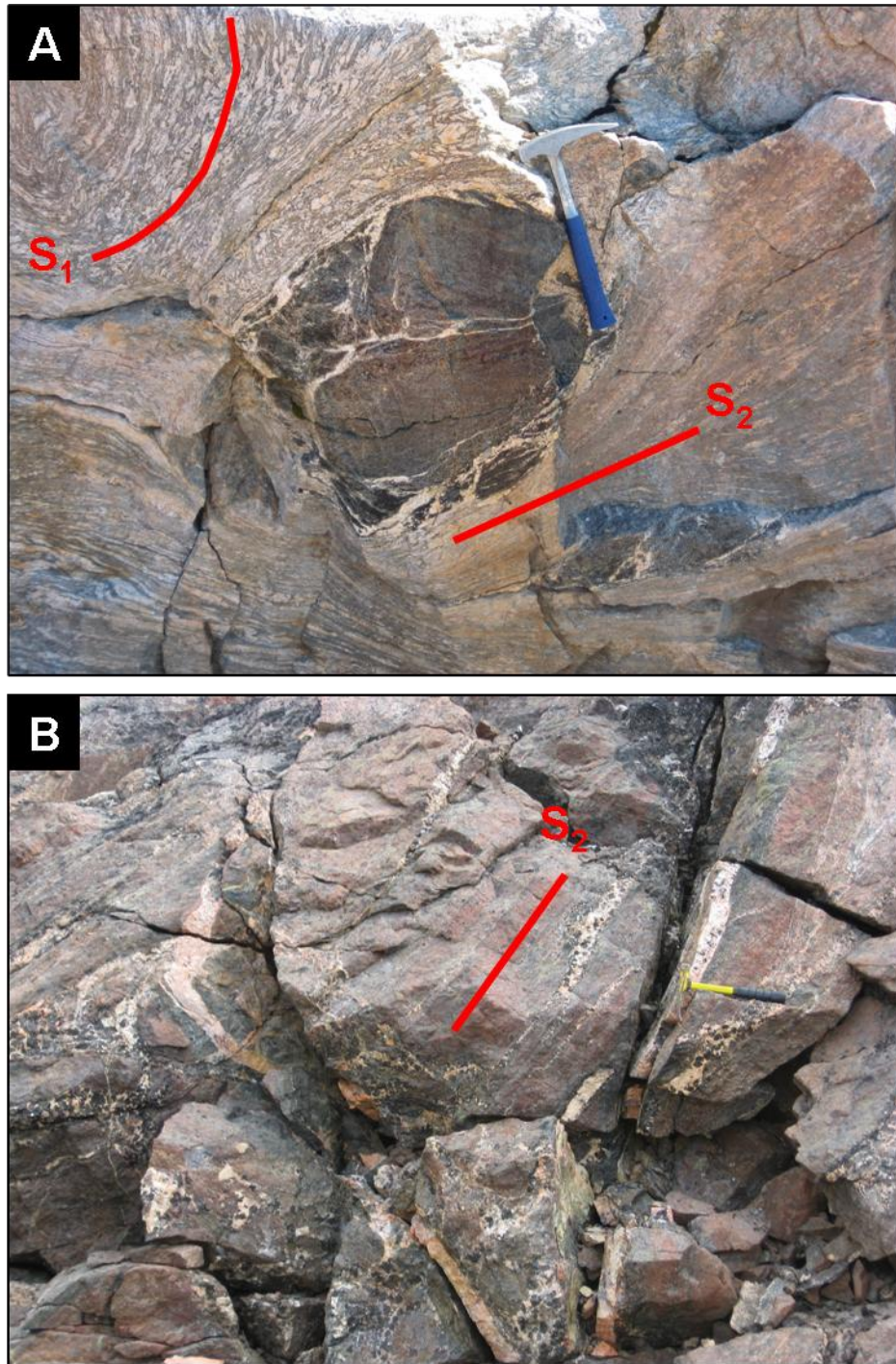


Figure 10. Field images of eclogites and related mylonites within the footwall of the Gubbedalen Shear Zone. **A.** Boudinaged eclogite pod within the felsic orthogneiss. Note the mylonitization (S_2) of the migmatite around the boudin and the presence of felsic veins interpreted to be decompressional melts. **B.** Eclogite CP-52A with garnet-rich layers (S_2 , eclogite-facies compositional layering) and felsic decompressional melt veins with large amphibole crystals.

(Figure 7F) portions of the orthogneiss complex. They were also observed cutting across granitic veins and dikes.

S_2 shears along the margins of the eclogite pods are retrogressive, non-coaxial crystal-plastic mylonitic shear zones that have comminuted minerals and obliterated fabrics within their felsic orthogneiss hosts (Figures 10A, 11A, 11B, and 11C). These are generally narrow, 10-30 cm wide shear zones. The mylonitic foliation, S_2 , is defined by alternating layers of sheared fine-grained quartz, feldspar, and lesser amounts of muscovite, biotite, and amphibole. Quartz and feldspar mostly occur in elongated ribbons and sigma clasts, respectively (Figure 11C) defining a mineral stretching lineation, L_2 .

One particularly well exposed mafic boudin that provided good three-dimensional control of the upper, domal-shaped surface containing S_2 and L_2 was carefully mapped and analyzed and is illustrated in Figure 11. The S_2 mylonitic foliation that wraps over the top of this eclogite boudin is variably striking and has sub-horizontal dips (Figures 11D and 12), reflecting a domal geometry. L_2 elongation lineations measured are subhorizontal and trend roughly N50°W/S50°E (Figure 11D). When plotted together with all L_2 lineation readings from shear zones wrapping mafic pods and those measured for “rogue” shears throughout the southern field area (Figure 13B), a conical fold distribution is documented with a cone-axis plunging 21° toward N27°W.

Petrographic analysis of mylonites found wrapping the eclogite pods imply that the original mylonite fabric has been partially annealed (Figures 11E and 11F). S-C fabrics, however, are preserved within some of the mylonites. C-planes are defined by recrystallized, strain-free quartz and feldspar ribbons, and S-planes are defined by biotite

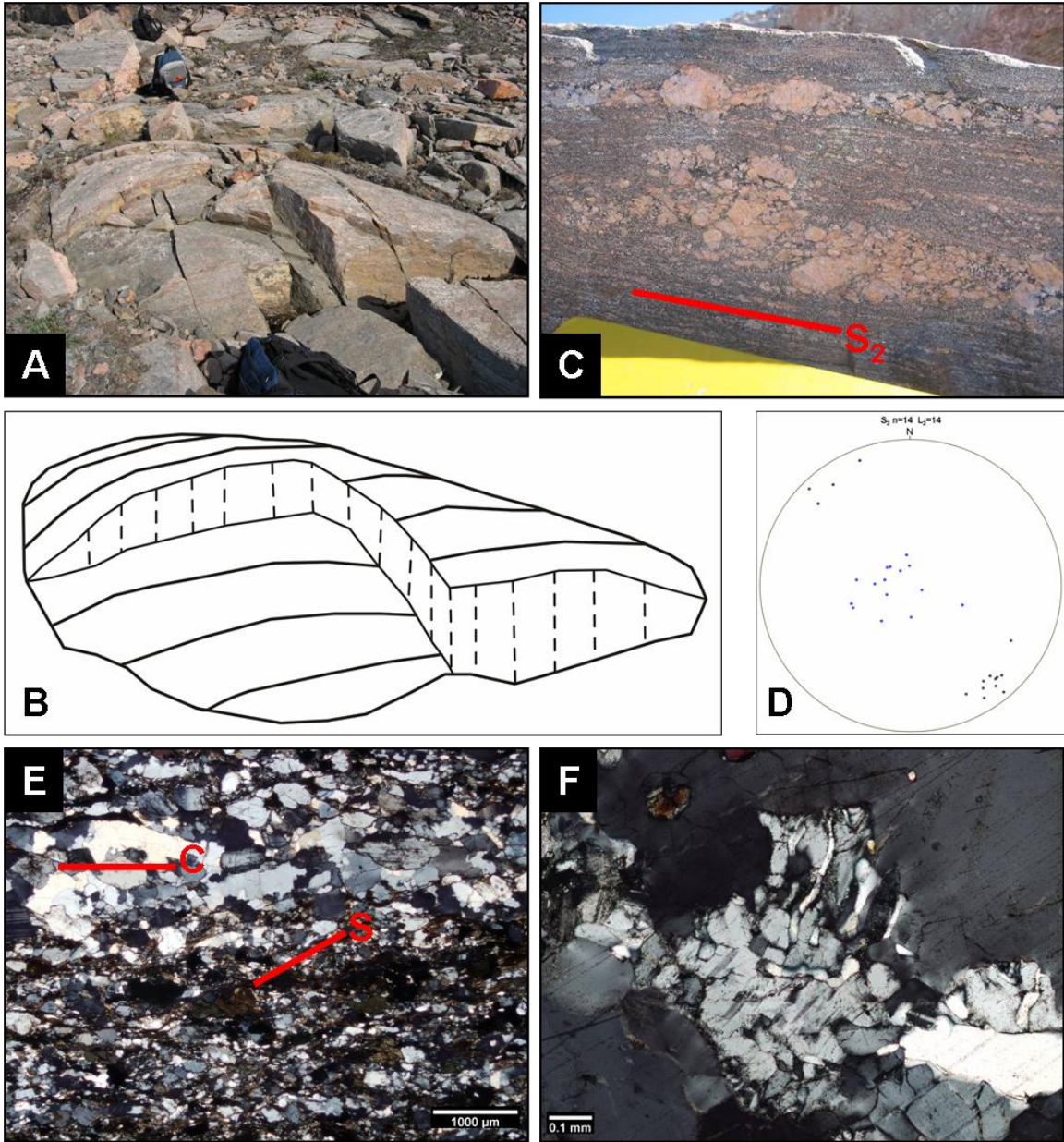


Figure 11. **A.** View of a sigmoidal shaped crystal-plastic mylonite wrapping over the top of a small mafic boudin (backpack for scale). **B.** Line drawing of a mylonite sheathed boudin in A. Solid lines represent mineral elongation lineation and dashed lines represent the vertical joint faces. **C.** Mylonite (looking perpendicular to foliation and parallel to lineation) from vertical face of a boudin sheathing a mafic lens with large (2.5 cm) potassium feldspar sigma clasts entrained and rotated with tops-right movement. **D.** Stereogram of data for outcrop shown in A, B, and C, with S_2 mylonitic foliation in blue and L_2 mineral elongation lineation in black. **E.** Photomicrograph in cross polarized light of a mylonite wrapping an eclogite boudin. S-C fabric is preserved indicating dextral movement. The shear fabric has been mostly recrystallized and annealed. **F.** Photomicrograph of myrmekite grains found throughout the boudin wrapping mylonites.

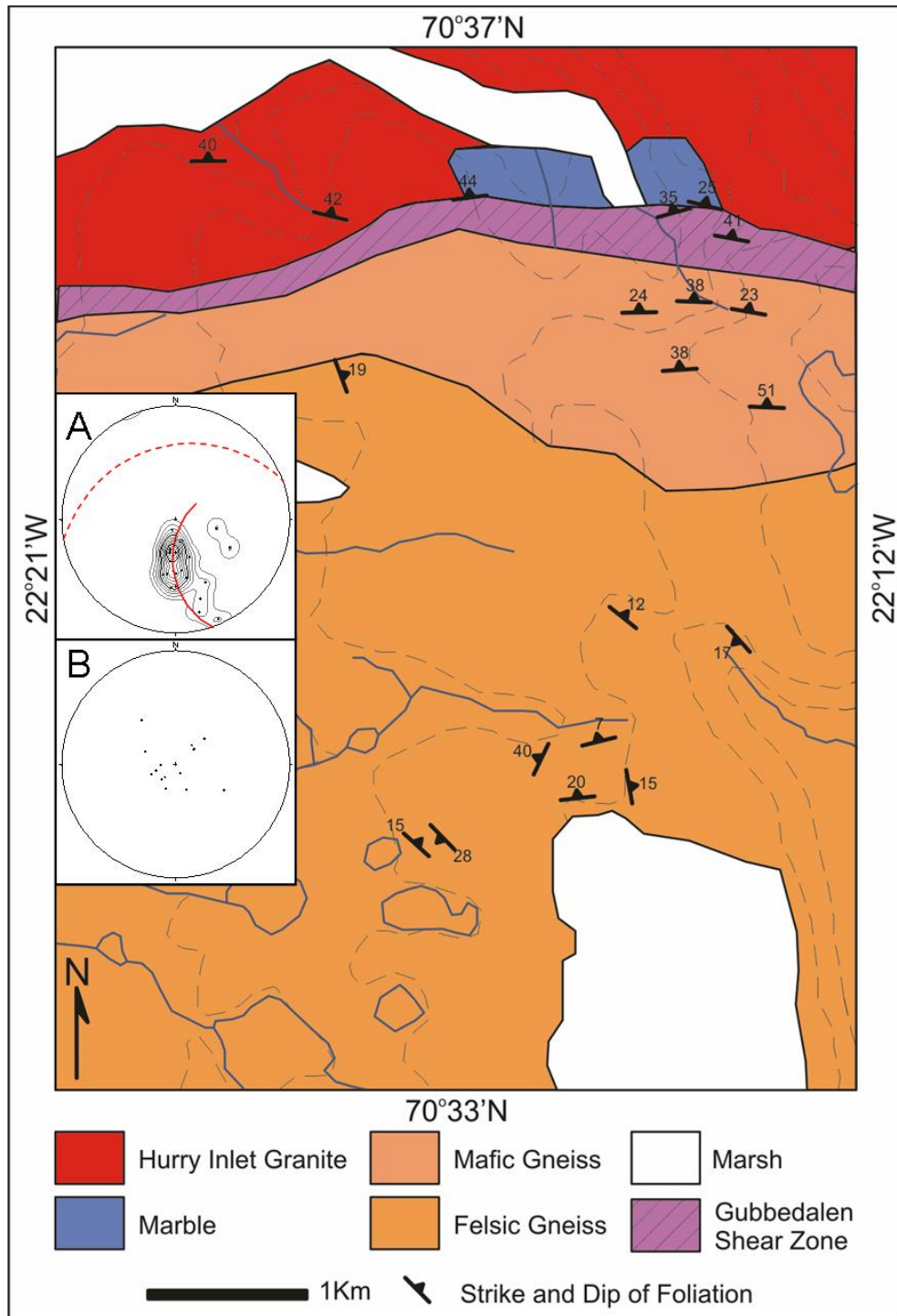


Figure 12. Geologic map illustrating S_2 and S_3/S_4 foliation planes measured in the southern field area. Inset is a lower hemisphere stereographic projection of poles to foliation planes. **A.** S_3/S_4 foliations within the Gubbedalen Shear Zone; $n = 24$. Dashed red line is an average S_0/S_1 foliation plane. Small circle fit through data (red partial circle) indicates a cone axis at $N32^\circ W$, $25^\circ W$. **B.** S_2 foliations of mylonite shear zones associated with eclogite boudins and “rogue” shears; $n = 14$.

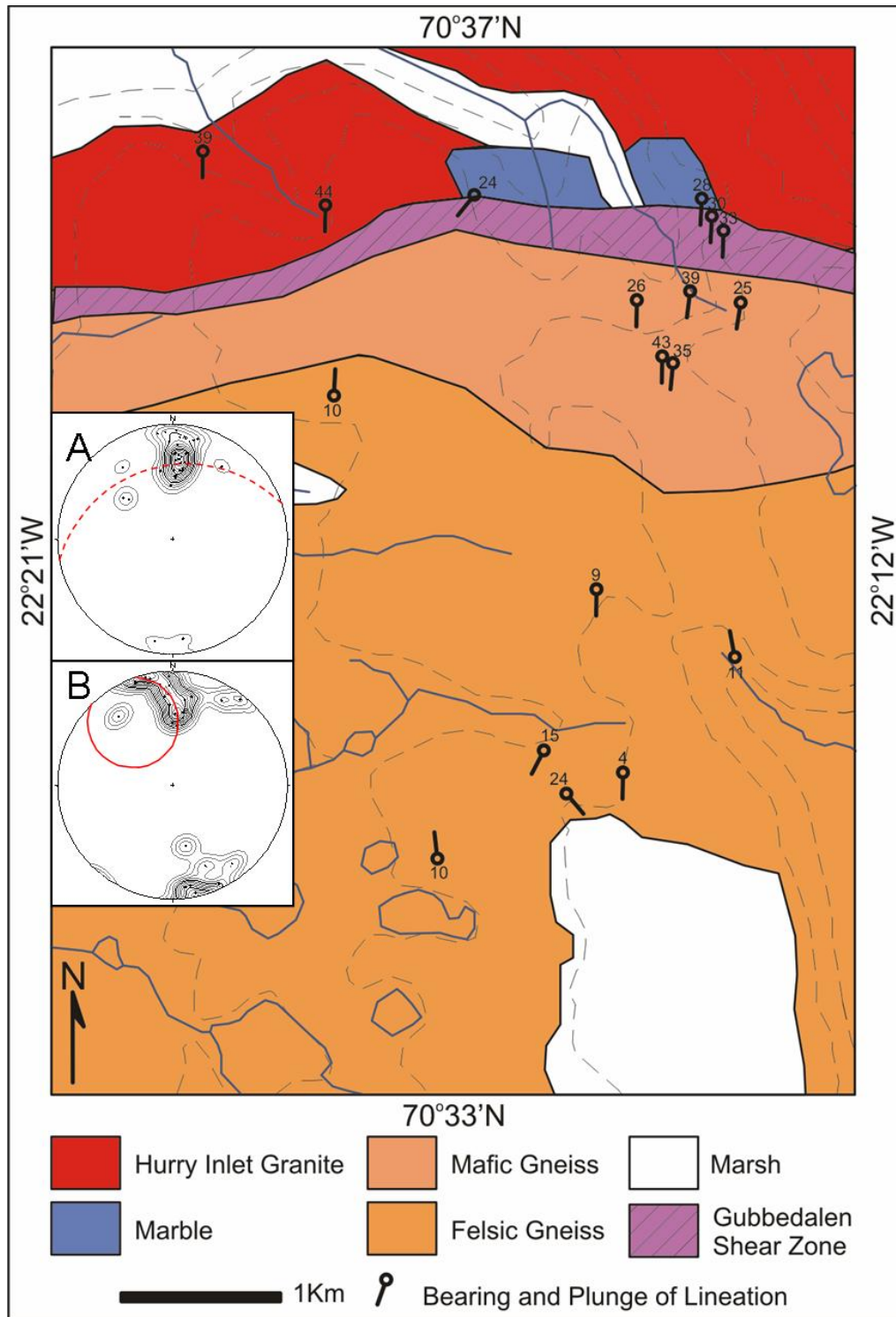


Figure 13. Geologic map illustrating L_2 and L_3/L_4 lineations. Inset is a lower hemisphere stereographic projection of elongation lineations. **A.** L_3/L_4 lineations within the Gubbedalen Shear Zone; $n = 34$. Dashed red line is an average S_0/S_1 foliation plane. **B.** L_2 lineations of shear zones associated with eclogite boudins and “rogue” shears; $n = 25$. Small circle fit through data (red circle) indicates a cone axis at $N27^\circ W, 19^\circ NW$.

and lesser amounts of muscovite. Amphibole and garnet have grown within the previously formed mylonitic fabric (Figure 11E). Some feldspar grains have a myrmekitic texture with quartz exsolved out of the interior of grains (Figure 11F). Although no petrographic analysis on “rogue” shears was performed, they are interpreted to have formed under the same D_2 crustal and deformational conditions as the shears encompassing the eclogite pods. This interpretation is based on their similar fault rock types that are derived from the same protoliths and their co-planar and co-linear fabrics.

Field relations combined with amphibolite-facies conditions for D_2 mylonitization (i.e., dynamic recrystallization of feldspar) require that this shearing post-dated eclogitization. Microstructures indicate that the mylonites stayed at elevated, annealing temperatures during the amphibolite-facies retrogression event that Augland (2008) dated at 388 Ma. D_2 shear zones are, therefore, interpreted to have formed in response to non-coaxial simple shearing during exhumation from eclogite-facies conditions to mid-crustal levels. The rigid eclogite bodies apparently were stretched and rotated along a present-day, shallow $N50^\circ W/S50^\circ E$ axis during their ascent into the middle crust.

Gubbedalen Shear Zone

The Gubbedalen Shear Zone (Figures 4) is the boundary between the northern hanging wall and southern footwall blocks. The shear zone has an east-west trend, dips shallowly to moderately to the north, is approximately 500 meters thick, and records a complex polyphase history. The main lithologies in the lower 400 meters of the shear zone are footwall mafic gneisses and syntectonic felsic granites injected into the shear

zone. In the structurally higher levels (upper 100 meters) protoliths are derived from the Krummedal Sequence. The shear zone fabric comprises mylonites, ultramylonites, phyllonites and in the structurally upper most parts cataclasites and breccias.

Shear sense indicators within the lower 400 meters of the Gubbedalen Shear Zone record tops-up-to-the-south reverse dip-slip motion. This contractional phase of the shear zone produced mylonitic and ultramylonitic shear fabrics (S_3 ; Figures 14A-C). S-C fabrics and rotated porphyroclasts are the most common shear-sense indicators within mylonites. Mylonitic shears in the Gubbedalen Shear Zone were observed to cut and fold the previously formed gneissosity (S_0), migmatitic foliation (S_1), and mylonitic shears (S_2) in the footwall block documenting tops-south thrust movement (Figure 14C). L_3 is defined by pronounced quartz elongation lineations.

Microstructures within the mylonites unambiguously confirm the tops-south thrusting. Dextral mica fish with connecting trails of sheared pieces of mica are prevalent within samples from the lower parts of the shear zone (Figure 14D). Sigma type porphyroclasts of single feldspar grains or aggregates of feldspars are common and preserve stepping up-to-the-right dextral geometries (Figure 14E). Feldspars have deformed brittlely by internal fracturing. Slight bulging of grain boundaries within some smaller feldspars and core-mantle structures in larger ones indicate some degree of crystal-plastic deformation. Most quartz within the mylonite has been dynamically recrystallized. Quartz ribbons with prominent subgrains are observed around the margins of competent feldspar porphyroclasts. Mineral assemblages (i.e., quartz + feldspar + biotite + muscovite) and microstructures (i.e., crystal-plastic quartz [$\sim 300^\circ\text{C}$] and crystal-brittle feldspars [$\sim 450^\circ\text{C}$]; Scholtz, 1988; Simpson and Wintsch, 1989) support upper

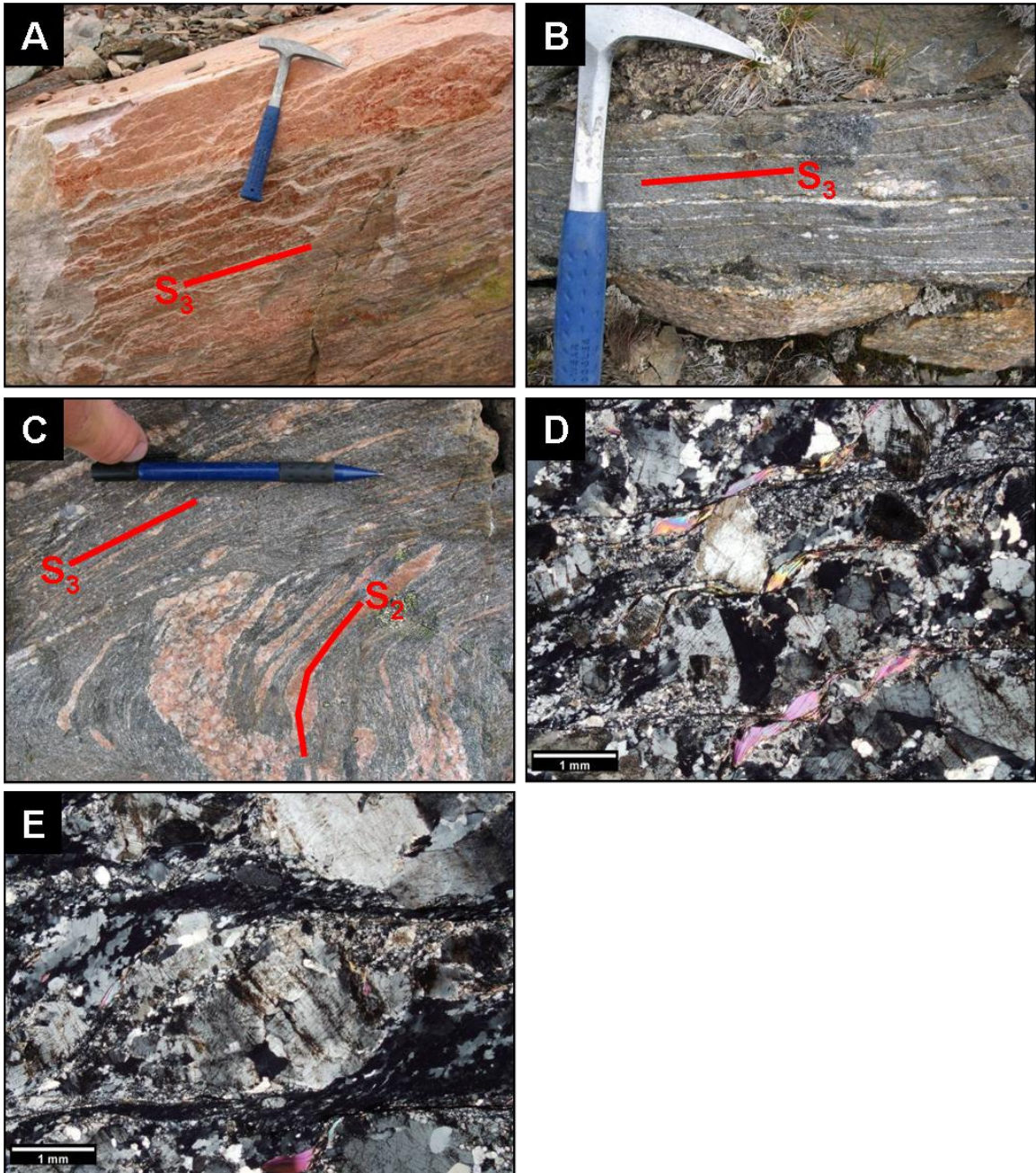


Figure 14. Images and photomicrographs of the contractional lower part of the Gubbedalen Shear Zone. All photos perpendicular to foliation and parallel to lineation. **A.** Mylonitized migmatitic gneiss and syntectonic granite found within the lower part of the shear zone. **B.** Mafic-rich ultramylonites with feldspar sigma clasts indicating tops-right (south) thrust movement. **C.** Ultramylonite (S3) cutting across a mylonitized migmatite (S2), documenting tops-right (south) thrust movement. **D.** Photomicrograph in cross polarized light from granitic mylonite in image A. Micafish and sigma clasts indicate dextral (tops-up and south) reverse slip movement. Note quartz has subgrains and the shear fabric is dynamically recrystallized. **E.** Photomicrograph in cross polars from same thin section as D showing a dextral quartz and feldspar aggregate sigma clast.

greenschist-facies conditions within the contractional, lower 400 meters of the Gubbedalen Shear Zone. These conditions contrast sharply with the high-temperature annealed mylonites in the footwall (i.e., shears around mafic pods and “rogue” shears).

The upper 100 meters of the Gubbedalen Shear Zone is characterized by tops-north, down-dip, extensional movement. Extensional strains were accommodated in several different fashions. In some places, new mylonites and ultramylonites (S_4) formed that cut across the previous S_3 mylonitic foliation (Figure 15A). Previous structures have been stretched by this extension. Syntectonic granitic dikes, for instance are excellent markers of this extensional strain (Figure 15B). Extension was largely accommodated parallel to the previously formed contractional structures and fabrics such as those preserved in the lower parts of the Gubbedalen Shear Zone away from the extensional overprint. Numerous reverse-slip crenulations (Figure 15C) and C' shears were observed in outcrops that document tops-north extension of the previously formed S_3 mylonitic foliation. Like the structurally lower parts of the shear zone, L_4 is defined by a pronounced quartz elongation lineation. The uppermost 20 meters of the shear zone has been chopped by several late-stage, brittle faults marked by carbonate-rich breccias (Figure 15D).

Microstructures in rocks collected from within the upper shear zone mylonites also confirm tops-north extensional movement. Quartz ribbons have been pulled, stretched, and rotated (folded) into tops-down-to-the north reverse slip crenulations (Figures 15E and 15F). Subgrains within quartz ribbons preserve S-C composite fabrics indicating down-dip directional movement (Figure 15F). Elongated mica fish are stretched and sheared into a tops-north rotational sense. C' shear bands are common

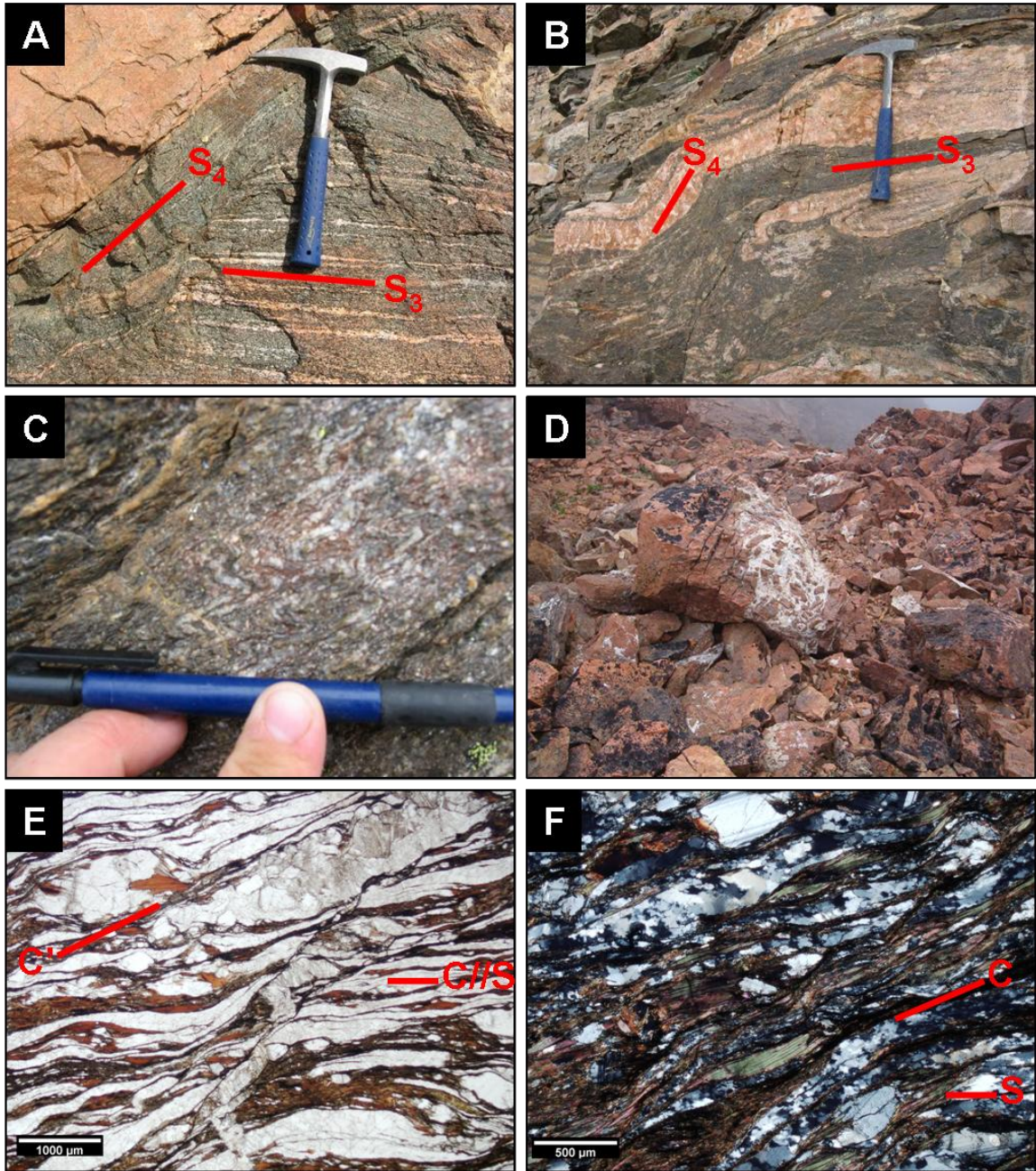


Figure 15. Studies from the extensional overprint in the upper parts of the Gubbedalen Shear Zone. **A.** Ultramylonitic extensional shear zone (S_4) cutting across and retrograding the prior contractional mylonitic fabric (S_3). **B.** S_4 extensional shear zone cutting a granitic injection. **C.** Reverse-slip crenulations documenting tops-down-to-the-left (north) extension. **D.** Carbonate breccia zone at the northern margin of the shear zone in contact with the Hurry Inlet Granite. **E.** Photomicrograph in plane light of extensional overprint upon the S_3 mylonitic fabric. Note the microfolds within the quartz ribbons, and C' shear bands. **F.** Photomicrograph in cross polarized light of dextral mica fish. Polycrystalline quartz ribbons contain subgrains and recrystallized grain shape preferred orientation documenting sinistral extensional shear.

tops-north extensional shear indicators (Figure 15E). Brittle deformation of feldspar is indicated by microfaults and fractures (Figures 15E and 15F). Much more biotite occurs within the mylonites in the upper parts of the shear zone, which is interpreted to reflect incorporation of Krummedal Sequence metasedimentary rocks; Figures 15E and 15F could be referred to as phyllonites. The presence of crystal-plastic quartz and crystal-brittle feldspar within the upper part of the Gubbedalen Shear Zone documents a deformational temperature around $\sim 300^{\circ}\text{C}$, indicating lower greenschist-facies conditions. The D_4 structures and fabrics are interpreted to reflect further exhumation of the footwall and its mylonitic carapace into the upper crust and then to near Earth surface conditions to form the latest-stage brittle faults and carbonate breccias.

The mylonitic and ultramylonitic foliations (S_3/S_4) and mineral elongation lineations (L_3/L_4) measured within the Gubbedalen Shear Zone are plotted on Figure 12 and Figure 13, respectively. Stereographic projections of S_3/S_4 mylonitic foliations indicate that the shear zone is east-west trending (Figure 12, Inset A), and L_3/L_4 mineral stretching lineations are almost exclusively down-dip to the north (Figure 13, Inset A).

The Gubbedalen Shear Zone affects footwall block rocks for at least 1 kilometer structurally beneath the main zone of mylonites. Figure 16 is a composite figure including a profile across the shear zone documenting its widespread affects. Gneissosity (S_0), migmatitic foliations (S_1), and the brittle stockwork of granitic veins have been rotated into parallelism with the shear zone. Mineral lineations (L_0), stretched neosomal “cigars” (L_1), and mineral elongation lineations (L_2) have been elongated and stretched within the shear zone parallel to L_3/L_4 .

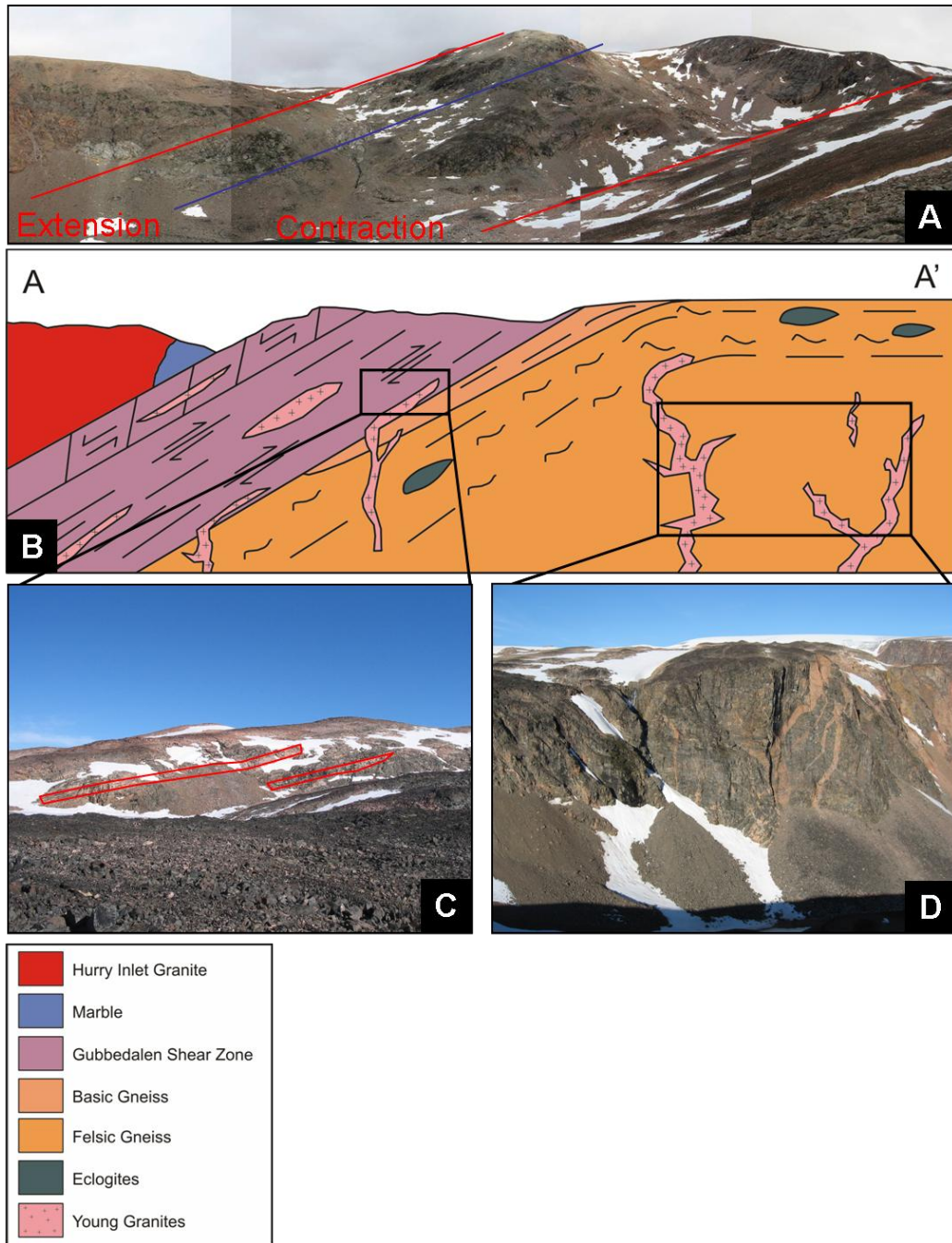


Figure 16. **A.** Photo mosaic of the Gubbedalen Shear Zone (outlined in red) looking to the east along a valley wall. Extensional and contractional zones are separated by the blue line. **B.** Schematic cross section from A to A' of the Gubbedalen Shear Zone and surrounding terranes (location of cross section marked in Figure 6). Shear couples within the shear zone represent the direction of shear. Straight lines represent the mylonitic foliation and wavy lines represent the migmatitic foliation. **C.** Felsic dikes within the bottom of the shear zone (looking north) pulled into parallelism with the shear zone's foliation. **D.** Unaffected felsic dikes from a canyon wall (looking east) well south of the shear zone.

Figure 17 summarizes all the structural data that was collected within the southern field area. Figure 17A plots gneissosity (S_0), migmatitic foliation (S_1), and mylonitic foliation (S_2). A great circle fits through the data, indicating that the Gubbedalen Shear Zone is a monocline with an axis oriented N88°E, 4°NE (Figure 16B); this monoclinial style for the hinge to the shear zone is expressed in the cross section in Figure 16B. Figure 17B depicts mineral alignment (L_0), neosomal “cigars” (L_1), and elongation lineations (L_2). A small circle fits through the data indicating the axis of a cone at N27°W, 21°NW. This cone axis likely reflects sheath fold geometries created by the Gubbedalen Shear Zone as rock fabric and structures of the footwall are swept into it. Another trend indicated in Figure 17B is that lineations trend progressively more toward the northwest as the dip of foliation shallows. As described above for the investigated shear zones illustrated in Figure 11A through 11D, it appears that the eclogite-pod and “rogue” shears initiated with a more easterly-westerly trend that was rotated about this conical fold axis. Data are also skewed toward a preponderance of readings from the domal crest of the Liverpool Land eclogite-containing core, as the Gubbedalen Shear Zone projects just above the footwall block of the southern study area. In other words, the data are skewed towards more contractional measurements from the basal parts of the Gubbedalen Shear Zone reflecting the contractional history that may have been directed more towards the southeast rather than due south.

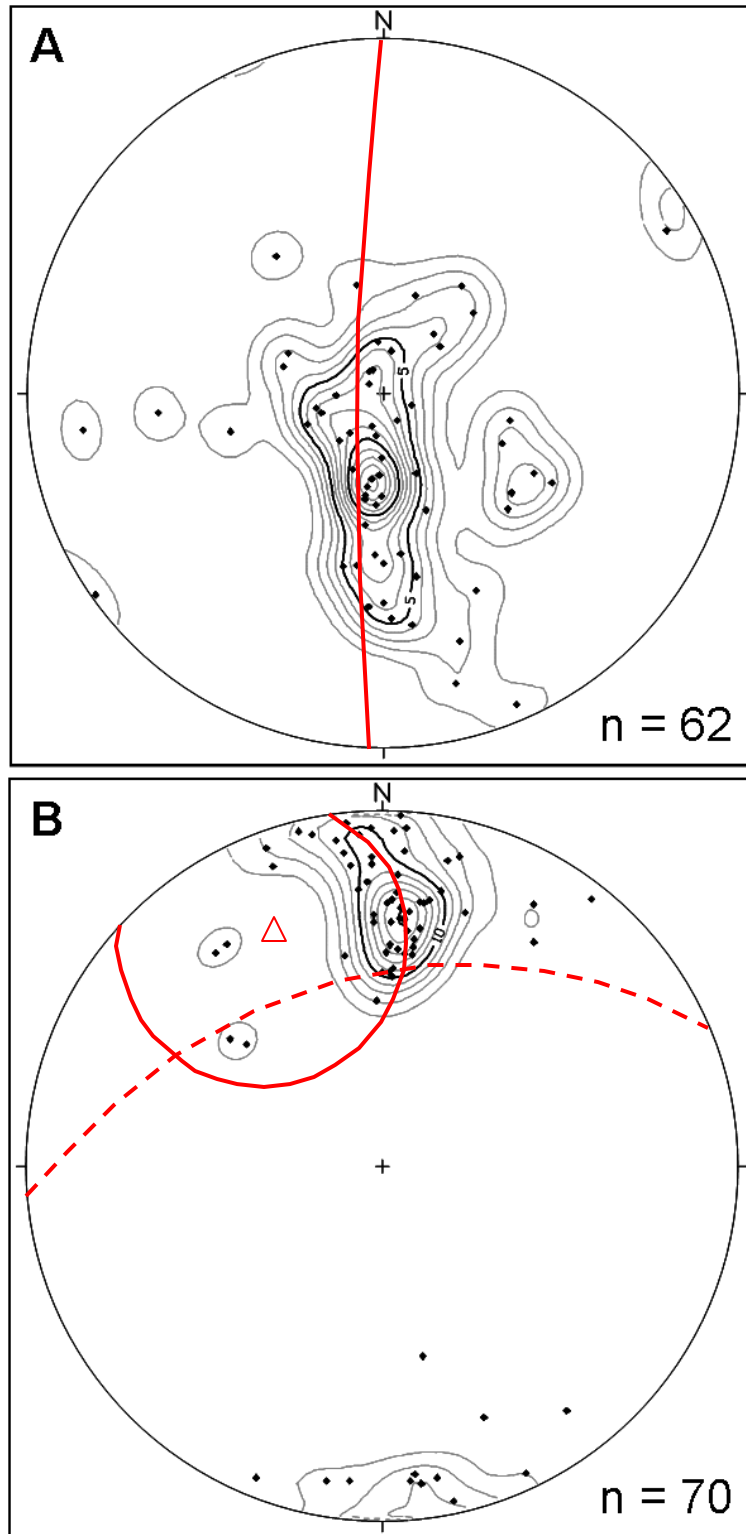


Figure 17. **A.** Stereographic projection of poles to planes from all foliation data (S_0 , S_1 , S_2 , S_3 , and S_4) collected in the southern field area. **B.** Stereographic projection of all lineations (L_0 , L_1 , L_2 , L_3 , and L_4) collected in the southern field area (n equals the number of measurements)

III. PETROLOGY AND PETROGRAPHY OF ECLOGITES

Petrography

Three eclogite samples (CP-47, CP-52A, and CP-92) were chosen for petrologic and petrographic analyses due to their differing levels of retrogression (Figure 18). The samples contain two mineral assemblages, one equilibrated under eclogite-facies and then a later one that was retrogressed to granulite-facies conditions. The eclogite-facies assemblage contains garnet + omphacite + quartz \pm zircon \pm rutile \pm ilmenite. The granulite-facies assemblage is garnet + low-sodium clinopyroxene + plagioclase + amphibole + quartz. Samples CP-47 and CP-92 both include pyroxene-plagioclase-amphibole symplectites. The symplectites formed after the breakdown of omphacite during decompression and can be used to infer prior, peak eclogite-facies conditions (Anderson and Moecher, 2007). Some mafic pods within the field area contain an amphibolite-facies retrogression assemblage, but this study focused on more pristine eclogite samples.

Sample CP-52A (Figure 19A) is the most pristine and least retrograded eclogite sample. CP-52A contains light pink, heavily fractured, hypidioblastic garnets that have inclusions of quartz, zircon, rutile, monazite, and sparse omphacite. Quartz inclusions do not exhibit radial fracture patterns around the inclusions, which might be indicative of ultra-high pressure metamorphism. Hypidioblastic omphacite grains have a slight pale

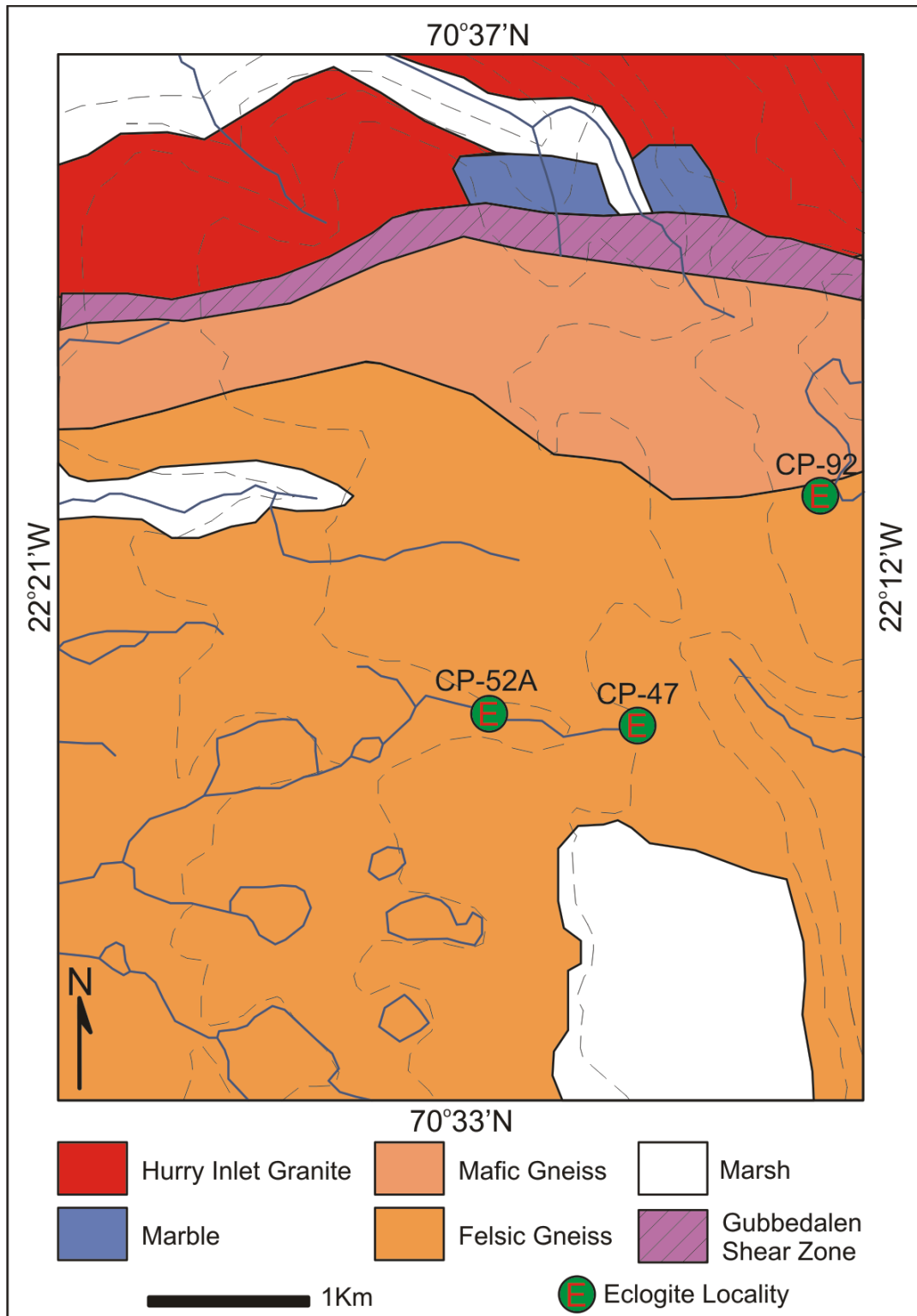


Figure 18. Simplified geologic map showing the location of eclogite samples that were petrographically and chemically analyzed (CP-47: 70° 34.937'N, 22° 13.770'W; CP-52A: 70° 34.633'N, 22° 15.220'W; and CP-92: 70° 35.362'N, 22° 12.106'W).

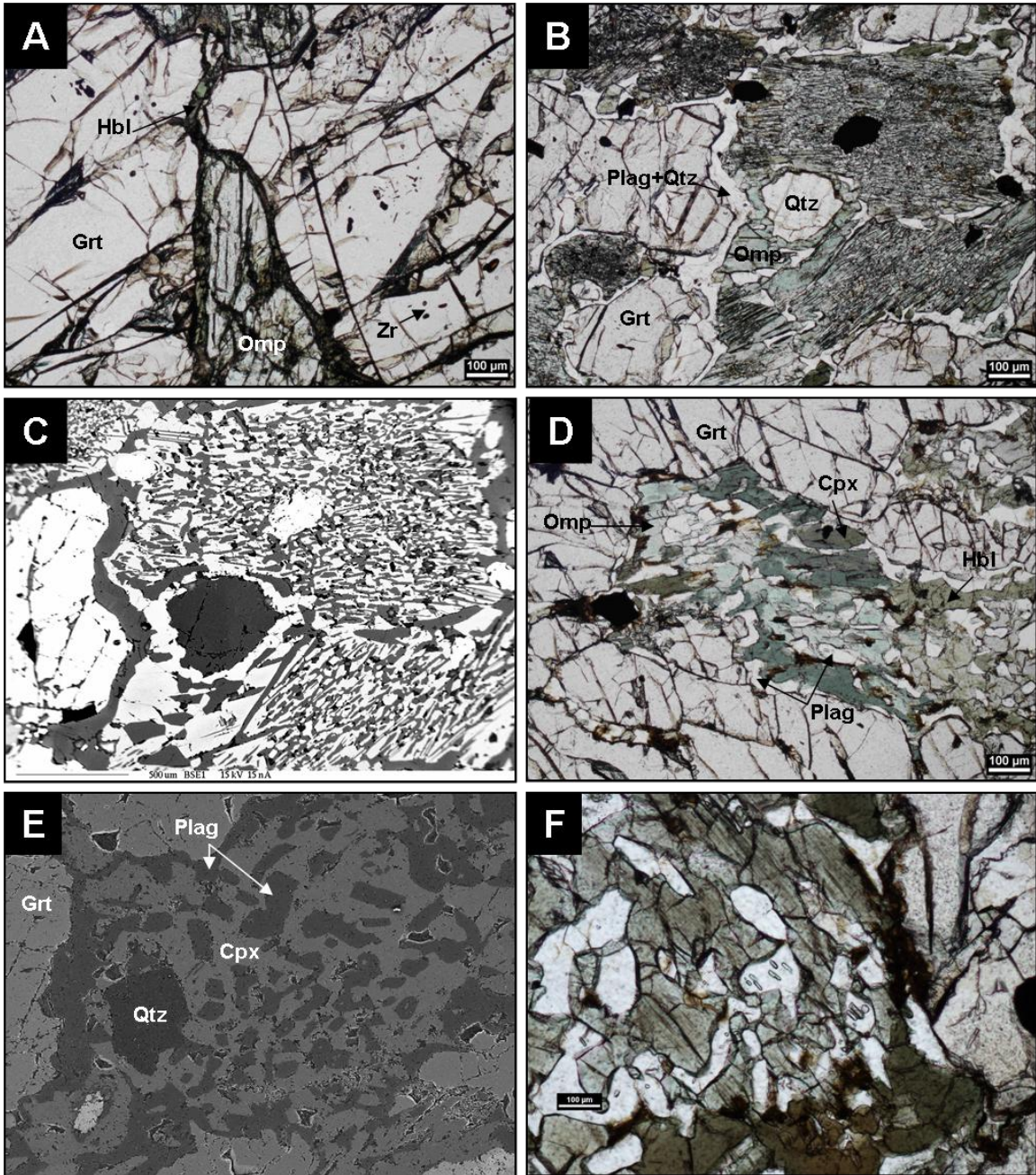


Figure 19. **A.** Eclogite CP-52A in plane light, notice the thin rim of retrograde hornblende growing on the omphacite grain. **B.** Eclogite CP-92 in plane light with fine-grained lamellar plagioclase-clinopyroxene-hornblende symplectites. **C.** Zoomed in Back Scatter Electron image of the area depicted in B. **D.** Eclogite CP-47 in plane light showing coarse grained wormy plagioclase-clinopyroxene-hornblende symplectites. **E.** Back Scatter Electron image of sample CP-47 (field of view is ~1 cm). **F.** Quartz exsolution rods within remnant omphacite grain and small low-sodium clinopyroxene nucleating in plagioclase within sample CP-47 in plane light. Abbreviations used in figure. Grt = Garnet, Cpx = low-Na clinopyroxene, Qtz = quartz, Plag = Plagioclase, Zr = Zircon, Omp = Omphacite, Hbl = Hornblende.

green pleochroism and are also heavily fractured. Omphacite cores are still pristine, but grain boundaries are retrogressed into hornblende.

Sample CP-92 (Figure 19B and 19C) is heavily retrogressed and contains few relict grains from the prograde mineral assemblage. Garnets are light pink, hypidioblastic, but not as heavily fractured as sample CP-52A. Garnets contain fewer inclusions of zircon, rutile, and monazite than CP-52A. Omphacite has been replaced by fine grained symplectites of lobate low-sodium clinopyroxene, plagioclase, and hornblende, and have a slight lamellar texture. Each symplectite is rimmed with a corona of quartz and plagioclase. Prograde quartz is more abundant in CP-92 than in CP-52A.

Sample CP-47 has the same mineral assemblage as sample CP-92 but the symplectites have a very different texture. Symplectites have a wormy texture and are coarser grained than CP-92. Symplectitic-grain cores still preserve richer omphacite compositions, but the edges of the symplectites are dominated by low-sodium pyroxenes and amphiboles (Figure 19D and 19E). Pyroxene grains contain quartz rods that have exsolved from the pyroxene, and very fine grained pyroxenes have nucleated in the plagioclase portions of the symplectites (Figure 19F). Both of these features demonstrate the mineral assemblages attempted to reach equilibrium as the rock was retrograded.

Mineral Chemistry

Mineral compositions for garnet, pyroxene, plagioclase, and amphibole were determined using quantitative Wavelength-Dispersive System (WDS) microprobe analysis. Table 2 contains averaged mineral compositions for garnet, pyroxene, plagioclase, and amphibole for all eclogite samples. Data from all microprobe analyses

are in Appendix B. Garnet formulae were recalculated based on 12 oxygens, pyroxene on 6 oxygens, plagioclase on 8 oxygens, and amphibole on 23 oxygens. Fe²⁺ and Fe³⁺ of garnet and pyroxene were estimated by stoichiometry (Droop, 1987); all Fe for plagioclase and amphibole were assumed to be Fe²⁺.

Sample	Garnet			Pyroxene			Plagioclase			Amphibole		
	CP-47 <i>n</i>	CP-52A	CP-92	CP-47	CP-52A	CP-92	CP-47	CP-52A	CP-92	CP-47	CP-52A	CP-92
	10	9	5	14	11	12	17	1	10	5	1	5
SiO ₂	39.22	39.49	39.05	50.47	53.74	50.26	59.82	68.56	63.48	43.72	41.30	41.30
TiO ₂	0.06	0.08	0.07	0.29	0.28	0.31	0.00	0.01	0.00	1.38	0.51	1.33
Al ₂ O ₃	22.17	22.29	21.82	3.92	12.35	7.03	25.23	19.88	23.09	11.45	15.47	14.32
Cr ₂ O ₃	0.01	0.00	0.01	0.02	0.01	0.01	0.01	0.00	0.01	0.01	0.00	0.01
FeO	19.58	18.62	22.23	10.32	4.81	10.53	0.21	0.11	0.23	14.07	11.77	13.65
MnO	0.30	0.21	0.36	0.11	0.03	0.12	0.01	0.07	0.01	0.06	0.06	0.09
MgO	7.60	7.76	6.64	12.28	8.41	10.60	0.00	0.00	0.00	12.22	13.23	12.21
CaO	11.17	11.98	10.29	21.57	15.08	19.17	7.32	0.32	4.44	11.61	11.10	11.31
Na ₂ O	0.02	0.01	0.05	0.61	5.61	1.94	7.44	11.56	9.28	1.68	2.65	3.13
K ₂ O	0.01	0.00	0.00	0.01	0.00	0.00	0.23	0.06	0.01	0.54	0.90	0.02
Total	100.16	100.45	100.53	99.60	100.33	99.98	100.29	100.57	100.57	96.75	96.99	97.38
Si	2.977	2.980	2.983	1.893	1.917	1.865	2.663	2.981	2.793	6.519	6.114	6.136
Ti	0.004	0.005	0.004	0.008	0.007	0.009	0.000	0.000	0.000	0.155	0.057	0.149
Al	1.983	1.983	1.964	0.173	0.519	0.307	1.324	1.019	1.198	2.013	2.700	2.508
Cr	0.001	0.000	0.001	0.001	0.000	0.001	0.000	0.000	0.001	0.004	0.000	0.004
Total Fe	1.243	1.175	1.420	0.323	0.144	0.327	0.008	0.004	0.009	1.754	1.456	1.696
Mn	0.019	0.013	0.023	0.003	0.001	0.004	0.001	0.003	0.001	0.008	0.007	0.011
Mg	0.860	0.873	0.756	0.686	0.448	0.587	0.000	0.000	0.000	2.716	2.921	2.704
Ca	0.909	0.968	0.842	0.867	0.577	0.762	0.349	0.015	0.210	1.854	1.760	1.800
Na	0.003	0.002	0.007	0.044	0.387	0.139	0.642	0.975	0.791	0.487	0.762	0.902
K	0.001	0.000	0.000	0.000	0.000	0.000	0.013	0.003	0.000	0.104	0.170	0.004
Total	8.000	8.000	8.000	4.000	4.000	4.000	5.002	4.999	5.003	15.613	15.946	15.913

n - number of analyses averaged

Table 2. Table contains averaged weight percent oxides from multiple (*n* = number) microprobe analyses of garnet, pyroxene, plagioclase, and amphibole.

The three eclogite samples had garnets with very similar average compositions of Alm+Sps₄₂Grs₃₀Prp₂₈ for CP-47, Alm+Sps₃₉Grs₃₂Prp₂₉ for CP-52A, and Alm+Sps₄₇Grs₂₈Prp₂₅ for CP-92 (Figure 20). The differing garnet compositions between samples can be contributed to bulk composition, as opposed to chemical changes due to retrograde metamorphism. Elemental mapping of garnets show homogenous cores without zoning, indicating complete equilibrium at eclogite-facies conditions. There are slight differences in the iron and magnesium contents at grain boundaries with pyroxene as a result of re-equilibration during the retrograde event.

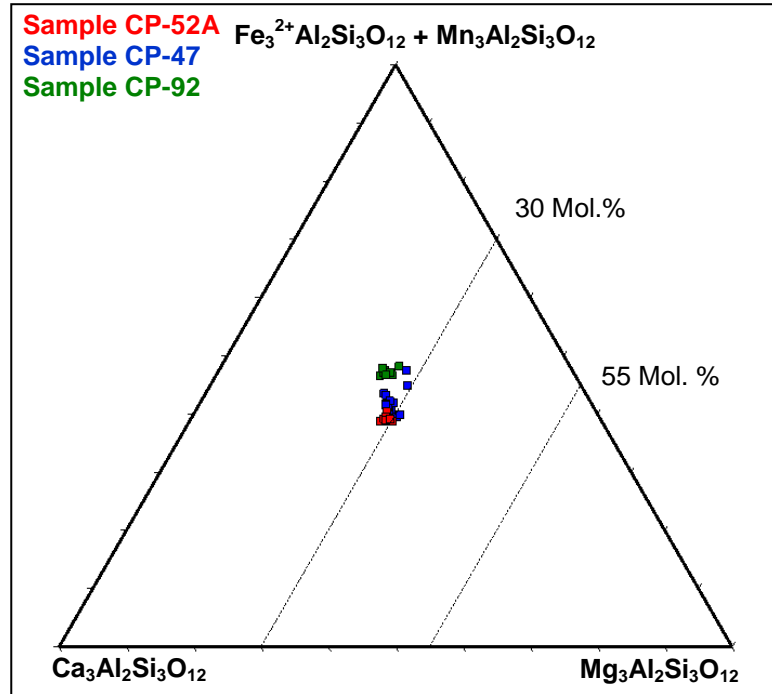


Figure 20. End member compositions of analyzed garnet grains from eclogite samples displayed on a ternary diagram (after Coleman et al., 1965).

Compositions of minerals other than garnet change dramatically between the pristine and retrograde eclogites. Pyroxenes from the most pristine eclogite (CP-52A) plot in the omphacite field on the ternary diagram, whereas pyroxenes that make up the symplectites (CP-47 and CP-92) plot in the Quad end of the diagram (Figure 21). As omphacite chemically breaks down to form the symplectites, sodium is released from pyroxene and is accommodated by plagioclase, as seen in element maps where sodium is depleted at the grain boundary (Figure 22). The amphiboles are calcium and sodium-rich and belong to the hornblende group. Amphibole compositions were plotted on a silicon versus sodium plus potassium diagram (Figure 23), and are more Edenite and Pargasite-rich, which are higher temperature and pressure amphiboles.

Geothermobarometry

Eclogite sample CP-52A was chosen for geothermobarometric calculations because the sample contains the most pristine eclogite-facies assemblage. Microprobe analysis was performed on six pairs of garnet and omphacite grains. The cores of adjacent grains were analyzed, because they should preserve the peak pressure and temperature conditions of eclogitization. The following sections describe the calculations necessary for determining the P-T conditions.

Thermometry Calculations

The traditional Ellis and Green (1979) calibration of the Fe-Mg exchange thermometer between garnet and clinopyroxene could not be used. The grossular content of the garnets being used for geothermometry was upwards of 30%. The calibration of

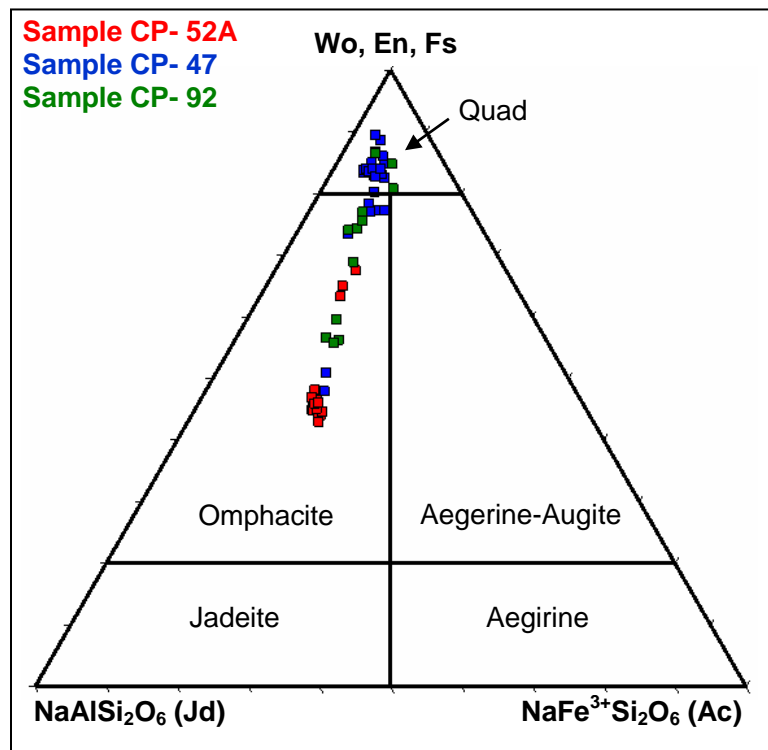


Figure 21. End member compositions of analyzed clinopyroxene grains from eclogite samples displayed on a ternary diagram (after Morimoto et al., 1988).

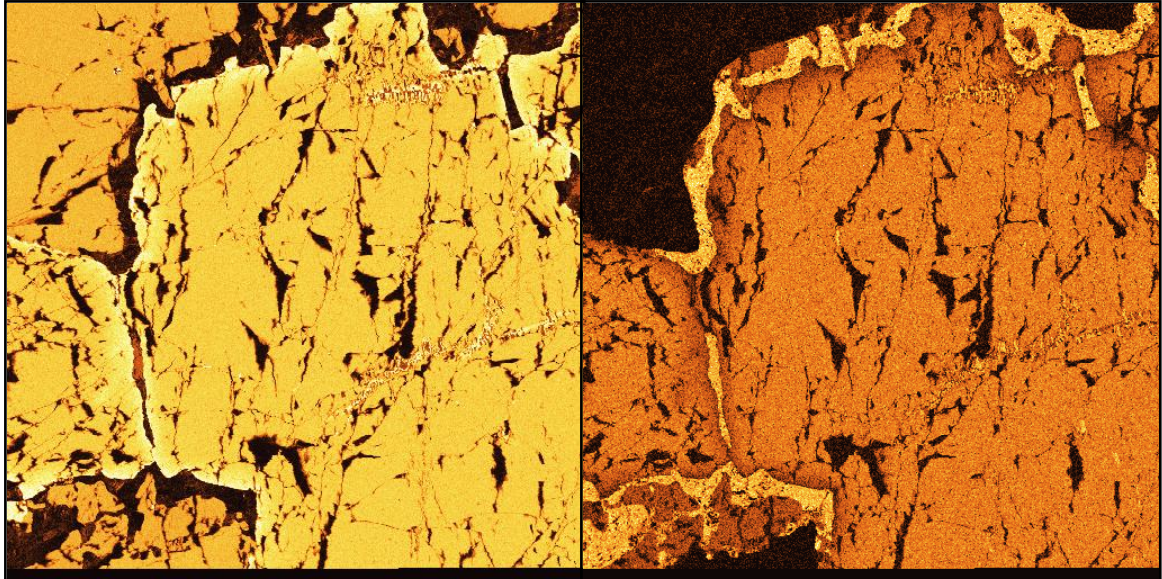


Figure 22. Element maps of calcium (left) and sodium (right) of eclogite CP-52A, with lighter colors being more enriched in the element. The central grain is an omphacite with a garnet grain to the top left of each image. Notice the fine grained symplectite that is forming along fractures within the omphacite. Image is approximately 1 cm.

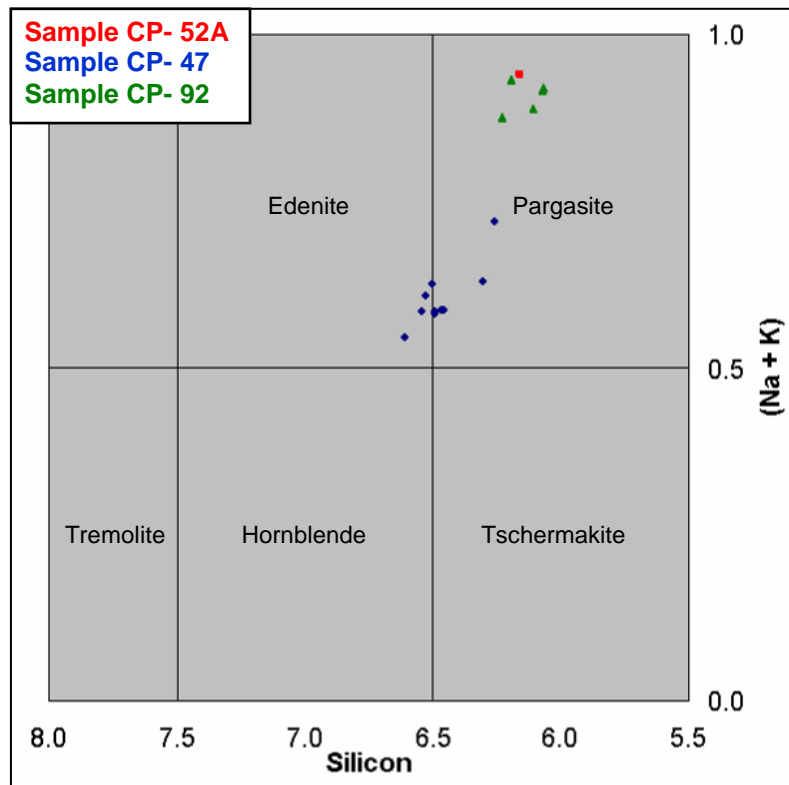
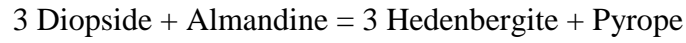


Figure 23. End member compositions of analyzed amphibole grains from eclogite samples on a Silicon versus Na+K diagram (after Deer et al., 1992).

the Ellis and Green (1979) thermometer is not suited for calcium levels that high, and the newer updated calibration of Krogh Ravna (2000) was used. The peak temperature of the eclogite-facies event was estimated using the garnet-clinopyroxene Fe²⁺- Mg exchange thermometer according to the following mineral reaction (Ellis and Green, 1979):



The P-T compositional relationship was determined by the following equation (Krogh Ravna, 2000):

$$T(^{\circ}\text{C}) = [(1939.9 + 3270 X_{Ca}^{Grt} - 1396(X_{Ca}^{Grt})^2 + 3319 X_{Mn}^{Grt} - 3535(X_{Mn}^{Grt})^2 + 1105 X_{Mg\#}^{Grt} - 3561(X_{Mg\#}^{Grt})^2 + 2324(X_{Mg\#}^{Grt})^3 + 169.4P(\text{GPa})) / (\ln K_D + 1.223)] - 273$$

where $K_D = (\text{Fe}^{2+}/\text{Mg})^{\text{Grt}} / (\text{Fe}^{2+}/\text{Mg})^{\text{Cpx}}$, $X_{Ca}^{Grt} = \text{Ca} / (\text{Ca} + \text{Mn} + \text{Fe}^{2+} + \text{Mg})$ in garnet,

$X_{Mn}^{Grt} = \text{Mn} / (\text{Ca} + \text{Mn} + \text{Fe}^{2+} + \text{Mg})$ in garnet, and $X_{Mg\#}^{Grt} = \text{Mg} / (\text{Mg} + \text{Fe}^{2+})$ in garnet.

Temperature calculations were based on the procedures outlined in Krogh Ravna (2000) and further information on the Fe-Mg thermometer can be found therein.

Barometry Calculations

Due to the absence of orthopyroxene in the eclogite-facies assemblage, absolute pressures of formation could not be estimated using a two pyroxene system. However, minimum pressures of formation could be calculated using the Jadeite component of omphacite grains following the equilibrium reaction:



The P-T compositional relationship was determined by the following equation (Holland, 1980):

$$P = 0.35 + 0.0265T(^{\circ}\text{C}) \pm \Delta P$$

where pressure is in kbars and ΔP is a pressure correction based on the Jadeite content of the clinopyroxene. The value of ΔP is given by the equation (Holland, 1980):

$$\Delta P = -(RT / \Delta V^{\circ}) \ln \alpha_{Jd}$$

where R is the gas constant, T is the absolute temperature of formation, the volume change of the reaction, ΔV° , was found to be 1.734 J/bar, and α_{Jd} is the activity of Jadeite in the pyroxene. The activity of Jadeite is given by (Holland, 1979):

$$\alpha_{Jd} = X_{Jd}^2 \gamma_{Jd}$$

where X_{Jd} and γ_{Jd} are the mole fraction and activity coefficient of Jadeite, respectively.

The activity of Jadeite was determined by (Holland, 1979):

$$\gamma_{Jd} = \exp[(W / RT)(1 - X_{Jd})^2]$$

where the interaction energy, W, was found to be 24 KJ. Pressure calculations were based on the previous equations and procedures outlined in Holland (1979; 1980) and further information on the albite = jadeite + quartz reaction can be found therein.

Results

Calculations from the aforementioned thermometry and barometry sections are summarized in Table 3. The Pressure-Temperature equations were simultaneously solved using an Excel® spreadsheet developed by the author using 100 iterations and a tolerance of 0.001. A mean temperature of ~867°C and a minimum pressure of 18.2

kbars were estimated for the peak of eclogite formation. These conditions constrain the metamorphism to high pressure conditions, in contrast to the ultra high pressure conditions reported in the abstract by Hartz et al. (2005). High pressure eclogitization in Liverpool Land also contrast with the ultra high pressure event documented in the North Eastern Greenland Eclogite Province (Gilotti and Ravna, 2002), further to the north of the study area.

Pressure - Temperature Calculations						
Grt-Cpx Pair	#1	#2	#3	#4	#5	#6
X_{Ca}^{Grt}	0.3220	0.3336	0.3244	0.3221	0.3266	0.3283
X_{Mn}^{Grt}	0.0043	0.0051	0.0042	0.0046	0.0055	0.0048
$X_{Mg\#}^{Grt}$	0.4392	0.4330	0.4382	0.4329	0.4428	0.4556
K_D	4.8285	4.8927	4.5103	5.3906	5.4011	3.9290
X_{Jd}^{Cpx}	0.3790	0.3702	0.3810	0.3861	0.3731	0.3792
α_{Jd}	2.7204	2.7815	2.6330	2.7584	2.8760	2.5215
γ_{Jd}	0.3908	0.3812	0.3823	0.4113	0.4004	0.3626
P (kbar)	18.07	18.09	18.73	17.31	17.19	20.00
T (°C)	857.72	864.73	892.24	812.32	813.35	962.39

Table 3. Summary table of geothermobarometric calculations.

IV. $^{40}\text{Ar}/^{39}\text{Ar}$ GEOCHRONOLOGY OF LAMPROPHYRE DIKES

Samples M-14C and M-21 are from two NNE-SSW trending lamprophyre dikes in Figure 4. Sample M-14C ($70^{\circ} 52.644'\text{N}$, $22^{\circ} 20.091'\text{W}$) was collected near to where the lamprophyre intruded the contact between the Krummedal Sequence and the Hodal-Storefjord Monzodiorite pluton. Sample M-21 ($70^{\circ} 52.696'\text{N}$, $22^{\circ} 17.493'\text{W}$) was collected where the lamprophyre intruded the Hodal-Storefjord Monzodiorite pluton. The two lamprophyre sampling locations are approximately 0.75 kilometers apart.

Petrography

Sample M-14C contains euhedral phenocrysts of plagioclase and phlogopite with very sharp grain boundaries and little to no alteration (Figure 24A). Phlogopite crystals are strongly pleochroic, changing from a tan-brown to colorless in plane light. Minor inclusions of plagioclase within the phlogopite are common. Phlogopite grains have very prominent mica cleavage traces. Some phlogopite grains may have a radial crystal form, which can be explained by the crystal being cut by the thin section at an odd angle, due to the large size of the phenocrysts. Compositional zoning is ubiquitous in plagioclase phenocrysts (Figure 24B). The matrix comprises very fine grained phlogopite, sodium plagioclase, and opaque minerals. Calcite can be seen filling late stage cracks with the matrix and in the interior portions of some mineral grains. Sample M-21 (Figure 24C) contains the same mineral assemblage as the M-14C lamprophyre. The only difference

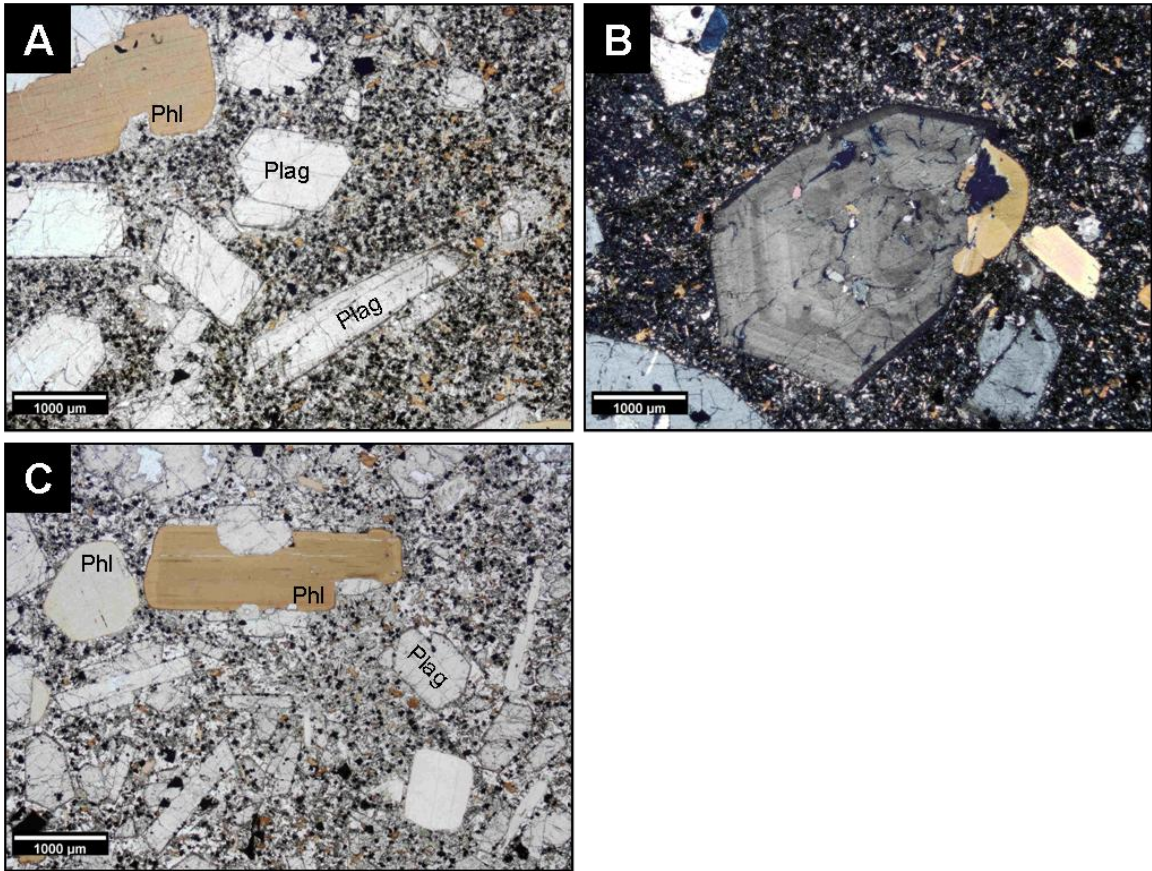


Figure 24. **A.** Photomicrograph in plane light from sample M-14C of euhedral phlogopite and plagioclase phenocrysts within a matrix of phlogopite, plagioclase, and opaques (in images Phl = phlogopite and Plag = plagioclase). **B.** Optically zoned plagioclase phenocryst within M-14C (cross-polarized light). Steel blue birefringence of the plagioclase is believed to be a result of the thin section being slightly too thick. **C.** Phlogopite and plagioclase phenocrysts within M-21 (plane light). Note the radiogenic halo within the tan-brown phlogopite grain in contact with matrix feldspar (lower right).

between the two samples is the matrix of M-21 contains less opaque minerals than M-14C and contains small amounts of chlorite. The presence of phlogopite phenocrysts and sodium plagioclase within the matrix makes both of these lamprophyres of the Kersantite variety.

$^{40}\text{Ar}/^{39}\text{Ar}$ Methods

The lamprophyre samples were crushed and approximately 50 phlogopite grains were picked from each sample using a binocular microscope and were prepared for $^{40}\text{Ar}/^{39}\text{Ar}$ analysis in the Auburn Noble Isotope Mass Analysis Laboratory (ANIMAL). Both Single Crystal Total Fusion (SCTF) and Incremental Heating (IH) techniques were used to analyze the phlogopite grains in order to check for consistency between the methods. Nine grains from each sample were analyzed using SCTF and one grain from each sample was analyzed using IH. Further information concerning $^{40}\text{Ar}/^{39}\text{Ar}$ methods and raw data are included in Appendix C.

$^{40}\text{Ar}/^{39}\text{Ar}$ Results

The IH analyses for sample M-14C provide a plateau age of 261.56 ± 0.38 Ma (calculated with 1σ error and a 95% confidence level; Figure 25) with 96.9% of the total $^{39}\text{Ar}_K$ released. IH analysis was performed for sample M-21, and the data yield a plateau age of 263.93 ± 0.93 Ma (Figure 26) with 97.1% of the total $^{39}\text{Ar}_K$ included. The SCTF analyses all yielded very consistent ages grouping around the plateau age dates. For both samples, the probability that the SCTF data was part of a normal distribution was 0.00%, showing that the age variations seen in the data are due to differences in the age of

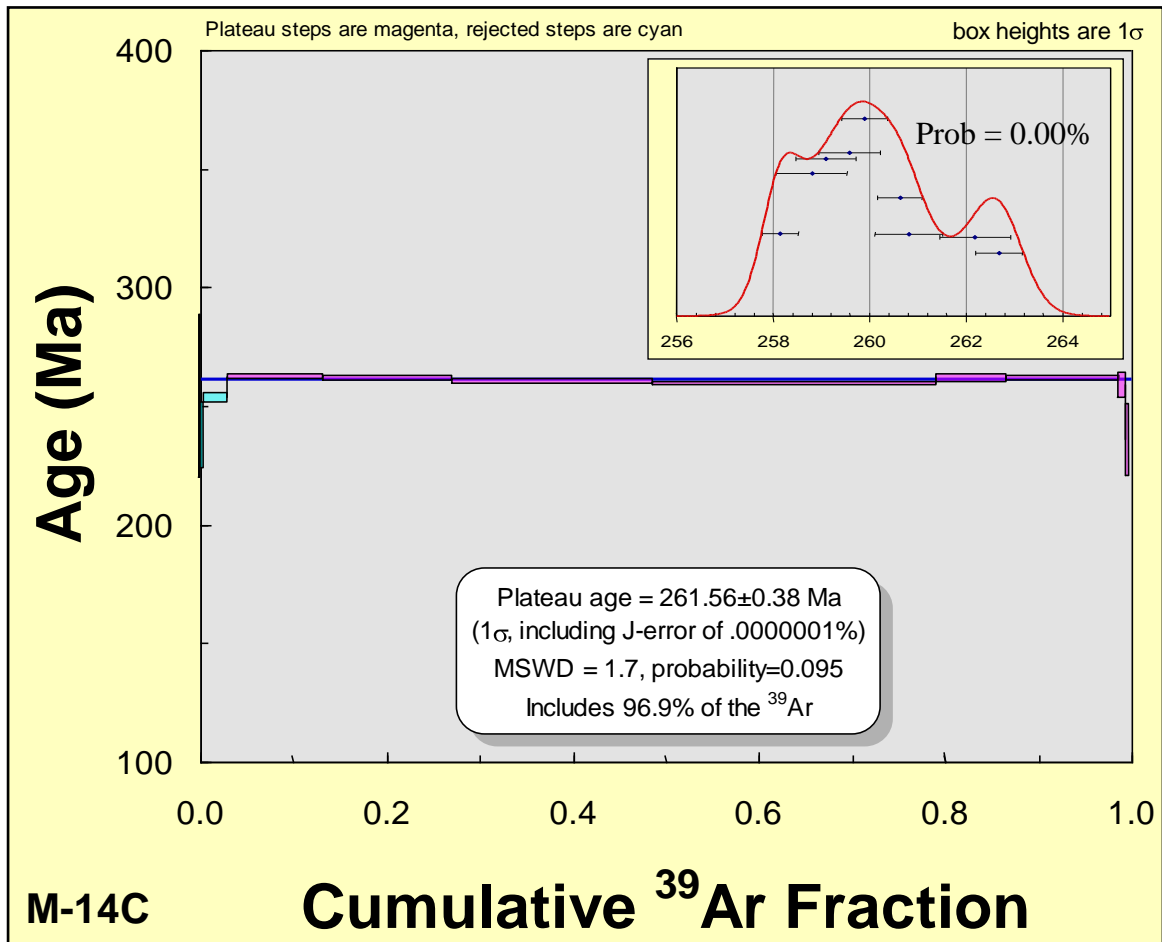


Figure 25. Plateau diagram produced from the incremental heating data collected from sample M-14C. **Inset.** Probability density diagram created from the SCTF data from sample M-14C. Individual crystal data represented as points with error bars (error bars are 1σ). Prob. = the probability that the SCTF data could be part of a normal distribution.

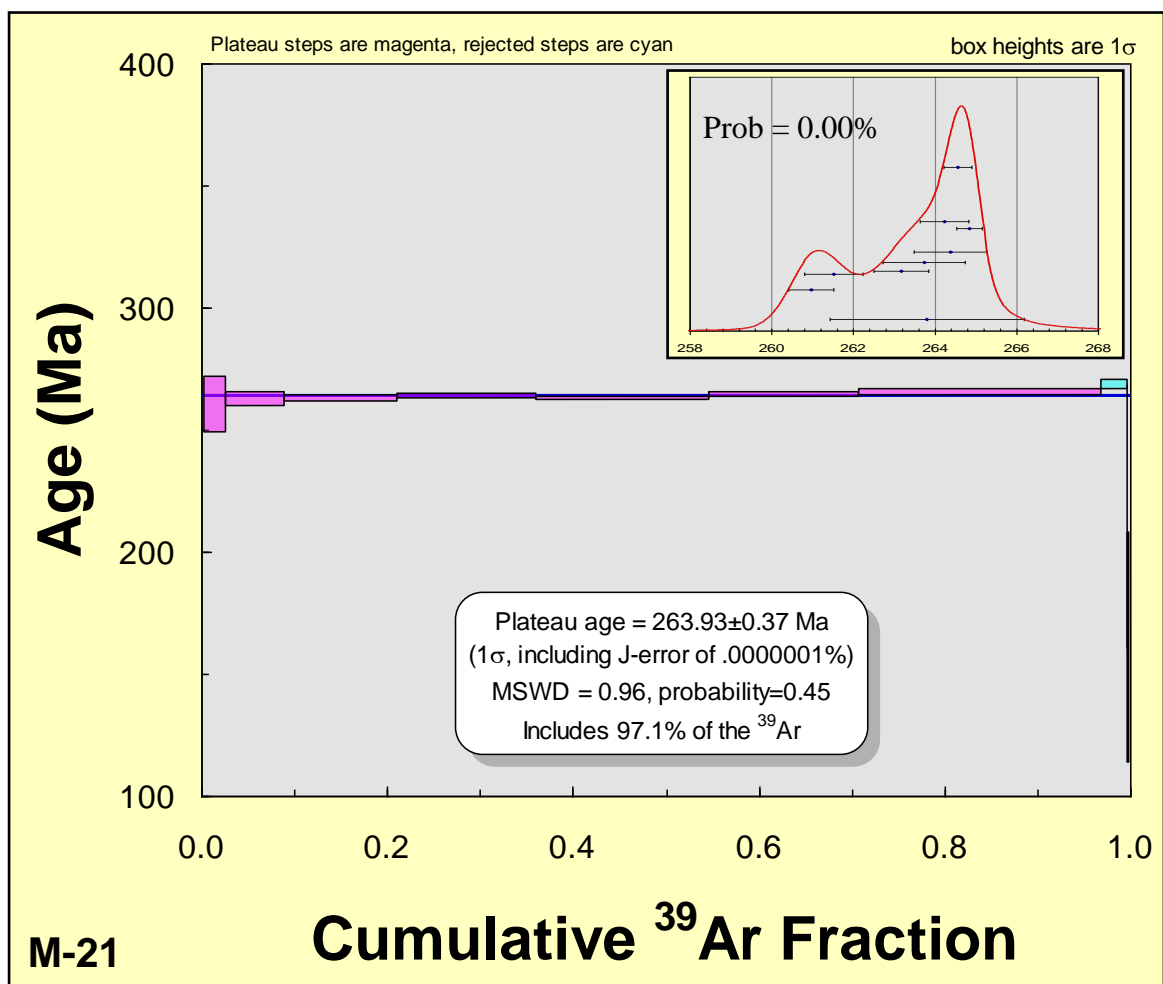


Figure 26. Plateau diagram produced from the incremental heating data collected from sample M-21. **Inset.** Probability density diagram created from the SCTF data from sample M-21. Individual crystal data represented as points with error bars (error bars are 1σ). Prob. = the probability that the SCTF data could be part of a normal distribution.

individual crystals and not internal analytical error. Linear regression of the SCTF data showed no correlation and a tight clustering of data. These results are taken to indicate that extraneous argon is not present in the phlogopite mineral grains analyzed. The results of the laser SCTF and IH analyses for samples M-21C and M-21 are interpreted to indicate lamprophyre crystallization at ca. 262 and 264 Ma.

V. DISCUSSION

To synthesize the tectonic evolution of rocks exposed in Liverpool Land, results from the present study are combined with data from other members of the 2006 expedition, summarized in Table 1. The Gubbedalen Shear Zone is herein interpreted to be essentially a detachment fault along a Caledonian metamorphic core complex (Coney, 1980). As such, the geologic history of the hanging wall is less important to understanding the evolution of the metamorphic core; this is why work was concentrated in the southern map area. Hanging wall block evolution during the Caledonian is linked to the intrusion of the calc-alkaline Hurry Inlet Granite with pulses at 445 and 438 Ma, and the intrusion of the Hodal-Storefjord Monzodiorite at 424 Ma (Augland, 2007).

The orthogneiss terrane of the footwall block to the Liverpool Land metamorphic core complex has a much more varied and significant history in regards to Caledonian evolution than the hanging wall block. The protolith age of the orthogneiss in the footwall is not well dated. An upper intercept age of 1660 Ma on zircons separated from one of the eclogites is interpreted as the time of crystallization for mafic bodies intruded into the gneissic complex (Augland, 2007). Likewise, the first deformational event (D_0) recorded within the footwall block is not absolutely dated. D_0 must occur after the emplacement of mafic bodies within the footwall at 1660 Ma, but before Caledonian migmatization (S_1) that overprints the gneissic foliation (S_0) of the felsic orthogneiss terrane, placing minimum and maximum ages on the timing of deformation.

During D₁, the southern Liverpool Land orthogneiss complex was tectonically buried as the Caledonian orogenic belt grew, initializing migmatization of the orthogneiss (L. Augland, personal communication, 2008). As the footwall block orthogneisses were brought deeper into the crust they reached eclogite-facies conditions (middle D₂ in Table 1) at 399 Ma (Augland, 2007). Results of the present study estimate peak eclogite-facies conditions were achieved at ~867°C and >18.2 kbars, representing a burial depth of approximately 70 kilometers.

Syn-collisional normal faulting is a possible mechanism for exhumation of the high pressure orthogneiss terrane during continental subduction (Figure 27: Chemenda et al., 1995; Chemenda et al., 1996). The continental slab is subducted to a maximum depth, which is proportional to the strength of the crust and inversely proportional to the pressure within the plate created by collision. At maximum depth, the crust fails and imbricates, allowing for buoyancy driven uplift of a subducted crustal slice, as the rest of the lithospheric slab continues to subduct. This uplifting creates reverse movement along the bottom contact of the crustal slice and down-going lithosphere and the appearance of normal movement along the contact of the crustal slice and overriding plate (Chemenda et al., 1995; Chemenda et al., 1996). It appears that the orthogneiss terrane is an uplifted crustal slice that delaminated from the down-going lithosphere; however, the normal fault that brought the eclogite-containing orthogneiss terrane to the surface is not observed within Liverpool Land. This normal fault would have been positioned at a high structural level and may have been cut out by the Gubbedalen Shear Zone or possibly by other post-Caledonian faulting that has segmented and chopped the orogen (Figure 3: Haller, 1985).

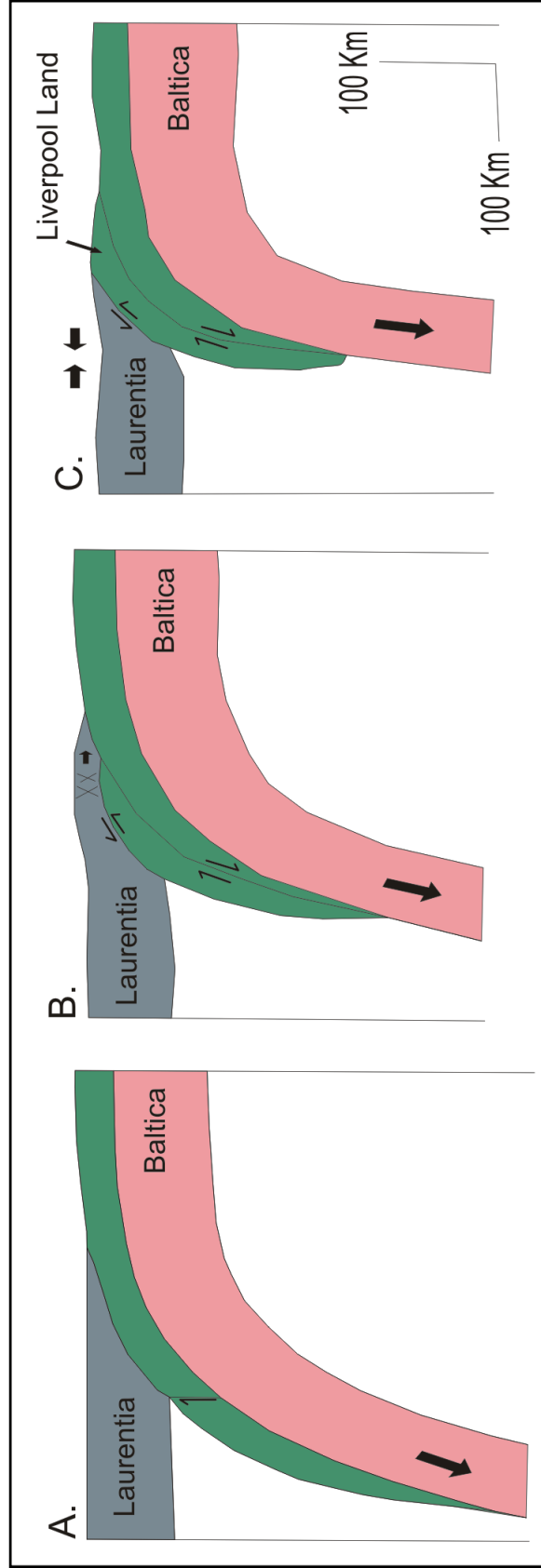


Figure 27. A. Subduction of the Baltic lithospheric slab underneath Laurentia during continental subduction. B. Failure of the upper crust after reaching eclogite-facies conditions, resulting in the uplift of a crustal slice (orthogneiss footwall terrane), creating a sense of normal movement along the contact with the overlying plate. X's represent brittle faulting occurring in the overlying Laurentian crust. C. Continued uplift of the crustal slice to shallow crustal levels (modified from Chemenda et al., 1995).

The Liverpool Land eclogites share a great number of similarities with eclogites of the Western Gneiss Region of Norway, leading the author to suggest that the former may be an orphaned block of the latter that was sutured onto the Laurentian margin, corroborating the idea that the orthogneiss footwall terrane is a crustal slice from the down-going Baltic slab. Paleogeographic reconstructions (Blakey, 2007; Bowman, 2008) depict the Western Gneiss Region adjacent to Liverpool Land during the Silurian collision with Baltica. Eclogites in both regions occur as boudinaged mafic pods within a felsic orthogneiss complex (Dunn and Medaris, 1989). Protolith ages for the eclogites in Liverpool Land and the Western Gneiss Region are comparable (~1660 Ma: Root et al., 2004; Augland, 2007). Likewise, the country rocks of both terranes include ultramafic rocks that are absent outside of the eclogite-bearing terranes (Smith and Cheeney, 1981; Brueckner, 1998). The timing of eclogitization in both regions is also of comparable age (~399 Ma; Root et al., 2004; Augland, 2007). Liverpool Land eclogites are herein found to have formed at temperature and pressure conditions of approximately 867°C and >18.2 kbars. Dunn and Medaris (1989) report Western Gneiss Region eclogites found at ~800°C and > 18-19 kbars. Eclogite-facies mineral compositions also are comparable, and they have very similar coarse-grained wormy symplectites of low-sodium clinopyroxene, plagioclase, and amphibole, after the decompression breakdown of omphacite. All the above mentioned similarities lead the author to interpret that the southern orthogneiss terrane of Liverpool Land is a crustal slice of the Western Gneiss Region left behind in East Greenland.

During the exhumation of southern Liverpool Land, the orthogneiss terrane was brought through granulite-facies conditions (middle D₂) as recorded by the eclogite

symplectites. Upon further exhumation, late D₂ deformation produced mylonitic shears wrapping the eclogite pods as well as the “rogue” shears in the footwall block. The footwall terrane was brought up rapidly to middle-crustal levels where amphibolite-facies metamorphism at approximately 388 Ma (Augland, 2007) caused partial annealing of the fabrics within the mylonites. Wormy low-sodium clinopyroxene-plagioclase-amphibole symplectites like those in the Liverpool Land eclogites have been documented in other continental eclogites and interpreted to have formed due to rapid exhumation (Anderson and Moecher, 2007).

D₃ marks a renewed pulse of contraction along the Gubbedalen Shear Zone, which emplaced the orthogneiss footwall block against the hanging wall block containing the Krummedal Sequence and the Caledonian plutons. D₃ contraction likely cut out the earlier normal fault that exhumed the eclogite-containing orthogneiss terrane. Syntectonic dikes within the Gubbedalen Shear Zone, dated to ~386 Ma (Augland, 2007), likely injected at the beginning of contractional D₃ shearing.

Extensional movement along the Gubbedalen Shear Zone is recorded by D₄ structures. Extensional faults commonly overprint, or reactivate, previously formed thrust faults and have been documented in other parts of East Greenland (Strachan, 1994). Last movements along the Gubbedalen Shear Zone occurred at 380 Ma as dated by ⁴⁰Ar/³⁹Ar analysis of muscovite recovered from rocks within the shear zone (Bowman, 2008). This timing for extensional faulting is synchronous with other Devonian-aged detachment faults within both the East Greenland and Norwegian Caledonides (Figure 28; Braathen et al., 2000; Hartz et al., 2002; Ebbing et al., 2006), and is compatible with

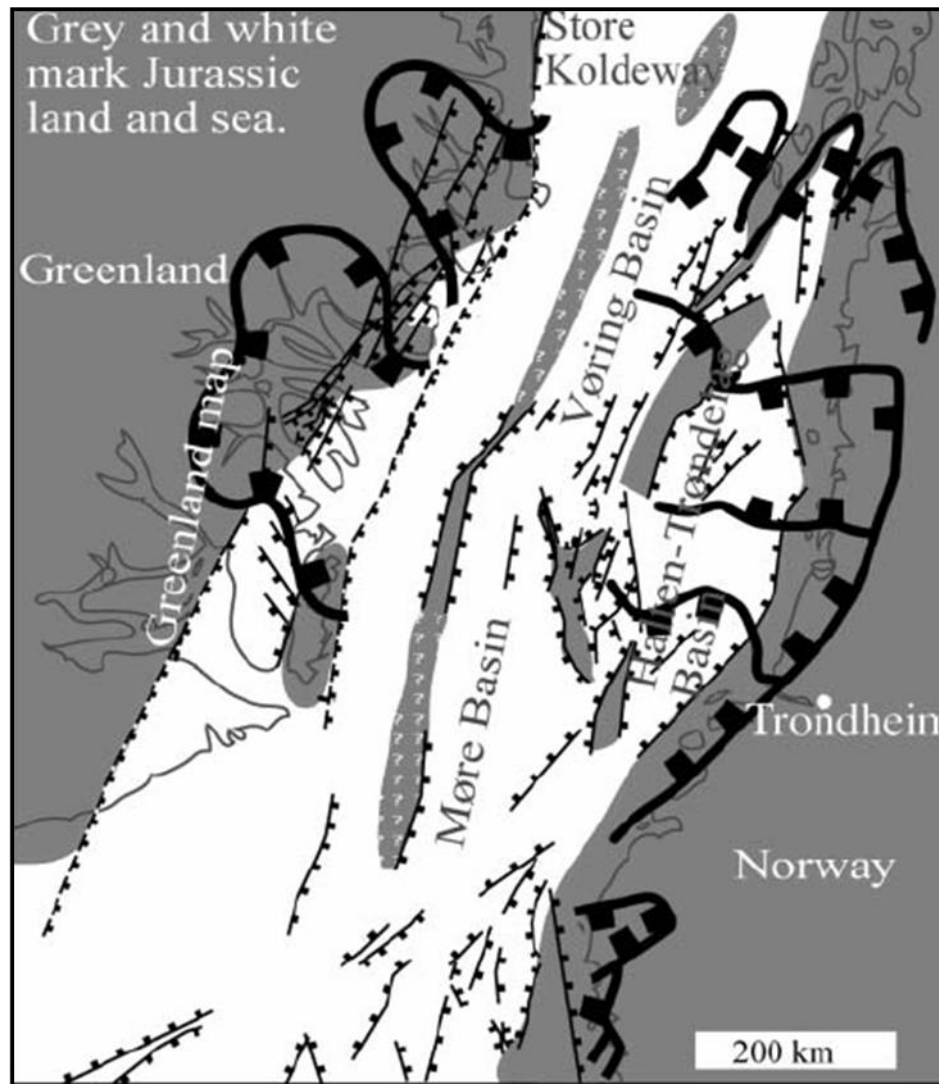


Figure 28. Devonian detachment faults within the East Greenland and Scandinavian Caledonides (Ebbing et al., 2006).

Devonian Sediments having been deposited onto the Hurry Inlet Granite within the hanging wall block of the Gubbedalen Shear Zone (Figure 4).

Lamprophyres in the northern field area record another pulse of extension within East Greenland that occurred during the Late Permian (~262 and ~264 Ma), synchronously with deposition of Permian clastic sediments in Liverpool Land (Figure 3). Paleogeographic plate reconstructions position Liverpool Land near the Lofoten region of north Norway at this time (Figure 29; Blakey, 2007) when the Lofoten metamorphic core complex was forming (Steltenpohl et al., 2004). $^{40}\text{Ar}/^{39}\text{Ar}$ data from both regions overlap on a probability density diagram (Figure 30), implying that Permian extension was occurring on both sides of the orogen as well as further south (i.e., Oslo Rift; Wilson et al., 2004). Sedimentation continued to occur in the region, filling the Triassic and Jurassic basins of Jameson Land to the west of Liverpool Land (Figure 3). Finally, Eocene rifting emplaced basaltic sills and dikes into the Jameson Land sedimentary basins. This rifting covered the southern Scoresby Sund landscape with large volumes of flood basalts (Figure 3).

Alternate Explanation of Liverpool Land Eclogites

To explain the occurrence of eclogites in the Laurentian upper plate of the Caledonian collisional zone, Hartz et al. (2005) suggested that the Liverpool Land eclogites can not be simply attributed to metamorphic processes due to overburden (i.e., pressure to depth relationship). Later, Hartz et al. (2007) hypothesized that eclogite formation was due to the effects of tectonic overpressure, introducing a new theoretical concept of “reaction overpressure.”



Figure 29. Paleogeographic plate reconstruction during the Permian (~260 Ma) showing the Liverpool Land region (red star) against Lofoten, Norway (blue star; Blakey, 2007).

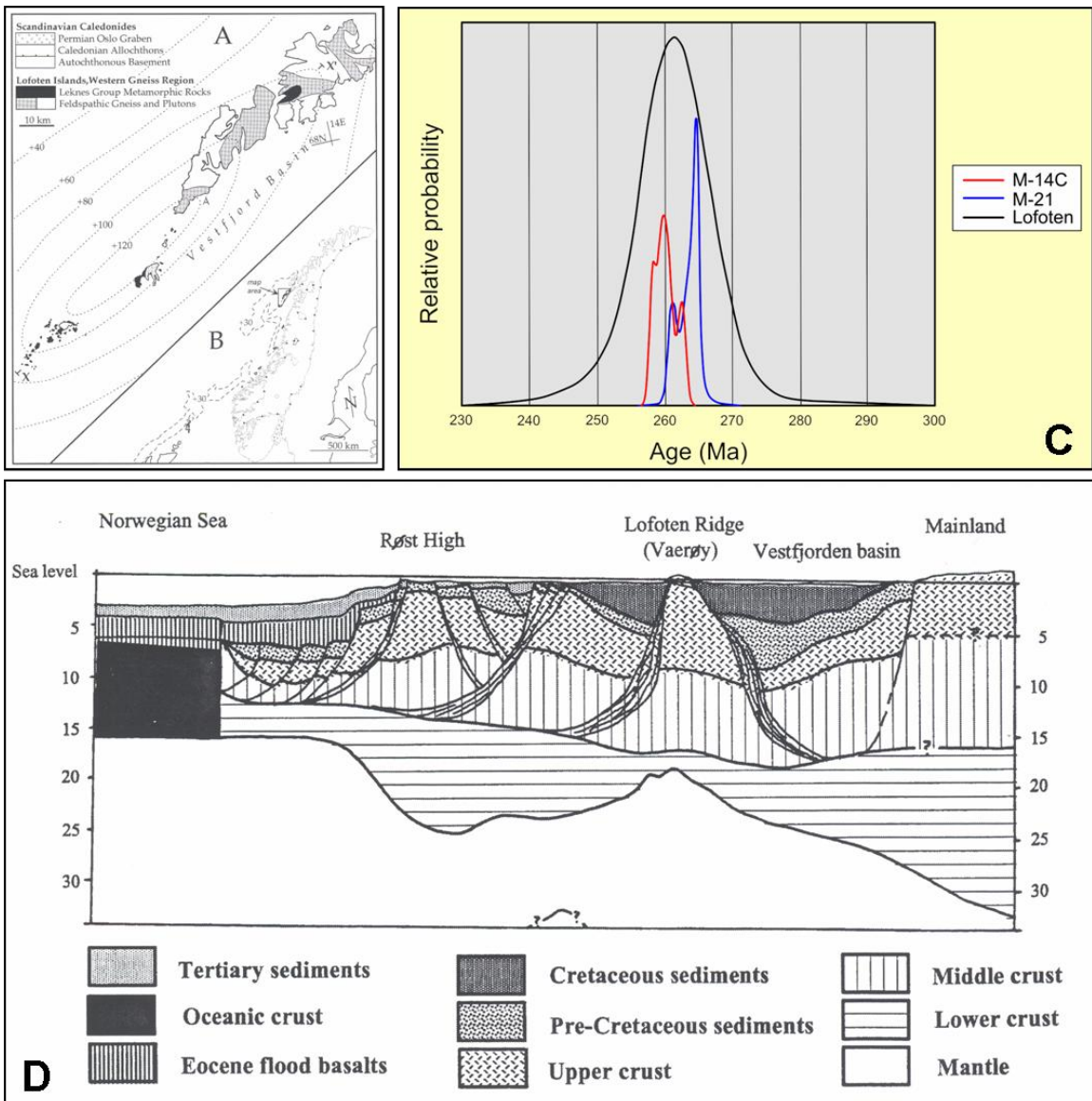


Figure 30. **A** and **B.** Location of the Lofoten Islands of northern Norway (Steltenpohl et al., 2004). **C.** Probability density diagram with hydrothermal muscovite age from Lofoten fault zone in black (data from Steltenpohl et al., 2004) and phlogopite crystallization age from Liverpool Land lamprophyres in blue and red. **D.** Diagram depicting the Permian metamorphic core complex of Lofoten (Steltenpohl et al., 2004).

Tectonic overpressure is the concept that within a convergent tectonic setting, pressure can be considerably higher than lithostatic (pressure = density x gravity x depth). Tectonic overpressure is theoretically created by plate tectonic derived horizontal stresses coupled with flexural vertical loads caused by the deflection of the upper crust and lower mantle during collision (Petrini and Podladchikov, 2000). “Reaction overpressure” as hypothesized by Hartz et al. (2007) is based on the same principle as a pressure cooker. It requires a rock inclusion enclosed in a stronger rock container. As the inclusion is heated, it will start to expand creating ultra-high pressures. When pressures exceed the strength of the container, it will fracture, and Hartz et al. (2007) predicted that the mafic inclusion will show evidence of decompressional melting.

Field observations from this study indicate that tectonic overpressure is not necessary to account for the formation of the eclogites in Liverpool Land. First, the concept of “reaction overpressure” can be dispelled by considering the eclogite-bearing host rocks. In the study area, the eclogite container was the felsic orthogneisses, which were not at all strong and rigid during eclogitization. In all observed cases, the orthogneiss around the eclogite boudins behaved in a plastic manner, resulting in migmatites and mylonites. There are decompressional melts originating within the eclogite pod themselves, but these are more parsimoniously explained by rapid tectonic exhumation of the eclogite terrane. Second, Hartz et al. (2007) presumed that the Liverpool Land eclogite terrane was positioned in the overriding plate of the Caledonian collision, a concept that is challenged by the model for tectonic evolution of the orthogneiss footwall terrane as described in this study.

VI. CONCLUSIONS

Field studies and laboratory analysis on rocks in southern Liverpool Land, East Greenland provide new constraints on Caledonian tectonic evolution in an important area where very little was previously known. Key contributions to this understanding that resulted from the present study are summarized below.

- The relative deformational sequence contained in rocks of Liverpool Land (Table 1) has been constrained for the first time. By combining this relative sequence with previous, ongoing, and new isotopic work reported herein, the absolute sequencing of metamorphic and deformational episodes has also been outlined for the first time.
- The Gubbedalen Shear Zone was discovered and documented by the 2006 expedition team. Work presented herein documents that the Gubbedalen Shear Zone is a greenschist-facies, east-west trending, shallowly to moderately north-dipping shear zone that is approximately 500 meters thick. The lower 400 meters of the shear zone records tops-up-to-the-south reverse dip-slip motion, and the upper 100 meters is characterized by tops-north, down-dip, extensional movement.
- Little had been published about the petrography and pressure-temperature conditions of eclogite-facies metamorphism within rocks of Liverpool Land. Geothermobarometric calculations conducted using microprobe data determined

that peak conditions of eclogitization occurred at $\sim 867^{\circ}\text{C}$ and >18.2 kbars.

Petrographic studies document granulite-facies symplectic replacement textures formed after the decompressional breakdown of omphacite, aiding in our understanding of the exhumation history of these lower-crustal continental basement rocks.

- Lamprophyre dikes in the northern field area were shown on the geologic map (Friderichsen and Surlyk, 1976) but have never been described or dated. The age of intrusion is particularly important for understanding their significance for the extensional evolution of East Greenland; based on what was previously known, these dikes could have intruded at any point between the Middle Devonian and the Eocene, a 300 million year gap of time. I used $^{40}\text{Ar}/^{39}\text{Ar}$ methods to separate and date phlogopite grains from the lamprophyres. The resulting 262 Ma and 264 Ma dates are interpreted to record the time of intrusion, which helps us to understand that the Permian was an important period of extension in East Greenland and now must be considered together with related Permian extension in Norway (i.e., Lofoten and the Oslo graben).

Through the course of this research, it has become evident that further research needs to be conducted on rocks in Liverpool Land. First, granulite- and amphibolite-facies metamorphism was recognized to have variably retrograded the high-pressure assemblages in the eclogite pods but only amphibolite-facies assemblages were found within the country rocks that encapsulate them. Microprobe analyses and geothermobarometric information constraining the pressure and temperature conditions

for both the granulite- and amphibolite-facies portions of this retrograde path would be important to further understand their exhumation history. Secondly, additional geochronologic and thermochronologic studies are needed on rocks from the orthogneiss terrane to determine the timing of protolith emplacement and to further constrain the timing of the Caledonian migmatization and subsequent exhumation. Lastly, in this thesis, most of the field studies and laboratory analyses were focused on the Gubbedalen Shear Zone and the eclogite-containing footwall terrane. The hanging wall block needs to be mapped and characterized in much greater detail, especially the rocks within the Krummedal Sequence, which are lithologically variable and have uncertain tectonostratigraphic affinities.

REFERENCES CITED

- Anderson, E.D., and Moecher, D.P., 2007, Omphacite breakdown reactions and relation to eclogite exhumation rates: *Contributions to Mineralogy and Petrology*, v. 154, p. 253-277.
- Augland, L.E., 2007, The Gubbedalen Shear Zone; a terrane boundary in the East Greenland Caledonides: Master's Thesis in Geosciences, University of Oslo, p. 127.
- Blakey, R.B., 2007, Paleogeography and geologic evolution of North America: <http://jan.ucc.nau.edu/~rcb7/nam.htm>.
- Braathen, A., Nordgulen, Ø., Osmundsen, P.T., Andresen, T.B., Solli, a., and Roberts, D., 2000, orogen-parallel, opposed extension in the Central Norwegian Caledonides: *Geology*, vol. 28, p. 615-618.
- Brueckner, H.K., 1998, Sinking intrusion model for the emplacement of garnet-bearing peridotites into continent collision orogens: *Geology*, vol. 26, no. 7, p. 631-634.
- Bowman, D.R., 2008, Exhumation history of Caledonian eclogites in Liverpool Land, East Greenland, and comparisons with eclogite in Norway: Master's Thesis in Geology, Auburn University, p. 99.
- Buchanan, J.W., Bowman, D., Steltenpohl, M.G., Augland, L.E., and Andresen, A., 2007, Discovery of the Gubbedalen Shear Zone (GSZ): An important terrane boundary within the East Greenland Caledonides of Liverpool Land: *Geological Society of America Abstracts with Programs*, v. 39, no. 2, p. 81.
- Chemenda, A.I., Mattauer, M., Malavieille, J., and Bokun, A.N., 1995, A mechanism for syn-collisional rock exhumation and associated normal faulting: Results from physical modeling: *Earth and Planetary Science Letters*, v. 132, p. 225-232.
- Chemenda, A.I., Mattauer, M., and Bokun, A.N., 1996, Continental subduction and a mechanism for exhumation of high-pressure metamorphic rocks: new modeling and field data from Oman: *Earth and Planetary Science Letters*, v. 143, p. 173-182.
- Coe, K., 1975. The Hurry Inlet granite and related rocks of Liverpool Land, East Greenland. *Grønlands Geologiske Undersøgelse Bulletin*, v. 115, p. 34.

- Coe, K. and Cheeney, R. F., 1972, Preliminary results of mapping in Liverpool Land, East Greenland: Rapport Grønlands Geologiske Undersøgelse, v. 48, p. 7-20.
- Coleman, R.G., Lee, D.E., Beatty, L.B. and Brannock, W.W., 1965, Eclogites and eclogites: the differences and similarities: Bulletin of the Geological Society of America, v. 76, p. 483-580.
- Coney, P.J., 1980, Cordilleran metamorphic core complexes: An overview: Geological Society of America Memoir 153, p. 7-31.
- Cox, S.G., Griffin, P.F., Adams, C.S., DeMille, D., and Riis, E., 2003, Reusable ultrahigh vacuum viewport bakeable to 240 C: Review of Scientific Instruments, v. 74, no. 6, p. 3185-3187.
- Cross, W.G., 1951, Two-directional focusing of charged particles with a sector-shaped, uniform magnetic field: Reviews of Scientific Instruments, v. 22, p. 717-722.
- Deer, W.A., Howie, R.A., and Zussman, J., 1992, An introduction to the rock-forming minerals: John Wiley and Sons, New York.
- Droop, G.T.R., 1987, A general equation for estimating Fe³⁺ concentrations in ferromagnesian silicates and oxides from microprobe analyses, using stoichiometric criteria: Mineralogical Magazine, v. 51, p. 431-435.
- Dunn, S.R., and Medaris, L.G., 1989, Retrograded eclogites in the Western Gneiss Region, Norway, and thermal evolution of a portion of the Scandinavian Caledonides: Lithos, v. 22, p. 229-245.
- Ebbing, J., Lundin, E., Olesen, O., and Hanses, E.K., 2006, The mid-Norwegian margin: a discussion of crustal lineaments, mafic intrusions, and remnants of the Caledonian root by 3D density modeling and structural interpretation: Journal of the Geological Society, London, vol. 163, p. 47-59.
- Ellis, D.J. and Green, D.H., 1979, An experimental study of the effect of Ca upon garnet-clinopyroxene Fe-Mg exchange equilibria: Contributions to Mineralogy and Petrology, vol. 71, p. 13-22.
- Fossen, personal communication to M.G. Steltenpohl, 2005.
- Friderichsen, J.D., and Surlyk, F. (eds), 1976, Hurry Inlet 70 Ø.1 Nord, Danmark Grønland 1:100,000: Grønlands Geologiske Undersøgelse.

- Gilotti, J.A., and Ravna, E.J.K., 2002, First evidence for ultra-high pressure metamorphism in the North-East Greenland Caledonides: *Geology*, v. 30, p. 551-554.
- Haller, J., 1971, *Geology of the East Greenland Caledonides*: New York, Interscience Publishers, 415 p.
- Haller, J., 1985, The East Greenland Caledonides – reviewed. In: Gee, D.G., and Sturt, B.A. (eds): *The Caledonide Orogen – Scandinavia and Related Areas*: John Wiley and Sons Ltd, 1985.
- Hansen, B. T. and Steiger, R. H., 1971. The Geochronology of the Scoresby Sund area. *Rapport Grønlands Geologiske Undersøgelse*, 37: 55-57.
- Hartz, E.H., Eide, E.A., Andresen, A., Midbøe, P., Hodges, K.V., and Kristiansen, S.N., 2002, $^{40}\text{Ar}/^{39}\text{Ar}$ geochronology and structural analysis: basin evolution and detrital feedback mechanisms, Hold with Hope region, East Greenland: *Norsk Geologisk Tidsskrift*, Vol. 82, p. 341-358.
- Hartz, E.H., Condon, D. Austrheim, H., and Erambert, M., 2005, Rediscovery of the Liverpool Land eclogites (Central East Greenland): A post and supra-subduction UHP province: *Mitteilungen der Österreichischen Mineralogischen Gesellschaft*, v. 150, abstract.
- Hartz, E.H., Podladchikov, Y.Y., and Dabrowski, M., 2007, Tectonic and reaction overpressure: Theoretical models and natural examples: *Geophysical Research Abstracts*, v. 9, 10430.
- Henriksen, N., Higgins, A.K., Kalsbeek, F. & Pulvertaft, T.C.R. 2000: Greenland from Archaean to Quaternary. Descriptive text to the Geological map of Greenland, 1:2 500 000. *Geology of Greenland Survey Bulletin*: vol. 185, pp. 93.
- Higgins, A.K., 1988, The Krummedal supracrustal sequence in East Greenland, in Winchester, J.A., ed., *Later Proterozoic stratigraphy of the northern Atlantic regions*: Glasgow and London, Blackie and Sons Ltd., p. 86-96.
- Higgins, A. K. and A. G. Leslie, A. G., 2000, Restoring thrusting in the East Greenland Caledonides: *Geology*, v. 28, p. 1019-1022.
- Hodges, K.V., Bartley, J.M., and Burchfiel, B.C., 1982, Structural evolution of an A-type subduction zone, Lofoten Rombak area, Northern Scandinavian Caledonides: *Tectonics*, v.1, p. 441-462.
- Holland, T.J.B., 1980, The reaction albite = jadeite + quartz determined experimentally in the range 600-1200°C: *American Mineralogist*, v. 65, p. 129-134.

- Holland, T.J.B., 1979, Reversed hydrothermal determination of jadeite-diopside activities: EOS, v. 60, p. 405.
- Kalsbeek, F., Nutman, A.P., and Jepsen, H.F., 1998, Granites in the Caledonian fold belt, East Greenland. In: Frederiksen, K.S., and Thrane, K. (eds): Symposium on Caledonian geology in East Greenland. Danmarks og Grønlands Geologiske Undersøgelse Rapport, 1998.
- Kranck, E. H., 1935. On the crystalline complex of Liverpool Land. Meddelelser om Grønland, 95(7): 1-122.
- Krogh Ravn, E., 2000, The garnet-clinopyroxene Fe²⁺-Mg geothermometer: an updated calibration: Journal of Metamorphic Geology, v. 18, p. 211-219.
- Ludwig, K.R., 2003, User's manual for Isoplot, v. 3.0, a geochronological toolkit for Microsoft Excel: Berkeley Geochronological Center, Special Publication no. 4
- Mandler, H.A.F., and Jokat, W., 1998, The crustal structure of central East Greenland: results from combined land – sea seismic refraction experiments: Geophysical Journal International, vol. 135, p. 63-76.
- McDougall, I. and Harrison, T.M., 1999, Geochronology and Thermochronology by the ⁴⁰Ar/³⁹Ar Method, 2nd edn: Oxford University Press, Oxford, p. 269.
- Morimoto, N., Fabries, J., Ferguson, A.K., Ginzburg, I.V., Ross, M., Siefert, F.A., Zussman, J., Aoki, K., Gottardi, G., 1988, Nomenclature of pyroxenes: American Mineralogist, v. 73, p. 1123-1133.
- Petrini, K., and Podladchikov, Y., 2000, Lithospheric pressure-depth relationship in compressive regions of thickened crust: Journal of Metamorphic Geology, v. 18, p. 67-77.
- Renne, P.R., Swisher, C.C., Deino, A.L., Karner, D.B., Owens, T.L., and DePaolo, D.J., 1998, Intercalibration of standards, absolute ages and uncertainties in ⁴⁰Ar/³⁹Ar dating: Chemical Geology, v. 145, no.1-2, p. 117-152
- Roberts, D. and Gee, D.G, 1985, An introduction to the structure of the Scandinavian Caledonides, in Gee, D.G., and Sturt, B.A. eds., The Caledonian Orogen-Scandinavia and Related Areas: London, Wiley & Sons, p. 55-68.
- Root, D. B., Hacker, B. R., Mattinson, J. M. and Wooden, J. L., 2004, Zircon geochronology and ca. 400 Ma exhumation of Norwegian ultrahigh pressure rocks; an ion microprobe and chemical abrasion study: Earth and planetary science letters, vol. 228, no. 3-4, p. 325-341.

Sahlstein, T. G., 1935. Petrographie der Eklogiteinschlüsse in den Gneisen des südwestlichen Liverpool-Landes in Ost-Grønland. *Meddelelser om Grønland*, 95(5): 1-43.

Scholz, C.H., 1988, The brittle-plastic transition and the depth of seismic faulting: *Geologische Rundschau*, vol. 77, p. 319-329.

Simpson, C., and Wintsch, R.P., 1989, Evidence for deformation-induced K-feldspar replacement by mermerite: *Journal of Metamorphic Geology*, vol. 7, no. 2, p. 261-275.

Smith, D. C. and Cheeney, R. F., 1981, A new occurrence of garnet-ultrabasic in the Caledonides; a Cr-rich chromite-garnet-ilmenite from Tvaerdalen, Liverpool Land, East Greenland: *Terra cognita*, vol. 1, no. 1, p. 74.

Stampfli, 2004, Tethyan Plate Tectonic Home Page: last updated 9-10-2004, accessed 2-4-2008, http://www.sst.unil.ch/Research/plate_tecto/index_files/Caledonides.gif.

Steltenpohl, M.G., Hames, W.E., Andresen, A., 2004, The Silurian to Permian history of a metamorphic core complex in Lofoten, northern Scandinavian Caledonides: *Tectonics*, vol. 23.

Strachan, R. A., 1994. Evidence in North-East Greenland for late Silurian - early Devonian regional extension during the Caledonian orogeny: *Geology*, v.22, p. 916-916.

Strachan, R.A., Nutman, A.P., and Friderichsen, J.D., 1995, SHRIMP U-Pb geochronology and metamorphic history of the Smaldefjord sequence, NE Greenland Caledonides: *Journal of the Geological Society (London)*, vol. 152, p. 779-784.

Wilson, M., Neuman, E.R., Davies, G.R., Timmerman, M.J., Heeremans, M., and Larsen, B.T., 2004, Permo-Carboniferous magmatism and rifting in Europe: introduction: *Geological Society (London), Special Publications*, vol. 223, p. 1-10

APPENDIX A
STRUCTURAL DATA AND STATION LOCATIONS

Appendix A contains structural data obtained from metamorphic and mylonitic fabrics at specified stations. Station locations are given by latitude and longitude coordinates. The structural data are divided based on deformation history using the aforementioned nomenclature. The data are reported using azimuth directions and the right hand rule.

CP-2A	Latitude N:	70° 35.522'			
	Longitude W:	22° 14.114'			
Fabric	Strike	Dip	Lineation	Bearing	Plunge
S ₀	273	19	L ₀	174	13
S ₀	76	26			
CP-3	Latitude N:	70° 36.046'			
	Longitude W:	22° 14.530'			
Fabric	Strike	Dip	Lineation	Bearing	Plunge
C Plane	273	21	L ₀	8	37
S Plane	279	59			
CP-4	Latitude N:	70° 36.089'			
	Longitude W:	22° 15.229'			
Fabric	Strike	Dip	Lineation	Bearing	Plunge
S ₀	273	19	L ₀	3	18
CP-5	Latitude N:	70° 35.086'			
	Longitude W:	22° 14.245'			
Fabric	Strike	Dip			
S ₀	218	38			
CP-6	Latitude N:	70° 35.216'			
	Longitude W:	22° 14.191'			
Fabric	Strike	Dip			
S ₀	223	40			
CP-7	Latitude N:	70° 35.210'			
	Longitude W:	22° 14.256'			
Fabric	Strike	Dip	Lineation	Bearing	Plunge
S ₁	203	30	L ₁	358	31
CP-9	Latitude N:	70° 35.078'			
	Longitude W:	22° 14.001'			
			Lineation	Bearing	Plunge
			L ₂	143	14
			L ₂	358	29
			L ₂	8	25
			L ₂	12	21

CP-10	Latitude N:	70° 35.044'			
	Longitude W:	22° 13.872'			
Fabric	Strike	Dip	Lineation	Bearing	Plunge
S ₂	23	24	L ₂	168	3
S ₂	310	12	L ₂	346	2
			L ₂	158	24
			L ₂	353	11
			L ₂	348	4
			L ₂	358	13
CP-11	Latitude N:	70° 34.978'			
	Longitude W:	22° 13.767'			
Fabric	Strike	Dip	Lineation	Bearing	Plunge
S ₁	57	6	L ₁	175	11
S ₁	84	12	L ₁	186	11
			L ₁	354	15
CP-13	Latitude N:	70° 34.929'			
	Longitude W:	22° 13.567'			
Fabric	Strike	Dip			
S ₁	348	16			
CP-14	Latitude N:	70° 34.781'			
	Longitude W:	22° 13.460'			
Fabric	Strike	Dip	Lineation	Bearing	Plunge
S ₁	203	7	L ₁	354	2
CP-16	Latitude N:	70° 34.669'			
	Longitude W:	22° 13.298'			
Fabric	Strike	Dip	Lineation	Bearing	Plunge
S ₂	343	15	L ₂	358	4
CP-18	Latitude N:	70° 34.778'			
	Longitude W:	22° 14.165'			
Fabric	Strike	Dip	Lineation	Bearing	Plunge
C Plane	213	42	L ₂	38	4
S Plane	278	40	L ₂	30	15
S ₂	208	40			
CP-20	Latitude N:	70° 34.583'			
	Longitude W:	22° 14.295'			
Fabric	Strike	Dip	Lineation	Bearing	Plunge
S ₁	33	4	L ₁	3	0

CP-21	Latitude N:	70° 34.478'			
	Longitude W:	22° 14.586'			
Fabric	Strike	Dip			
S ₀	353	75			
CP-22	Latitude N:	70° 34.476'			
	Longitude W:	22° 14.882'			
Fabric	Strike	Dip	Lineation	Bearing	Plunge
S ₁	346	37	L ₂	173	10
S ₁	355	54			
S ₂	138	28			
CP-23	Latitude N:	70° 34.471'			
	Longitude W:	22° 15.012'			
Fabric	Strike	Dip			
S ₂	358	11			
S ₂	313	15			
S ₂	292	19			
CP-24	Latitude N:	70° 34.336'			
	Longitude W:	22° 14.624'			
Fabric	Strike	Dip	Lineation	Bearing	Plunge
S ₁	278	20	L ₁	3	23
CP-25	Latitude N:	70° 34.524'			
	Longitude W:	22° 13.822'			
Fabric	Strike	Dip	Lineation	Bearing	Plunge
S ₂	248	20	L ₂	322	24
CP-27	Latitude N:	70° 35.455'			
	Longitude W:	22° 13.200'			
Fabric	Strike	Dip	Lineation	Bearing	Plunge
S ₀	268	54	L ₀	310	43
CP-28	Latitude N:	70° 35.472'			
	Longitude W:	22° 13.124'			
Fabric	Strike	Dip			
S ₀	263	56			
CP-30	Latitude N:	70° 35.655'			
	Longitude W:	22° 12.735'			
Fabric	Strike	Dip			
C Plane	232	56			
S Plane	256	58			

CP-31	Latitude N:	70° 35.644'			
	Longitude W:	22° 12.763'			
Fabric	Strike	Dip			
S ₁	247	86			
CP-32	Latitude N:	70° 35.664'			
	Longitude W:	22° 12.734'			
Fabric	Strike	Dip			
S ₂	256	74			
S ₂	274	51			
CP-34					
Fabric	Strike	Dip	Lineation	Bearing	Plunge
C Plane	243	68	L ₂	13	58
S Plane	278	59			
CP-35	Latitude N:	70° 35.653'			
	Longitude W:	22° 13.486'			
			Lineation	Bearing	Plunge
			L ₂	3	43
			L ₂	8	39
			L ₂	350	39
CP-36	Latitude N:	70° 35.669'			
	Longitude W:	22° 13.509'			
Fabric	Strike	Dip	Lineation	Bearing	Plunge
S ₁	253	63	L ₁	3	45
S ₂	264	38	L ₂	4	35
CP-40	Latitude N:	70° 34.022'			
	Longitude W:	22° 11.621'			
Fabric	Strike	Dip	Lineation	Bearing	Plunge
S ₀	108	24	L ₀	18	25
CP-42	Latitude N:	70° 34.520'			
	Longitude W:	22° 13.137'			
Fabric	Strike	Dip			
S ₀	100	10			
CP-50	Latitude N:	70° 34.867'			
	Longitude W:	22° 15.260'			
Fabric	Strike	Dip	Lineation	Bearing	Plunge
S ₁	280	10	L ₁	340	10

CP-56	Latitude N:	70° 34.888'			
	Longitude W:	22° 16.321'			
Fabric	Strike	Dip	Lineation	Bearing	Plunge
S ₀	15	24	L ₀	202	5
S ₁	65	6	L ₁	4	4
CP-58	Latitude N:	70° 35.679'			
	Longitude W:	22° 15.183'			
Fabric	Strike	Dip	Lineation	Bearing	Plunge
S ₁	192	30	L ₁	325	24
S ₁	208	45	L ₁	312	47
CP-60	Latitude N:	70° 35.864'			
	Longitude W:	22° 16.333'			
Fabric	Strike	Dip	Lineation	Bearing	Plunge
S ₁	290	8	L ₁	352	7
S ₂	338	19	L ₂	190	10
CP-62	Latitude N:	70° 35.707'			
	Longitude W:	22° 17.968'			
Fabric	Strike	Dip			
S ₀	325	90			
CP-65	Latitude N:	70° 36.171'			
	Longitude W:	22° 18.168'			
Fabric	Strike	Dip	Lineation	Bearing	Plunge
S ₀	245	52	L ₀	358	51
CP-66	Latitude N:	70° 36.463'			
	Longitude W:	22° 18.190'			
Fabric	Strike	Dip			
S ₀	270	50			
CP-67	Latitude N:	70° 36.455'			
	Longitude W:	22° 17.954'			
Fabric	Strike	Dip	Lineation	Bearing	Plunge
S ₂	270	40	L ₂	1	39

CP-70	Latitude N:	70° 35.779'			
	Longitude W:	22° 13.477'			
Fabric	Strike	Dip	Lineation	Bearing	Plunge
S ₂	271	24	L ₂	2	5
			L ₂	10	24
			L ₂	9	32
			L ₂	2	25
			L ₂	358	15
			L ₂	1	26
			L ₂	4	11
			L ₂	4	30
CP-71	Latitude N:	70° 35.892'			
	Longitude W:	22° 13.357'			
Fabric	Strike	Dip	Lineation	Bearing	Plunge
S ₂	273	38	L ₂	6	39
CP-72	Latitude N:	70° 35.892'			
	Longitude W:	22° 13.357'			
Fabric	Strike	Dip	Lineation	Bearing	Plunge
S ₂	278	31	L ₂	2	31
CP-73	Latitude N:	70° 36.039'			
	Longitude W:	22° 12.995'			
Fabric	Strike	Dip	Lineation	Bearing	Plunge
S ₂	274	26	L ₂	4	27
S ₂	280	22	L ₂	14	10
S ₂	280	24	L ₂	9	25
CP-74	Latitude N:	70° 36.217'			
	Longitude W:	22° 13.095'			
Fabric	Strike	Dip	Lineation	Bearing	Plunge
S ₂	279	41	L ₂	6	33
S ₂	272	15	L ₂	12	12
CP-75	Latitude N:	70° 36.255'			
	Longitude W:	22° 13.267'			
Fabric	Strike	Dip	Lineation	Bearing	Plunge
S ₂	250	29	L ₂	5	30

CP-76	Latitude N:	70° 36.271'			
	Longitude W:	22° 13.196'			
Fabric	Strike	Dip			
C Plane	250	35			
S Plane	250	51			
CP-77	Latitude N:	70° 36.317'			
	Longitude W:	22° 13.207'			
Fabric	Strike	Dip	Lineation	Bearing	Plunge
S ₂	280	25	L ₂	6	28
CP-78	Latitude N:	70° 36.290'			
	Longitude W:	22° 16.493'			
Fabric	Strike	Dip	Lineation	Bearing	Plunge
S ₂	283	42	L ₂	2	44
			L ₂	356	6
CP-83	Latitude N:	70° 36.323'			
	Longitude W:	22° 15.390'			
Fabric	Strike	Dip	Lineation	Bearing	Plunge
S ₂	260	44	L ₂	34	24
CP-84	Latitude N:	70° 35.106'			
	Longitude W:	22° 14.058'			
	S ₂			L ₂	
	Strike	Dip		Bearing	Plunge
84.1	58	11	84.1	138	15
84.2	85	12	84.2	139	15
84.3	45	16	84.3	140	19
84.4	82	18	84.4	146	15
84.5	40	17	84.5	154	17
84.6	8	30	84.6	120	24
84.7	344	34	84.7	148	9
84.8	5	20	84.8	144	19
84.9	16	15	84.9	136	14
84.10	340	34	84.10	141	11
84.11	342	14	84.11	140	4
84.12	310	25	84.12	338	8
84.13	270	17	84.13	323	14
84.14	200	30	84.14	312	17
84.15	196	6	84.15	314	5

CP-85	Latitude N:	70° 34.875'			
	Longitude W:	22° 13.943'			
Fabric	Strike	Dip	Fabric	Bearing	Plunge
S ₂	243	7	L ₂	8	35
			L ₂	357	20
			L ₂	355	22
			L ₂	2	37
			L ₂	0	44
			L ₂	4	38
			L ₂	340	4
CP-87	Latitude N:	70° 34.976'			
	Longitude W:	22° 12.567'			
Fabric	Strike	Dip	Fabric	Bearing	Plunge
S ₂	140	17	L ₂	170	11
CP-88	Latitude N:	70° 35.190'			
	Longitude W:	22° 11.210'			
Fabric	Strike	Dip	Fabric	Bearing	Plunge
S ₂	52	41	L ₂	168	44
CP-89	Latitude N:	70° 35.296'			
	Longitude W:	22° 10.385'			
Fabric	Strike	Dip	Fabric	Bearing	Plunge
S ₂	130	18	L ₂	155	4
M-10	Latitude N:	70° 51.573'			
	Longitude W:	22° 19.459'			
Fabric	Strike	Dip			
S ₁	126	31			
M-11	Latitude N:	70° 52.378'			
	Longitude W:	22° 19.255'			
Fabric	Strike	Dip			
S ₁	150	82			

APPENDIX B

MINERAL CHEMISTRY DATA FROM MICROPROBE ANALYSIS

PART I

Appendix B, Part I contains mineral chemical data obtained from microprobe analysis performed at the Institute of Geosciences, University of Oslo, Norway, under the supervision of Dr. Muriel Erambert. The data were collected on the 29th, 30th, and 31st of May 2007. Pyroxene, garnet, plagioclase, and amphibole were analyzed from three eclogite samples, CP-47, CP-52A, and CP-92, which represented a spectrum of retrogression. The following tables are grouped by sample number and mineral type. The number at the top of the column corresponds to the order of the analyses done in a particular day.

Quantitative analyses were performed in Wavelength-Dispersive System (WDS) mode on a Cameca Sx100 electron microprobe. Analytical conditions were: accelerating voltage 15 kV, current 15 nA, and counting time 10 s on peak (and 5 s on each background position). Na and K were analyzed first. Calibration standards were wollastonite (Ca and Si), MgO (Mg), Al₂O₃ (Al), Fe metal, pyrophanite (Mn and Ti), Cr₂O₃ (Cr), orthoclase (K), albite and omphacite. For pyroxene, garnet, and amphibole analyses, a focused electron beam was used, but when analyzing feldspars a defocalized electron beam with a diameter of 10 micrometers was used, due to the sensitivity of feldspar to the electron beam. Qualitative Energy-Dispersive System (EDS) analysis was used to quickly identify minerals prior to WDS analysis. The Cameca Sx100 is fitted with an EDS system from Princeton Gamma Tech.

MICROPROBE ANALYSES OF PYROXENE FROM ECLOGITE SAMPLE CP-47

	#1	#7	#8	#11	#14	#15	#24	#26	#31	#32	#33	#39	#43	#45
<u>Weight % oxide</u>														
SiO ₂	51.268	49.229	49.993	49.858	50.141	50.553	51.379	50.472	50.791	49.858	50.799	50.699	50.455	51.052
TiO ₂	0.244	0.344	0.367	0.432	0.375	0.305	0.255	0.289	0.227	0.240	0.235	0.259	0.275	0.217
Al ₂ O ₃	2.632	4.903	4.894	4.988	4.244	3.866	2.949	4.542	3.376	4.036	4.147	3.412	4.040	2.910
Cr ₂ O ₃	0.009	0.038	0.000	0.000	0.016	0.022	0.058	0.000	0.016	0.018	0.000	0.016	0.003	0.025
FeO	10.895	10.364	10.127	9.198	9.914	9.283	9.717	13.903	10.534	10.917	9.950	9.975	9.710	9.928
MnO	0.142	0.147	0.121	0.111	0.099	0.044	0.085	0.118	0.068	0.165	0.116	0.142	0.103	0.068
MgO	12.875	12.069	12.043	12.339	12.094	12.475	12.625	12.563	11.961	12.036	11.931	12.452	12.006	12.396
CaO	21.284	21.634	21.174	21.924	22.222	21.960	22.462	17.953	22.378	20.713	21.538	22.078	22.388	22.294
Na ₂ O	0.446	0.667	0.621	0.489	0.551	0.623	0.739	0.613	0.821	0.710	0.790	0.474	0.642	0.373
K ₂ O	0.000	0.011	0.019	0.039	0.007	0.005	0.000	0.006	0.025	0.002	0.001	0.000	0.006	0.000
Total	99.799	99.411	99.363	99.383	99.667	99.142	100.274	100.463	100.203	98.700	99.512	99.512	99.633	99.268
<u>Atoms per formula unit (4 cations, 6 oxygens)</u>														
Si	1.923	1.847	1.878	1.869	1.879	1.898	1.909	1.888	1.894	1.888	1.905	1.903	1.890	1.924
Ti	0.007	0.010	0.010	0.012	0.011	0.009	0.007	0.008	0.006	0.007	0.007	0.007	0.008	0.006
Al	0.116	0.217	0.217	0.220	0.187	0.171	0.129	0.200	0.148	0.180	0.183	0.151	0.178	0.129
Cr	0.001	0.003	0.000	0.000	0.001	0.002	0.004	0.000	0.001	0.001	0.000	0.001	0.000	0.002
Fe ³⁺	0.056	0.116	0.052	0.056	0.073	0.059	0.088	0.052	0.110	0.080	0.051	0.061	0.072	0.036
Fe ²⁺	0.285	0.209	0.266	0.233	0.238	0.233	0.214	0.383	0.218	0.265	0.261	0.252	0.232	0.277
Mn	0.005	0.005	0.004	0.004	0.003	0.001	0.003	0.004	0.002	0.005	0.004	0.005	0.003	0.002
Mg	0.720	0.675	0.674	0.689	0.676	0.698	0.699	0.701	0.665	0.680	0.667	0.697	0.671	0.696
Ca	0.855	0.870	0.852	0.880	0.892	0.883	0.894	0.720	0.894	0.840	0.865	0.888	0.899	0.900
Na	0.032	0.049	0.045	0.036	0.040	0.045	0.053	0.044	0.059	0.052	0.057	0.035	0.047	0.027
K	0.000	0.001	0.001	0.002	0.000	0.000	0.000	0.000	0.001	0.000	0.000	0.000	0.000	0.000
Sum	4.000	4.000	4.000	4.000	4.000	4.000	4.000	4.000	4.000	4.000	4.000	4.000	4.000	4.000

MICROPROBE ANALYSES OF GARNET FROM ECLOGITE SAMPLE CP-47

	#3	#4	#5	#17	#18	#28	#35	#36	#47	#48
<u>Weight % oxide</u>										
SiO ₂	38.879	38.794	39.046	39.416	39.247	39.423	39.172	39.147	39.624	39.446
TiO ₂	0.058	0.078	0.067	0.063	0.038	0.053	0.068	0.073	0.085	0.063
Al ₂ O ₃	22.108	22.337	22.205	22.250	22.084	22.008	22.271	22.494	22.014	21.966
Cr ₂ O ₃	0.000	0.028	0.000	0.026	0.000	0.028	0.000	0.018	0.000	0.000
FeO	20.272	18.750	18.879	18.835	22.226	19.728	19.277	18.959	19.556	19.292
MnO	0.281	0.298	0.296	0.328	0.456	0.322	0.287	0.243	0.307	0.210
MgO	7.039	7.635	7.725	7.655	7.491	7.695	7.760	7.790	7.664	7.541
CaO	11.046	11.448	11.200	11.617	9.188	10.957	11.470	11.819	11.556	11.441
Na ₂ O	0.020	0.000	0.000	0.000	0.042	0.000	0.000	0.000	0.129	0.047
K ₂ O	0.000	0.007	0.004	0.005	0.000	0.011	0.019	0.010	0.001	0.000
Total	99.709	99.380	99.425	100.201	100.777	100.228	100.329	100.555	100.939	100.012
<u>Atoms per formula unit (4 cations, 6 oxygens)</u>										
Si	2.975	2.961	2.980	2.985	2.980	2.991	2.964	2.952	2.982	2.997
Ti	0.003	0.004	0.004	0.004	0.002	0.003	0.004	0.004	0.005	0.004
Al	1.994	2.009	1.997	1.986	1.976	1.968	1.986	1.999	1.952	1.967
Cr	0.000	0.004	0.000	0.004	0.000	0.004	0.000	0.003	0.000	0.000
Fe ³⁺	0.051	0.057	0.036	0.033	0.066	0.041	0.079	0.087	0.093	0.038
Fe ²⁺	1.246	1.140	1.169	1.160	1.345	1.210	1.141	1.108	1.138	1.188
Mn	0.018	0.019	0.019	0.021	0.029	0.021	0.018	0.016	0.020	0.014
Mg	0.803	0.869	0.879	0.864	0.848	0.870	0.875	0.876	0.860	0.854
Ca	0.906	0.936	0.916	0.943	0.747	0.891	0.930	0.955	0.932	0.931
Na	0.003	0.000	0.000	0.000	0.006	0.000	0.000	0.000	0.019	0.007
K	0.000	0.001	0.000	0.000	0.000	0.001	0.002	0.001	0.000	0.000
Sum	8.000	8.000	8.000	8.000	8.000	8.000	8.000	8.000	8.000	8.000

MICROPROBE ANALYSES OF PLAGIOCLASE FROM ECLOGITE SAMPLE CP-47

	#2	#6	#9	#10	#16	#19	#20	#21	#23	#27	#30	#34	#37	#40	#42	#44	#46
<u>Weight % oxide</u>																	
SiO ₂	60.413	60.078	59.900	60.779	60.625	60.512	55.611	59.964	62.063	61.312	59.968	60.655	58.535	59.117	58.229	59.954	59.194
TiO ₂	0.000	0.003	0.000	0.003	0.000	0.012	0.025	0.000	0.003	0.000	0.000	0.010	0.000	0.000	0.000	0.000	0.000
Al ₂ O ₃	24.723	25.027	25.384	24.761	24.751	24.508	27.860	24.973	23.992	24.523	25.046	24.408	26.101	25.827	26.441	25.156	25.492
Cr ₂ O ₃	0.000	0.018	0.003	0.000	0.000	0.000	0.028	0.000	0.000	0.000	0.009	0.000	0.029	0.000	0.000	0.000	0.004
FeO	0.234	0.238	0.233	0.169	0.197	0.162	0.219	0.160	0.151	0.144	0.217	0.215	0.311	0.244	0.219	0.198	0.259
MnO	0.022	0.050	0.001	0.009	0.030	0.040	0.000	0.036	0.012	0.021	0.000	0.017	0.012	0.000	0.000	0.000	0.000
MgO	0.000	0.000	0.018	0.000	0.000	0.000	0.000	0.000	0.010	0.000	0.000	0.008	0.000	0.000	0.000	0.000	0.018
CaO	6.908	7.113	7.291	6.505	6.794	6.701	10.642	7.056	5.773	6.044	7.221	6.566	8.548	7.922	8.464	7.357	7.568
Na ₂ O	7.633	7.666	7.695	7.926	7.778	7.784	5.799	7.636	8.264	8.016	7.380	7.798	6.778	7.084	6.624	7.450	7.186
K ₂ O	0.196	0.178	0.169	0.205	0.242	0.223	0.116	0.219	0.271	0.266	0.275	0.359	0.220	0.257	0.202	0.285	0.279
Total	100.135	100.375	100.699	100.361	100.420	99.945	100.303	100.047	100.543	100.331	100.121	100.040	100.537	100.453	100.181	100.404	100.005
<u>Atoms per formula unit (5 cations, 8 oxygens)</u>																	
Si	2.690	2.672	2.658	2.697	2.692	2.698	2.501	2.675	2.742	2.717	2.673	2.703	2.610	2.633	2.602	2.667	2.646
Ti	0.000	0.000	0.000	0.000	0.000	0.000	0.001	0.000	0.000	0.000	0.000	0.000	0.000	0.000	0.000	0.000	0.000
Al	1.297	1.312	1.327	1.295	1.295	1.288	1.477	1.313	1.249	1.281	1.316	1.282	1.371	1.356	1.393	1.319	1.343
Cr	0.000	0.002	0.000	0.000	0.000	0.000	0.002	0.000	0.000	0.000	0.001	0.000	0.003	0.000	0.000	0.000	0.000
Fe	0.009	0.009	0.009	0.006	0.007	0.006	0.008	0.006	0.006	0.005	0.008	0.008	0.012	0.009	0.008	0.007	0.010
Mn	0.001	0.002	0.000	0.000	0.001	0.002	0.000	0.001	0.000	0.001	0.000	0.001	0.000	0.000	0.000	0.000	0.000
Mg	0.000	0.000	0.001	0.000	0.000	0.000	0.000	0.000	0.001	0.000	0.000	0.001	0.000	0.000	0.000	0.000	0.001
Ca	0.330	0.339	0.347	0.309	0.323	0.320	0.513	0.337	0.273	0.287	0.345	0.314	0.408	0.378	0.405	0.351	0.362
Na	0.659	0.661	0.662	0.682	0.670	0.673	0.506	0.660	0.708	0.689	0.638	0.674	0.586	0.612	0.574	0.643	0.623
K	0.011	0.010	0.010	0.012	0.014	0.013	0.007	0.012	0.015	0.015	0.016	0.020	0.013	0.015	0.012	0.016	0.016
Sum	5.000	5.000	5.000	5.000	5.000	5.000	5.000	5.000	5.000	5.000	5.000	5.000	5.000	5.000	5.000	5.000	5.000

MICROPROBE ANALYSES OF AMPHIBOLE FROM ECLOGITE SAMPLES

	47-#12	47-#13	47-#22	47-#38	47-#41	52A-#2	92-#65	92-#72	92-#73	92-#74	92-#80
<u>Weight % oxide</u>											
SiO ₂	43.472	43.913	43.674	44.166	43.351	41.297	41.541	41.010	40.972	40.974	41.990
TiO ₂	1.551	1.691	1.473	0.839	1.368	0.509	1.276	2.173	0.961	0.761	1.480
Al ₂ O ₃	11.431	11.871	11.295	10.843	11.826	15.473	13.670	14.203	15.374	14.925	13.441
Cr ₂ O ₃	0.000	0.000	0.013	0.041	0.019	0.000	0.022	0.000	0.000	0.037	0.009
FeO	13.952	12.860	14.039	14.625	14.850	11.765	14.371	12.947	13.385	13.526	14.028
MnO	0.075	0.061	0.049	0.070	0.052	0.058	0.102	0.075	0.089	0.121	0.053
MgO	12.295	12.560	12.283	12.074	11.867	13.233	12.028	12.031	12.238	12.611	12.129
CaO	11.668	11.525	11.384	11.799	11.661	11.095	11.048	11.399	11.261	11.465	11.378
Na ₂ O	1.738	1.868	1.763	1.464	1.588	2.654	3.205	3.059	3.191	3.170	3.033
K ₂ O	0.428	0.473	0.512	0.635	0.673	0.902	0.027	0.027	0.022	0.025	0.017
Total	96.614	96.826	96.488	96.559	97.258	96.991	97.293	96.929	97.497	97.619	97.562
<u>Atoms per formula unit (16 cations, 22 oxygens)</u>											
Si	6.492	6.502	6.527	6.612	6.460	6.114	6.195	6.108	6.070	6.073	6.231
Ti	0.174	0.188	0.166	0.094	0.153	0.057	0.143	0.243	0.107	0.085	0.165
Al	2.012	2.071	1.989	1.913	2.077	2.700	2.403	2.493	2.684	2.607	2.351
Cr	0.000	0.000	0.004	0.012	0.005	0.000	0.006	0.000	0.000	0.011	0.003
Fe	1.742	1.592	1.754	1.831	1.851	1.456	1.792	1.613	1.658	1.676	1.741
Mn	0.009	0.008	0.006	0.009	0.007	0.007	0.013	0.009	0.011	0.015	0.007
Mg	2.738	2.772	2.737	2.695	2.637	2.921	2.674	2.672	2.703	2.787	2.683
Ca	1.867	1.828	1.823	1.892	1.862	1.760	1.765	1.819	1.787	1.821	1.809
Na	0.503	0.536	0.511	0.425	0.459	0.762	0.927	0.883	0.916	0.911	0.873
K	0.082	0.089	0.098	0.121	0.128	0.170	0.005	0.005	0.004	0.005	0.003
Sum	15.620	15.587	15.615	15.604	15.638	15.946	15.923	15.846	15.941	15.991	15.865

MICROPROBE ANALYSES OF PYROXENE FROM ECLOGITE SAMPLE CP-52A

	#1	#3	#8	#10	#11	#12	#13	#16	#18	#20	#22
<u>Weight % oxide</u>											
SiO ₂	54.864	50.314	53.696	53.876	54.055	53.007	53.557	54.719	54.239	54.109	54.650
TiO ₂	0.187	0.255	0.285	0.354	0.420	0.402	0.374	0.202	0.209	0.165	0.207
Al ₂ O ₃	12.196	9.309	12.551	13.026	13.007	13.266	13.118	12.334	12.661	12.022	12.406
Cr ₂ O ₃	0.009	0.020	0.029	0.000	0.029	0.000	0.000	0.003	0.000	0.013	0.013
FeO	4.463	7.408	4.643	4.369	4.476	5.434	4.380	4.375	4.383	4.482	4.536
MnO	0.026	0.072	0.009	0.000	0.026	0.025	0.000	0.035	0.000	0.077	0.034
MgO	8.138	10.575	8.420	8.018	8.204	8.592	8.048	8.085	8.015	8.262	8.156
CaO	14.392	18.857	15.240	14.554	14.620	15.739	14.858	14.360	14.234	14.621	14.423
Na ₂ O	6.246	2.655	5.587	5.909	5.878	5.103	5.819	6.184	6.248	6.013	6.046
K ₂ O	0.002	0.000	0.000	0.000	0.000	0.000	0.002	0.000	0.027	0.001	0.010
Total	100.528	99.470	100.466	100.110	100.720	101.573	100.162	100.302	100.020	99.771	100.484
<u>Atoms per formula unit (4 cations, 6 oxygens)</u>											
Si	1.946	1.849	1.912	1.921	1.917	1.875	1.910	1.945	1.931	1.935	1.941
Ti	0.005	0.007	0.008	0.009	0.011	0.011	0.010	0.005	0.006	0.004	0.006
Al	0.510	0.403	0.527	0.547	0.544	0.553	0.551	0.517	0.531	0.507	0.519
Cr	0.000	0.001	0.001	0.000	0.001	0.000	0.000	0.000	0.000	0.000	0.000
Fe ³⁺	0.019	0.074	0.019	0.000	0.003	0.025	0.011	0.008	0.027	0.031	0.003
Fe ²⁺	0.114	0.154	0.120	0.130	0.130	0.136	0.120	0.122	0.103	0.103	0.131
Mn	0.001	0.002	0.000	0.000	0.001	0.001	0.000	0.001	0.000	0.002	0.001
Mg	0.430	0.579	0.447	0.426	0.434	0.453	0.428	0.428	0.426	0.440	0.432
Ca	0.547	0.742	0.581	0.556	0.556	0.596	0.568	0.547	0.543	0.560	0.549
Na	0.429	0.189	0.386	0.409	0.404	0.350	0.402	0.426	0.431	0.417	0.416
K	0.000	0.000	0.000	0.000	0.000	0.000	0.000	0.000	0.001	0.000	0.000
Sum	4.000	4.000	4.000	4.000	4.000	4.000	4.000	4.000	4.000	4.000	4.000

MICROPROBE ANALYSES OF GARNET FROM ECLOGITE SAMPLE CP-52A

	#5	#6	#9	#14	#15	#17	#19	#21	#23
<u>Weight % oxide</u>									
SiO ₂	39.335	39.292	39.632	39.819	39.757	39.553	39.707	39.555	38.757
TiO ₂	0.083	0.083	0.075	0.085	0.080	0.070	0.107	0.098	0.062
Al ₂ O ₃	22.373	22.348	22.237	22.469	22.180	22.443	22.322	22.235	22.036
Cr ₂ O ₃	0.000	0.018	0.000	0.001	0.000	0.004	0.006	0.013	0.000
FeO	18.546	18.848	18.305	19.053	18.628	18.537	18.849	18.485	18.299
MnO	0.178	0.200	0.241	0.142	0.199	0.195	0.214	0.257	0.221
MgO	7.763	7.783	7.622	7.581	7.732	7.811	7.780	7.858	7.906
CaO	12.138	11.785	12.358	11.557	12.047	11.984	11.963	12.078	11.887
Na ₂ O	0.000	0.036	0.000	0.066	0.004	0.000	0.000	0.000	0.003
K ₂ O	0.000	0.000	0.000	0.000	0.000	0.011	0.000	0.006	0.000
Total	100.420	100.398	100.475	100.777	100.630	100.612	100.952	100.589	99.175
<u>Atoms per formula unit (8 cations, 12 oxygens)</u>									
Si	2.969	2.967	2.991	2.999	2.997	2.979	2.984	2.980	2.959
Ti	0.005	0.005	0.004	0.005	0.005	0.004	0.006	0.006	0.004
Al	1.990	1.989	1.978	1.994	1.970	1.992	1.977	1.974	1.983
Cr	0.000	0.001	0.000	0.000	0.000	0.000	0.000	0.001	0.000
Fe ³⁺	0.063	0.071	0.032	0.008	0.028	0.043	0.043	0.054	0.093
Fe ²⁺	1.107	1.119	1.123	1.192	1.146	1.124	1.142	1.111	1.075
Mn	0.011	0.013	0.015	0.009	0.013	0.012	0.014	0.016	0.014
Mg	0.873	0.876	0.858	0.851	0.869	0.877	0.872	0.883	0.900
Ca	0.981	0.953	0.999	0.932	0.973	0.967	0.963	0.975	0.972
Na	0.000	0.005	0.000	0.010	0.001	0.000	0.000	0.000	0.000
K	0.000	0.000	0.000	0.000	0.000	0.001	0.000	0.001	0.000
Sum	8.000	8.000	8.000	8.000	8.000	8.000	8.000	8.000	8.000

MICROPROBE ANALYSES OF PYROXENE FROM ECLOGITE SAMPLE CP-92

	#49	#53	#55	#58	#59	#63	#64	#66	#67	#76	#77	#79
<u>Weight % oxide</u>												
SiO ₂	49.897	49.845	52.798	52.526	51.463	48.748	48.955	50.594	49.456	49.148	50.402	49.242
TiO ₂	0.249	0.227	0.097	0.137	0.330	0.585	0.599	0.207	0.564	0.237	0.188	0.295
Al ₂ O ₃	10.182	9.991	1.349	1.959	3.116	6.309	6.876	10.991	8.026	6.694	10.868	8.057
Cr ₂ O ₃	0.013	0.000	0.039	0.013	0.000	0.012	0.038	0.000	0.004	0.022	0.000	0.031
FeO	12.084	10.658	12.367	12.695	8.861	9.794	9.872	10.004	9.286	9.088	10.383	11.231
MnO	0.142	0.094	0.136	0.152	0.123	0.089	0.134	0.085	0.090	0.124	0.116	0.137
MgO	8.486	8.464	11.721	11.288	12.998	12.149	10.958	8.363	10.792	11.948	8.433	11.613
CaO	15.100	17.180	20.119	20.246	21.743	20.732	20.972	15.886	20.543	21.487	16.596	19.439
Na ₂ O	3.511	3.092	1.330	1.558	0.702	0.876	1.216	3.606	1.782	0.980	3.561	1.050
K ₂ O	0.002	0.000	0.000	0.000	0.000	0.005	0.006	0.000	0.000	0.000	0.000	0.000
Total	99.671	99.557	99.959	100.580	99.340	99.302	99.631	99.740	100.547	99.733	100.551	101.099
<u>Atoms per formula unit (4 cations, 6 oxygens)</u>												
Si	1.849	1.850	1.981	1.959	1.925	1.823	1.828	1.863	1.819	1.825	1.843	1.812
Ti	0.007	0.006	0.003	0.004	0.009	0.016	0.017	0.006	0.016	0.007	0.005	0.008
Al	0.445	0.437	0.060	0.086	0.137	0.278	0.303	0.477	0.348	0.293	0.468	0.349
Cr	0.001	0.000	0.003	0.001	0.000	0.001	0.003	0.000	0.000	0.002	0.000	0.002
Fe ³⁺	0.096	0.074	0.066	0.100	0.045	0.105	0.093	0.043	0.109	0.112	0.088	0.083
Fe ²⁺	0.278	0.257	0.322	0.296	0.232	0.201	0.215	0.265	0.176	0.170	0.230	0.263
Mn	0.004	0.003	0.004	0.005	0.004	0.003	0.004	0.003	0.003	0.004	0.004	0.004
Mg	0.469	0.468	0.656	0.628	0.725	0.677	0.610	0.459	0.592	0.662	0.460	0.637
Ca	0.599	0.683	0.809	0.809	0.871	0.831	0.839	0.627	0.810	0.855	0.650	0.766
Na	0.252	0.222	0.097	0.113	0.051	0.064	0.088	0.257	0.127	0.071	0.252	0.075
K	0.000	0.000	0.000	0.000	0.000	0.000	0.000	0.000	0.000	0.000	0.000	0.000
Sum	4.000	4.000	4.000	4.000	4.000	4.000	4.000	4.000	4.000	4.000	4.000	4.000

MICROPROBE ANALYSES OF GARNET FROM ECLOGITE SAMPLE CP-92

	#52	#61	#68	#69	#78
<u>Weight % oxide</u>					
SiO2	39.102	39.046	39.196	38.978	38.937
TiO2	0.057	0.098	0.065	0.072	0.077
Al2O3	22.004	21.872	21.844	21.666	21.723
Cr2O3	0.019	0.000	0.004	0.010	0.000
FeO	22.263	21.932	21.964	22.601	22.405
MnO	0.356	0.328	0.342	0.421	0.356
MgO	6.561	6.528	6.579	7.093	6.417
CaO	10.368	10.797	10.435	9.478	10.375
Na2O	0.000	0.018	0.137	0.000	0.085
K2O	0.000	0.001	0.004	0.000	0.016
Total	100.734	100.625	100.575	100.323	100.395
<u>Atoms per formula unit (8 cations, 12 oxygens)</u>					
Si	2.981	2.979	2.989	2.982	2.981
Ti	0.003	0.006	0.004	0.004	0.004
Al	1.977	1.967	1.963	1.953	1.960
Cr	0.003	0.000	0.001	0.001	0.000
Fe3+	0.050	0.066	0.072	0.073	0.042
Fe2+	1.369	1.333	1.329	1.373	1.392
Mn	0.023	0.021	0.022	0.027	0.023
Mg	0.746	0.743	0.748	0.809	0.732
Ca	0.847	0.883	0.852	0.777	0.851
Na	0.000	0.003	0.020	0.000	0.013
K	0.000	0.000	0.000	0.000	0.002
Sum	8.000	8.000	8.000	8.000	8.000

MICROPROBE ANALYSES OF PLAGIOCLASE FROM ECLOGITE SAMPLES CP-47 AND CP-52A

	#50	#51	#54	#56	#57	#60	#62	#70	#71	#75	CP-52A-#4
<u>Weight % oxide</u>											
SiO ₂	63.986	63.751	64.480	66.904	65.997	62.675	63.511	60.103	61.282	62.061	68.556
TiO ₂	0.000	0.000	0.012	0.000	0.008	0.007	0.003	0.010	0.005	0.000	0.010
Al ₂ O ₃	22.964	22.452	22.469	21.039	21.356	23.631	22.975	25.689	24.438	23.931	19.881
Cr ₂ O ₃	0.029	0.016	0.000	0.028	0.000	0.000	0.012	0.028	0.007	0.016	0.000
FeO	0.232	0.216	0.248	0.250	0.243	0.135	0.161	0.208	0.257	0.399	0.108
MnO	0.054	0.000	0.000	0.004	0.000	0.021	0.022	0.009	0.000	0.030	0.070
MgO	0.002	0.012	0.000	0.013	0.000	0.000	0.015	0.000	0.000	0.000	0.000
CaO	4.403	3.918	3.639	1.914	2.352	5.177	4.350	7.224	6.102	5.332	0.319
Na ₂ O	9.467	9.312	9.779	10.828	10.568	8.864	9.283	7.725	8.113	8.828	11.563
K ₂ O	0.000	0.008	0.001	0.005	0.005	0.018	0.010	0.005	0.022	0.000	0.060
Total	101.140	99.688	100.633	100.987	100.533	100.531	100.347	101.005	100.230	100.601	100.570
<u>Atoms per formula unit (5 cations, 8 oxygens)</u>											
Si	2.800	2.823	2.830	2.911	2.889	2.764	2.799	2.655	2.717	2.741	2.981
Ti	0.000	0.000	0.000	0.000	0.000	0.000	0.000	0.000	0.000	0.000	0.000
Al	1.184	1.172	1.162	1.079	1.102	1.228	1.193	1.337	1.277	1.246	1.019
Cr	0.002	0.001	0.000	0.002	0.000	0.000	0.001	0.002	0.001	0.001	0.000
Fe	0.008	0.008	0.009	0.009	0.009	0.005	0.006	0.008	0.010	0.015	0.004
Mn	0.002	0.000	0.000	0.000	0.000	0.001	0.001	0.000	0.000	0.001	0.003
Mg	0.000	0.001	0.000	0.001	0.000	0.000	0.001	0.000	0.000	0.000	0.000
Ca	0.206	0.186	0.171	0.089	0.110	0.245	0.205	0.342	0.290	0.252	0.015
Na	0.803	0.799	0.832	0.913	0.897	0.758	0.793	0.661	0.697	0.756	0.975
K	0.000	0.000	0.000	0.000	0.000	0.001	0.001	0.000	0.001	0.000	0.003
Sum	5.000	5.000	5.000	5.000	5.000	5.000	5.000	5.000	5.000	5.000	5.000

PART II

Appendix B, Part II contains mineral chemical data obtained from microprobe analysis performed at the University of Kentucky, in Lexington, Kentucky, under the direction of Dr. David Moecher. The data were collected on the 17th, 18th, and 19th of December 2007. Pyroxene, garnet, plagioclase, and amphibole were analyzed from three eclogite samples, CP-47, CP-52A, and CP-92, which represented a spectrum of retrogression. The following tables are grouped by sample number and mineral type. Each data column represents the average of two spot analyses taken a few microns apart.

Mineral compositions were determined using the ARL-SEMQ microprobe at the university of Kentucky. Most minerals were analyzed in point mode, using WDS at 15kV and 15 nA, except for plagioclase, which was analyzed using a rastered beam (10 X 10 μm) at 15kV and 10 nA to minimize loss of Na and K. Typical count times were 10-20 s on peak, and 5-10 s for background counts. Natural USNM standards were used, ZAF corrections were made using Probewin v, 5.32 (after Anderson and Moecher 2007).

ANALYSES OF GARNETS FROM ECLOGITES CP-52A, CP-92

	52A-C1	52A-C2	52A-C3	92-C1	92-C2	92-C3
<u>Weight % oxide</u>						
SiO ₂	39.748	39.692	40.004	39.479	39.360	39.104
TiO ₂	0.064	0.091	0.083	0.085	0.076	0.071
Al ₂ O ₃	22.979	23.173	22.864	22.368	22.593	22.007
FeO	18.101	18.004	18.190	21.460	21.770	21.394
MnO	0.253	0.299	0.275	0.345	0.375	0.358
MgO	7.673	8.023	7.822	6.851	6.751	6.613
CaO	11.703	11.479	11.515	9.929	9.998	10.206
Na ₂ O	0.000	0.034	0.070	0.026	0.003	0.032
K ₂ O	0.000	0.000	0.000	0.000	0.000	0.000
Total	100.521	100.795	100.823	100.543	100.925	99.786
<u>Atoms per formula unit (8 cations, 12 oxygens)</u>						
Si	2.994	2.976	3.002	3.007	2.989	3.004
Ti	0.004	0.005	0.005	0.005	0.004	0.004
Al	2.040	2.048	2.022	2.008	2.022	1.992
Fe 3+	0.000	0.000	0.000	0.000	0.000	0.000
Fe 2+	1.140	1.129	1.142	1.367	1.382	1.374
Mn	0.016	0.019	0.017	0.022	0.024	0.023
Mg	0.862	0.897	0.875	0.778	0.764	0.757
Ca	0.944	0.922	0.926	0.810	0.813	0.840
Na	0.000	0.005	0.010	0.004	0.000	0.005
K	0.000	0.000	0.000	0.000	0.000	0.000
Sum	8.000	8.000	8.000	8.000	8.000	8.000

ANALYSES OF PYROXENE FROM ECLOGITE SAMPLE CP-52A

	Omp 2 C	Omp 2 R1	Omp 2 R2	Omp 1 C	Omp 3C
<u>Weight % oxide</u>					
SiO2	54.095	49.793	49.255	54.289	54.458
TiO2	0.171	0.195	0.189	0.154	0.170
Al2O3	12.951	8.491	9.864	12.872	13.183
FeO	4.222	7.884	7.670	4.239	4.741
MnO	0.007	0.045	0.056	0.031	0.035
MgO	9.336	12.742	11.785	9.409	9.560
CaO	13.941	19.671	19.004	13.841	14.487
Na2O	5.495	1.791	2.033	5.746	5.617
K2O	0.000	0.000	0.000	0.000	0.000
Total	100.220	100.612	99.858	100.582	102.252
<u>Atoms per formula unit (4 cations, 8 oxygens)</u>					
Si	1.923	1.809	1.802	1.919	1.898
Ti	0.005	0.005	0.005	0.004	0.004
Al	0.543	0.364	0.424	0.536	0.541
Fe 3+	0.000	0.135	0.106	0.011	0.034
Fe 2+	0.126	0.105	0.129	0.115	0.105
Mn	0.000	0.001	0.002	0.001	0.001
Mg	0.495	0.690	0.644	0.496	0.497
Ca	0.531	0.766	0.746	0.524	0.541
Na	0.379	0.126	0.144	0.394	0.380
K	0.000	0.000	0.000	0.000	0.000
Sum	4.000	4.000	4.000	4.000	4.000

ANALYSES OF AMPHIBOLE FROM ECLOGITE SAMPLE CP-47

	G2 - AMP1	G2 - AMP2	CPX 1 - AMP1	CPX 1 - AMP2	CPX 1 - AMP3
<u>Weight % oxide</u>					
SiO ₂	42.826	42.766	44.563	44.333	44.297
TiO ₂	0.631	0.632	1.298	2.421	0.906
Al ₂ O ₃	14.467	14.086	11.686	11.524	12.291
FeO	13.891	14.008	13.992	11.491	13.484
MnO	0.072	0.072	0.096	0.051	0.066
MgO	12.863	12.513	12.764	13.673	13.054
CaO	11.088	11.216	11.273	12.015	11.566
Na ₂ O	2.249	1.928	1.910	1.893	1.928
K ₂ O	0.435	0.413	0.222	0.277	0.171
Total	98.522	97.633	97.804	97.678	97.762
<u>Atoms per formula unit (16 cations, 23 oxygens)</u>					
Si	6.259	6.307	6.544	6.470	6.496
Ti	0.069	0.070	0.143	0.266	0.100
Al	2.492	2.448	2.023	1.982	2.124
Fe	1.698	1.728	1.718	1.403	1.654
Mn	0.009	0.009	0.012	0.006	0.008
Mg	2.803	2.751	2.794	2.975	2.854
Ca	1.736	1.772	1.774	1.879	1.817
Na	0.637	0.551	0.544	0.536	0.548
K	0.081	0.078	0.042	0.052	0.032
Sum	15.785	15.714	15.594	15.567	15.633

MICROPROBE ANALYSES OF PYROXENE FROM ECLOGITE SAMPLE CP-47

	CPX - G2	CPX - G3	CPX1 - 1	CPX1 - 2	CPX1 - 3	CPX1 - 4	CPX1 - 5	CPX1 - 6	CPX2 - 1	CPX2 - 2	CPX2 - 3
<u>Weight % oxide</u>											
SiO2	51.603	52.477	49.129	48.872	49.273	48.779	51.410	50.938	51.613	50.572	48.942
TiO2	0.273	0.171	0.424	0.412	0.510	0.425	0.294	0.249	0.181	0.261	0.353
Al2O3	12.809	12.988	5.145	5.971	5.092	6.092	3.447	4.074	3.082	3.481	7.907
FeO	5.340	5.211	9.529	9.685	9.748	9.766	8.680	9.182	8.845	8.975	9.892
MnO	0.026	0.021	0.070	0.107	0.107	0.068	0.041	0.092	0.104	0.070	0.083
MgO	10.014	9.462	12.850	12.914	13.658	12.958	14.001	13.219	14.084	13.312	12.484
CaO	17.136	16.220	21.106	21.177	21.600	21.063	21.269	21.373	22.016	21.842	18.315
Na2O	4.246	4.890	0.911	0.637	0.733	0.719	0.833	0.776	0.524	0.646	1.208
K2O	0.000	0.000	0.000	0.000	0.000	0.000	0.000	0.000	0.000	0.000	0.000
Total	101.448	101.440	99.164	99.775	100.722	99.871	99.976	99.904	100.450	99.160	99.184
<u>Atoms per formula unit (4 cations, 6 oxygens)</u>											
Si	1.828	1.853	1.835	1.817	1.811	1.810	1.899	1.890	1.903	1.892	1.822
Ti	0.007	0.005	0.012	0.012	0.014	0.012	0.008	0.007	0.005	0.007	0.010
Al	0.535	0.541	0.227	0.262	0.221	0.266	0.150	0.178	0.134	0.153	0.347
Fe 3+	0.086	0.078	0.145	0.127	0.182	0.141	0.094	0.083	0.087	0.095	0.077
Fe 2+	0.072	0.076	0.153	0.174	0.118	0.162	0.174	0.201	0.186	0.185	0.231
Mn	0.001	0.001	0.002	0.003	0.003	0.002	0.001	0.003	0.003	0.002	0.003
Mg	0.529	0.498	0.716	0.716	0.748	0.717	0.771	0.731	0.774	0.742	0.693
Ca	0.650	0.614	0.845	0.844	0.851	0.838	0.842	0.850	0.870	0.875	0.731
Na	0.292	0.335	0.066	0.046	0.052	0.052	0.060	0.056	0.037	0.047	0.087
K	0.000	0.000	0.000	0.000	0.000	0.000	0.000	0.000	0.000	0.000	0.000
Sum	4.000	4.000	4.000	4.000	4.000	4.000	4.000	4.000	4.000	4.000	4.000

MICROPROBE ANALYSES OF PLAGIOCLASE FROM ECLOGITE SAMPLE CP-47

	G2 - P1	CPX1 - P1	CPX1 - P2	CPX1 - P3	CPX1 - P4	CPX1 - P5	CPX1 - P6	CPX2 - P1	CPX2 - P2	CPX2 - P3
<u>Weight % oxide</u>										
SiO2	57.402	59.724	59.117	61.342	60.052	60.505	60.798	57.962	59.875	60.485
Al2O3	28.354	26.077	26.105	24.858	25.314	25.620	25.215	26.485	26.169	25.329
FeO	0.280	0.207	0.195	0.182	0.232	0.140	0.191	0.139	0.220	0.232
CaO	8.748	6.582	6.616	5.738	6.190	6.126	6.276	7.183	6.917	6.627
Na2O	6.110	7.302	7.435	8.187	7.796	7.983	7.985	7.328	7.104	7.060
K2O	0.144	0.175	0.133	0.174	0.145	0.184	0.174	0.139	0.132	0.160
Total	101.038	100.066	99.602	100.481	99.727	100.558	100.639	99.235	100.417	99.893
<u>Atoms per formula unit (5 cations, 8 oxygens)</u>										
Si	2.543	2.655	2.643	2.712	2.679	2.677	2.689	2.609	2.653	2.688
Al	1.481	1.366	1.376	1.295	1.331	1.336	1.314	1.405	1.366	1.327
Fe	0.010	0.008	0.007	0.007	0.009	0.005	0.007	0.005	0.008	0.009
Ca	0.415	0.314	0.317	0.272	0.296	0.290	0.297	0.346	0.328	0.316
Na	0.525	0.629	0.645	0.702	0.674	0.685	0.685	0.639	0.610	0.608
K	0.008	0.010	0.008	0.010	0.008	0.010	0.010	0.008	0.007	0.009
Sum	4.983	4.982	4.995	4.997	4.997	5.003	5.002	5.013	4.973	4.957

MICROPROBE ANALYSES OF GARNETS FROM ECLOGITE SAMPLE CP-47

	G1 - C1	G1 - R2	G1 - C2	G1 - C3	G1 - R3	G1 - C4	G3 - C1	G3 - R1	G3 - C2	G3 - R2	G2 - C1	G2 - R1	G2 - R2	G2 - R3	G2 - C2
<u>Weight % oxide</u>															
SiO2	39.460	39.532	39.493	40.096	39.369	39.685	39.413	39.528	38.984	38.820	38.784	38.238	38.239	39.332	39.461
TiO2	0.087	0.010	0.079	0.053	0.034	0.027	0.073	0.042	0.031	0.049	0.048	0.046	0.004	0.097	0.065
Al2O3	22.437	22.267	22.475	22.439	21.920	22.131	22.183	21.927	21.907	22.523	23.185	22.626	22.810	23.339	23.304
FeO	18.908	23.262	19.954	19.411	24.141	20.682	19.275	22.612	18.930	23.696	18.503	22.125	21.605	18.449	18.666
MnO	0.350	0.521	0.347	0.313	0.578	0.324	0.287	0.499	0.302	0.576	0.291	0.555	0.510	0.297	0.326
MgO	7.388	7.205	7.094	7.344	7.157	7.706	7.282	6.981	7.227	8.039	8.122	7.420	7.735	7.956	8.190
CaO	11.046	7.785	10.904	10.836	7.063	9.418	11.206	8.434	11.110	6.224	11.189	8.248	8.440	11.238	10.881
Na2O	0.005	0.000	0.000	0.000	0.000	0.000	0.005	0.048	0.068	0.018	0.023	0.000	0.000	0.006	0.000
K2O	0.000	0.000	0.000	0.000	0.000	0.000	0.000	0.000	0.000	0.000	0.000	0.000	0.000	0.000	0.000
Total	99.681	100.583	100.346	100.494	100.262	99.974	99.724	100.070	98.559	99.945	100.146	99.258	99.343	100.714	100.892
<u>Atoms per formula unit (8 cations, 12 oxygens)</u>															
Si	3.008	3.019	3.001	3.036	3.024	3.025	3.007	3.033	3.007	2.975	2.927	2.947	2.936	2.954	2.958
Ti	0.005	0.001	0.005	0.003	0.002	0.002	0.004	0.002	0.002	0.003	0.003	0.003	0.000	0.005	0.004
Al	2.016	2.004	2.013	2.003	1.985	1.988	1.995	1.983	1.991	2.034	2.062	2.055	2.064	2.066	2.059
Fe 3+	0.000	0.000	0.000	0.000	0.000	0.000	0.000	0.000	0.002	0.013	0.082	0.046	0.064	0.015	0.018
Fe 2+	1.206	1.486	1.268	1.229	1.551	1.319	1.230	1.451	1.219	1.505	1.086	1.380	1.323	1.144	1.152
Mn	0.023	0.034	0.022	0.020	0.038	0.021	0.019	0.032	0.020	0.037	0.019	0.036	0.033	0.019	0.021
Mg	0.840	0.820	0.804	0.829	0.820	0.876	0.828	0.798	0.831	0.919	0.914	0.852	0.885	0.891	0.915
Ca	0.902	0.637	0.888	0.879	0.581	0.769	0.916	0.693	0.918	0.511	0.905	0.681	0.694	0.904	0.874
Na	0.001	0.000	0.000	0.000	0.000	0.000	0.001	0.007	0.010	0.003	0.003	0.000	0.000	0.001	0.000
K	0.000	0.000	0.000	0.000	0.000	0.000	0.000	0.000	0.000	0.000	0.000	0.000	0.000	0.000	0.000
Sum	8.000	8.000	8.000	8.000	8.000	8.000	8.000	8.000	8.000	8.000	8.000	8.000	8.000	8.000	8.000

97

APPENDIX C

$^{40}\text{Ar}/^{39}\text{Ar}$ ISOTOPIC AGE DATA

Appendix C contains argon isotope data collected on June 13, 2007 at the Auburn Noble Isotope Mass Analysis Laboratory (ANIMAL) performed at Auburn University, under the supervision of Dr. Bill Hames. Both Single Crystal Total Fusion and Incremental heating methods were used to date phlogopite grains separated from lamprophyre dike samples, M-14C and M-21. The appendix also includes data from air samples and monitor data, which were used to estimate the neutron flux parameter, J. The monitor mineral FC-2 (from a split prepared by New Mexico Tech) was used to determine J-values (see McDougall and Harrison, 1999) with the age of 28.02 Ma assigned to FC-2 (after Renee et al., 1998). All argon fraction data are recorded in moles. Table headings for argon fractions are reported in the following list.

^{40}Ar (*, atm) – Radiogenic ^{40}Ar derived from natural decay of ^{40}K
and the atmosphere

^{39}Ar (K) – ^{39}Ar derived from irradiation

^{38}Ar (Cl, atm) – ^{38}Ar derived from chlorine and the atmosphere

^{37}Ar (Ca) – ^{37}Ar derived from calcium

^{36}Ar (atm) – ^{36}Ar derived from the atmosphere

The following paragraphs contain an analytical description of the ANIMAL facility. The facility is equipped with an ultra-high vacuum, 90-degree sector, 10 cm radius spectrometer optimized for $^{40}\text{Ar}/^{39}\text{Ar}$ research (single-crystal and multigrain sample incremental heating). The spectrometer employs second-order focusing (Cross, 1951), and is fitted with a high sensitivity electron-impact source and a single ETP electron multiplier (with signal amplification through a standard pre-amplifier). Analyses are typically made using a filament current of 2.75 A, and potentials for the source and

multiplier of 2000 V and -1300 V, respectively. The total volume of the spectrometer is 400 cc. Resolution in the instrument (with fixed slits for the source and detector) is constrained to ~150, and the high sensitivity and low blank of the instrument permits measurement of 10^{-14} mole samples to within 0.2% precision. Analyses comprise 10 cycles of measurement over the range of masses and half-masses from $m/e=40$ to $m/e=35.5$, and baseline corrected values are extrapolated to the time of inlet, or averaged, depending upon signal evolution.

The extraction line for this system utilizes a combination of Varian 'mini' and Nupro pneumatic valves, and Varian turbomolecular and ion pumps. Analysis of samples and blanks is fully automated under computer control. Pumping of residual and sample reactive gases is accomplished through use of SAES AP-10 non-evaporable getters. Pressures in the spectrometer and extraction line, as measured with an ionization gauge, are routinely below $\sim 5 \times 10^{-9}$ torr. A pipette delivers standard aliquots of air for use in measuring sensitivity and mass discrimination. Typical recent measurements of $^{40}\text{Ar}/^{36}\text{Ar}$ in air are ~ 293 (e.g., from 5/15/07 — 5/23/07 mass discrimination was 0.9945 ± 0.00038 per amu, at the 95% confidence level for twelve measurements).

The extraction line is fitted with a 50W Synrad CO₂ IR laser for heating and fusing silicate minerals and glasses. The sample chamber uses a Cu planchet, KBr cover slips, and low-blank UHV ZnS window (manufactured at Auburn University and based on the design of Cox et al., 2003). In the present configuration, this laser system is suitable for incremental heating and fusion analysis of single crystals and multigrain samples. The laser beam delivery system utilizes movable optical mounts and a fixed sample chamber to further minimize volume and improve conductance of the extraction

line. (The time required to inlet, or equilibrate, a ‘half-split’ of a sample is less than 7 s, and the inlet time for a full sample is ca. 20 s.) Typical blanks for the entire system (4 minute gettering time) are as follows (in moles): ^{40}Ar , 7.6×10^{-17} ; ^{39}Ar , 1.3×10^{-17} ; ^{38}Ar , 2.8×10^{-18} ; ^{37}Ar , 2.0×10^{-18} ; ^{36}Ar , 1.2×10^{-18} .

Computer control of the laser, positioning of laser optics, extraction line, mass spectrometer, and data recording is enabled with National Instruments hardware and a Labview program written by lab personnel specifically for ANIMAL. Initial data reduction is accomplished through an in-house Excel spreadsheet, with final reduction using Isoplot (Ludwig, 2003). Figures drawn using Isoplot were constructed using uncertainties of 1σ .

M-14C SINGLE CRYSTAL TOTAL FUSION (J-Value = 0.01341)

	⁴⁰ Ar (*, atm)	³⁹ Ar (K)	³⁸ Ar (Cl, atm)	³⁷ Ar (Ca)	³⁶ Ar (atm)	%Rad	R	Age (Ma)
41	2.031E-14 ± 2.1E-17	1.751E-15 ± 3.7E-18	4.63E-18 ± 7.0E-20	1.16E-17 ± 7.5E-19	8.3E-19 ± 8.678E-20	0.988	11.453	260.8 ± 0.7
42	2.176E-14 ± 1.5E-17	1.900E-15 ± 1.7E-18	4.75E-18 ± 9.1E-20	1.72E-17 ± 8.8E-19	7.9E-19 ± 6.710E-20	0.989	11.327	258.1 ± 0.4
43	5.870E-14 ± 8.3E-17	5.152E-15 ± 1.2E-17	1.23E-17 ± 1.1E-19	3.40E-17 ± 1.2E-18	5.9E-19 ± 6.730E-20	0.997	11.359	258.8 ± 0.7
44	4.575E-14 ± 3.6E-17	3.984E-15 ± 9.0E-18	1.20E-17 ± 1.2E-19	2.53E-17 ± 1.4E-18	1.2E-18 ± 7.823E-20	0.992	11.395	259.6 ± 0.6
45	5.855E-14 ± 1.1E-16	5.039E-15 ± 9.8E-18	1.24E-17 ± 5.5E-20	2.41E-17 ± 9.3E-19	1.7E-18 ± 9.059E-20	0.991	11.518	262.2 ± 0.7
46	4.874E-14 ± 5.2E-17	4.197E-15 ± 6.2E-18	1.07E-17 ± 1.5E-19	2.69E-17 ± 1.1E-18	1.0E-18 ± 7.679E-20	0.994	11.542	262.7 ± 0.5
47	1.009E-13 ± 9.6E-17	8.789E-15 ± 1.3E-17	2.48E-17 ± 2.2E-19	9.12E-17 ± 2.4E-18	2.3E-18 ± 1.120E-19	0.993	11.410	259.9 ± 0.5
48	4.144E-14 ± 4.7E-17	3.579E-15 ± 7.1E-18	9.54E-18 ± 1.2E-19	2.15E-17 ± 1.0E-18	2.5E-18 ± 8.740E-20	0.982	11.372	259.1 ± 0.6
49	6.169E-14 ± 7.7E-17	5.337E-15 ± 6.3E-18	1.41E-17 ± 1.1E-19	3.28E-16 ± 2.9E-18	2.1E-18 ± 8.103E-20	0.990	11.445	260.6 ± 0.5

Total Gas Age: 257.2 Ma

Weighted Mean Age: 260.0±1.2 Ma

M-21 SINGLE CRYSTAL TOTAL FUSION (J-Value = 0.01341)

	⁴⁰ Ar (*, atm)	³⁹ Ar (K)	³⁸ Ar (Cl, atm)	³⁷ Ar (Ca)	³⁶ Ar (atm)	%Rad	R	Age (Ma)
51	2.379E-14 ± 2.3E-17	2.016E-15 ± 4.6E-18	2.80E-18 ± 1.1E-19	6.25E-17 ± 2.0E-18	2.1E-18 ± 7.757E-20	0.973	11.486	261.5 ± 0.7
52	5.969E-14 ± 3.7E-17	4.993E-15 ± 4.7E-18	1.41E-17 ± 1.1E-19	9.94E-17 ± 1.1E-18	5.5E-18 ± 1.115E-19	0.973	11.630	264.6 ± 0.3
53	5.553E-15 ± 7.8E-18	4.617E-16 ± 1.8E-18	1.08E-18 ± 5.4E-20	2.18E-18 ± 7.4E-19	6.8E-19 ± 1.436E-19	0.964	11.595	263.8 ± 2.4
54	4.620E-14 ± 7.5E-17	3.877E-15 ± 5.2E-18	1.01E-17 ± 8.7E-20	1.18E-16 ± 2.6E-18	3.9E-18 ± 1.026E-19	0.975	11.615	264.2 ± 0.6
55	1.179E-13 ± 1.2E-16	9.955E-15 ± 1.7E-17	2.84E-17 ± 2.8E-19	2.84E-16 ± 2.9E-18	1.3E-17 ± 1.623E-19	0.968	11.461	261.0 ± 0.6
56	1.254E-13 ± 1.8E-16	1.005E-14 ± 2.7E-17	3.12E-17 ± 1.6E-19	4.90E-16 ± 7.1E-18	2.9E-17 ± 2.808E-19	0.932	11.622	264.4 ± 0.9
57	2.735E-14 ± 3.1E-17	2.253E-15 ± 7.3E-18	6.52E-18 ± 9.0E-20	3.50E-17 ± 1.1E-18	4.2E-18 ± 1.097E-19	0.955	11.591	263.7 ± 1.0
58	4.616E-14 ± 8.3E-17	3.874E-15 ± 6.1E-18	1.11E-17 ± 1.3E-19	7.45E-17 ± 2.2E-18	4.6E-18 ± 9.034E-20	0.971	11.565	263.2 ± 0.7
59	8.897E-14 ± 5.7E-17	7.542E-15 ± 6.7E-18	2.02E-17 ± 1.5E-19	2.34E-16 ± 2.8E-18	3.9E-18 ± 1.127E-19	0.987	11.644	264.8 ± 0.3

Total Gas Age: 260.4 Ma

Weighted Mean Age: 263.9±1.1 Ma

M-14C INCREMENTAL HEATING (J-Value = 0.01341)

	⁴⁰ Ar (*, atm)	³⁹ Ar (K)	³⁸ Ar (Cl, atm)	³⁷ Ar (Ca)	³⁶ Ar (atm)	%Rad	R	Age (Ma)
3.5	1.156E-16 ± 2.3E-18	4.190E-18 ± 6.3E-19	1.17E-19 ± 7.9E-20	1.95E-19 ± 1.1E-18	2.48E-19 ± 8.1E-20	36.7%	10.127	232.5 ± 173.7
3.8	2.096E-16 ± 3.3E-18	1.508E-17 ± 4.2E-19	3.11E-19 ± 7.3E-20	3.84E-18 ± 1.3E-18	1.40E-19 ± 7.3E-20	80.3%	11.161	254.6 ± 34.4
4.1	5.598E-16 ± 2.9E-18	4.162E-17 ± 6.9E-19	4.19E-19 ± 8.7E-20	6.79E-18 ± 1.5E-18	4.31E-19 ± 7.8E-20	77.3%	10.392	238.2 ± 13.9
4.5	3.241E-15 ± 6.4E-18	2.810E-16 ± 7.2E-19	1.13E-18 ± 3.3E-20	5.50E-18 ± 1.2E-18	3.82E-19 ± 7.2E-20	96.5%	11.130	253.9 ± 1.9
4.9	1.328E-14 ± 1.8E-17	1.140E-15 ± 2.2E-18	3.35E-18 ± 6.7E-20	8.41E-18 ± 1.1E-18	3.71E-19 ± 7.6E-20	99.2%	11.548	262.8 ± 0.8
5.3	1.801E-14 ± 3.0E-17	1.555E-15 ± 4.3E-18	3.27E-18 ± 5.8E-20	2.06E-17 ± 1.6E-18	3.29E-19 ± 1.1E-19	99.5%	11.519	262.2 ± 1.0
5.6	2.775E-14 ± 2.7E-17	2.414E-15 ± 6.9E-18	5.55E-18 ± 5.9E-20	2.83E-17 ± 1.4E-18	2.85E-19 ± 1.0E-19	99.7%	11.461	261.0 ± 0.8
5.9	3.903E-14 ± 3.6E-17	3.413E-15 ± 1.0E-17	5.73E-18 ± 7.3E-20	3.57E-17 ± 1.5E-18	3.81E-19 ± 6.0E-20	99.7%	11.402	259.7 ± 0.8
6.2	9.851E-15 ± 1.2E-17	8.487E-16 ± 4.7E-18	1.69E-18 ± 3.7E-20	1.13E-17 ± 1.0E-18	2.06E-19 ± 6.4E-20	99.4%	11.536	262.6 ± 1.6
6.5	1.557E-14 ± 1.4E-17	1.345E-15 ± 4.8E-18	2.98E-18 ± 7.4E-20	3.77E-18 ± 9.4E-19	2.89E-19 ± 9.7E-20	99.5%	11.516	262.1 ± 1.1
7	1.103E-15 ± 2.4E-18	9.469E-17 ± 9.7E-19	2.74E-19 ± 3.7E-20	9.51E-19 ± 8.1E-19	8.81E-20 ± 6.3E-20	97.6%	11.378	259.2 ± 5.3

104

Total Gas Age: 257.8 Ma
Weighted Mean Age: 261.3±1.4 Ma
Plateau Age: 261.56±0.38 Ma

M-21 INCREMENTAL HEATING (J-Value = 0.01341)

	⁴⁰ Ar (*, atm)		³⁹ Ar (K)		³⁸ Ar (Cl, atm)		³⁷ Ar (Ca)		³⁶ Ar (atm)		%Rad	R	Age (Ma)	
3.5	8.580E-15	± 1.3E-17	2.521E-16	± 2.7E-18	4.77E-18	± 3.3E-19	9.16E-17	± 1.9E-18	1.93E-17	± 2.2E-19	33.6%	11.446	260.7	± 11.7
3.8	8.880E-15	± 1.6E-17	6.896E-16	± 5.0E-18	2.05E-18	± 5.9E-20	7.60E-18	± 7.3E-19	3.12E-18	± 1.2E-19	89.6%	11.542	262.7	± 2.5
4.1	1.620E-14	± 1.7E-17	1.300E-15	± 4.6E-18	3.84E-18	± 8.8E-20	8.19E-18	± 8.3E-19	3.96E-18	± 1.4E-19	92.8%	11.568	263.2	± 1.3
4.5	1.906E-14	± 1.8E-17	1.627E-15	± 3.7E-18	3.85E-18	± 4.6E-20	1.53E-17	± 6.5E-19	5.83E-19	± 1.2E-19	99.1%	11.609	264.1	± 0.8
4.8	2.358E-14	± 2.8E-17	2.027E-15	± 3.0E-18	4.97E-18	± 8.1E-20	1.87E-17	± 9.7E-19	5.23E-19	± 1.1E-19	99.3%	11.558	263.0	± 0.6
5.1	2.040E-14	± 1.9E-17	1.745E-15	± 4.5E-18	4.23E-18	± 4.3E-20	1.60E-17	± 1.1E-18	2.75E-19	± 6.7E-20	99.6%	11.641	264.8	± 0.8
5.6	3.305E-14	± 2.4E-17	2.817E-15	± 1.1E-17	6.86E-18	± 8.8E-20	7.54E-17	± 1.7E-18	5.56E-19	± 7.0E-20	99.5%	11.672	265.5	± 1.1
5.9	3.635E-15	± 3.9E-18	3.047E-16	± 1.5E-18	9.90E-19	± 4.6E-20	1.44E-17	± 9.0E-19	1.19E-19	± 6.4E-20	99.0%	11.815	268.5	± 2.0
6.2	1.020E-16	± 1.6E-18	1.012E-17	± 5.1E-19	1.89E-19	± 8.3E-20	2.96E-18	± 8.5E-19	1.11E-19	± 6.6E-20	67.8%	6.833	160.1	± 47.5
6.5	2.993E-17	± 2.5E-18	2.164E-18	± 6.6E-19	-6.46E-22	± -4.7E-21	2.04E-18	± 9.2E-19	-1.89E-20	± -5.9E-20	118.7%	16.411	363.0	± 197.5

105

Total Gas Age: 261.1 Ma
Weighted Mean Age: 264.1±1.1 Ma
Plateau Age: 263.93±0.37 Ma

SAMPLE FC-2 MONITOR DATA

	⁴⁰ Ar (*, atm)	³⁹ Ar (K)	³⁸ Ar (Cl, atm)	³⁷ Ar (Ca)	³⁶ Ar (atm)	%Rad	R	J Value
a	5.238E-14 ± 3.1E-17	4.439E-14 ± 3.5E-17	1.06E-16 ± 7.3E-19	3.34E-16 ± 4.6E-18	1.72E-18 ± 8.8E-20	99.0%	1.168	0.01340 ± 1.518E-05
b	5.469E-14 ± 3.3E-17	4.646E-14 ± 2.3E-17	1.28E-16 ± 8.1E-19	4.54E-16 ± 2.8E-18	2.29E-18 ± 9.7E-20	98.8%	1.163	0.01346 ± 1.304E-05
c	6.602E-14 ± 7.5E-17	5.450E-14 ± 5.2E-17	1.83E-16 ± 1.2E-18	6.82E-16 ± 4.2E-18	7.57E-18 ± 1.1E-19	96.6%	1.170	0.01337 ± 2.181E-05
d	1.084E-13 ± 1.1E-16	9.121E-14 ± 6.8E-17	2.45E-16 ± 6.8E-19	5.55E-16 ± 6.2E-18	9.47E-18 ± 1.5E-19	97.4%	1.158	0.01352 ± 1.815E-05
e	1.122E-13 ± 3.5E-17	9.293E-14 ± 4.1E-17	2.38E-16 ± 1.0E-18	5.75E-16 ± 5.4E-18	9.90E-18 ± 2.1E-19	97.4%	1.175	0.01332 ± 1.071E-05
							Mean	0.01341 ± 3.469E-05

106

MEASUREMENTS OF ARGON ISOTOPES IN AIR

	⁴⁰ Ar (*, atm)	³⁹ Ar (K)	³⁸ Ar (Cl, atm)	³⁷ Ar (Ca)	³⁶ Ar (atm)	(40/36)	(40/38)	M. Fract
a	6.950E-14 + 8.7E-17	-3.583E-18 + 3.6E-19	4.32E-17 + 3.6E-19	-1.89E-19 + 1.5E-19	2.32E-16 + 1.5E-18	299.69	1607.53	1.0035
b	7.145E-14 + 1.4E-16	-4.307E-18 + 4.2E-19	4.47E-17 + 5.7E-19	-2.50E-19 + 1.9E-19	2.35E-16 + 1.1E-18	303.43	1597.12	1.0067
c	7.128E-14 + 9.8E-17	-5.515E-18 + 1.2E-18	4.48E-17 + 5.7E-19	1.21E-19 + 1.6E-19	2.37E-16 + 1.2E-18	300.33	1590.94	1.0041
d	1.215E-13 + 1.5E-16	1.708E-18 + 1.5E-18	7.75E-17 + 1.2E-18	1.02E-18 + 1.2E-19	4.05E-16 + 1.9E-18	299.55	1566.58	1.0034
e	6.574E-14 + 6.4E-17	-5.893E-19 + 6.6E-19	4.19E-17 + 1.3E-18	2.81E-19 + 1.2E-19	2.19E-16 + 5.7E-19	300.21	1567.64	1.0040